University of Stavanger

FACULTY OF SCIENCE AND TECHNOLOGY

MASTER`S THESIS
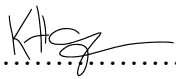
Study Programme/Specialisation:	Spring Semester, 2020
Marine- and Offshore Technology	**Open/~~Restricted Access~~**

Author:	
Kine Hagen	…………………………………………… (Signature of Author)

Faculty Supervisor: **Prof. Yihan Xing**

Title of thesis:

Collapse Design Optimisation of Ring-Stiffened Cylindrical Pressure Hulls

Credits (ECTS): **30**

Key Words:	Pages: **76**
Critical buckling pressure, Pressure hull, Weight of the pressure hull, Design variables, Optimisation, ANSYS, Uncertainty, ASME, Design factor	+ Supplementary Material: **8** **Stavanger,** **1st July 2020**

ABSTRACT

The pressure hull is a vital structural component of the underwater vehicle. It enables the underwater vehicle to withstand environmental loadings such as hydrostatic pressure. Pressure hull design seeks maximum strength capacity with minimum structural weight and is usually constructed as a ring-stiffened cylindrical shell. The shell has the potential to buckle and reduce its loading capacity. Hence, the critical collapse analysis of the pressure hull represents one of the most appealing areas to optimise in structural design.

This thesis aims to optimise the collapse performance of a ring-stiffened cylindrical pressure hull under uniform external hydrostatic pressure. This will be done by studying the influence of the design parameters on the two constraints, which are the critical buckling pressure and the corresponding weight of the steel construction. The optimisation process contains four design variables which include shell cylinder thickness, unsupported spacing, ring-stiffener height and ring-stiffener thickness. A pressure hull model was developed with ANSYS software, and the collapse design analysis is performed using the finite element method. The design influence of the performance output is investigated using eigenvalue analysis, and a parameter correlation study was performed to analyse the coefficient of correlation between the design variables and the performance output. Additionally, a probabilistic analysis was conducted for the pressure hull model in order to investigate the reliability of the critical buckling pressure due to uncertainties in the design parameters.

The findings from this study revealed that the design factor was reduced with 16.4% and the critical buckling pressure was increased by 7.09% when considering parameter uncertainties of cylinder thickness, diameter, unsupported spacing, ring-stiffener height and ring-stiffener thickness. The input design parameters with a significant influence on the performance of the ring-stiffened cylindrical pressure hull are the unsupported spacing between the ring-stiffeners and the cylinder thickness. The cylinder thickness also showed a strong coefficient of correlation with the critical buckling pressure and the corresponding weight of the pressure hull.

This thesis presents an in-depth insight into the design of an important component in the underwater vehicle. The method and analysis framework presented in this thesis can also be utilised in other structural applications.

II

PREFACE

This thesis was completed in the spring of 2020 as a final project of the Master of Science degree in Marine- and Offshore Technology at the University of Stavanger.

I want to offer my sincerest appreciation to my supervisor, Professor Yihan Xing from the University of Stavanger, for his proposal and idea for this thesis. Furthermore, I would like to thank him for his encouragement, enthusiasm and guidance throughout this time.

I would also like to thank my fellow co-students and friends for a collaborative environment, their words of encouragement and motivation these past two years, and my parents for always supporting me.

Stavanger, July 2020
Kine Hagen

TABLE OF CONTENT

LIST OF FIGURES

LIST OF TABLES

LIST OF SYMBOLS

B	-	bending stiffness parameter
$\boldsymbol{B}$	-	strain displacement matrix
C	-	extensional stiffness parameter
D	-	diameter, mm
$\{D\}$	-	displacement vector
$\boldsymbol{D}$	-	global degrees of freedom
E	-	Young's modulus, N/mm^2
$\boldsymbol{F}$	-	volume force vector
F_{ha}	-	allowable hoop compressive membrane stress
F_{he}	-	predicted elastic buckling stress
G	-	shear modulus, N/mm^2
I_r	-	the second moment of area, cm^4
$\boldsymbol{K_e}$	-	material stiffness matrix
$\boldsymbol{K_G}$	-	geometric stiffness matrix
$\boldsymbol{K_{e,ref}}$	-	reference geometric stiffness matrix
L	-	length of the circular cylinder, mm
L_e	-	effective length, mm
$M_x, M_\theta, M_{x,\theta}$	-	bending and twisting moments, Nmm/mm
$N_x, N_\theta, N_{x,\theta}$	-	normal and shearing forces, N/mm
$\boldsymbol{N}$	-	matrix of the shape function
P_a	-	allowable external pressure
P_{cr}	-	critical buckling pressure
P_m	-	elastic instability pressure
P_y	-	pressure midway between stiffeners reaching yield point
$\{P\}$	-	pressure
$\{P\}_{ref}$	-	reference pressure
Q_x, Q_θ	-	transverse shearing forces, N/mm
R, R_i	-	radius and internal radius, mm
S	-	unsupported spacing, mm
U	-	total strain energy

W_f	-	external work done by nodal force
W_p	-	external work due to surface pressure

$\boldsymbol{d}$	-	partial derivative matrix
$\{dD\}$	-	eigenvector
f_s	-	design stresses
h_r	-	stiffener height
n	-	number of observations
$\boldsymbol{q}$	-	nodal displacement matrix
s	-	factor related to the effective yield point
t_r	-	ring-stiffener thickness, mm
t_s	-	cylindrical shell thickness, mm
u, v, w	-	orthogonal coordinates
w_i	-	weight factor
x, θ, z	-	shell coordinates
y_i	-	prediction of the response surface

β	-	parameter of stiffened cylinder
ε	-	hoop strain
$\boldsymbol{\varepsilon}$	-	strain vector
$\boldsymbol{\varepsilon_o}$	-	initial strain in a domain
$\varepsilon_x, \varepsilon_\theta, \gamma_{x,\theta}$	-	membrane strains
$\chi_x, \chi_\theta, \chi_{x,\theta}$	-	curvature changes and twist
λ	-	scale multiplier
λ_{cr}	-	critical eigenvalue
ν	-	Poisson's ratio
σ	-	hoop stress
$\boldsymbol{\sigma}$	-	stress-strain relation
σ_{all}	-	allowable stress
σ_{SD}	-	standard deviations
σ_y	-	yield strength
$\sigma_x, \sigma_\theta, \tau_{x,\theta}$	-	normal stresses and shear stress

μ	-	mean
ρ	-	density
$\rho_{P1,P2}$	-	linear coefficient of correlation
α	-	the amplitude of initial imperfection
ϕ_β	-	design factor
Π	-	potential energy

CHAPTER 1   INTRODUCTION

This chapter presents the primary motivation and outline for this thesis. This includes an introduction to the subject and status of the primary developments and challenges of collapse buckling of a pressure hull.

1.1   Background and Motivation

For underwater vehicles, the pressure hull is a significant structural component. It is the main watertight fundamental component and needs to be designed to withstand environmental loadings associated with diving to third dimension (depth), such as hydrostatic pressure. The pressure hull may either be a single or a double hull. For a single hull, the entire structure has to withstand the external pressure. The doubled pressure hull is presented in Figure 1.1, where the outer hull structure is flooded in order to be hydrostatically balanced. This allows for it to behave as a main ballast tank (MBT) for stability where the pressure hull is designed to withstand the external pressures (Ref. Mackay *et al.* [1]).
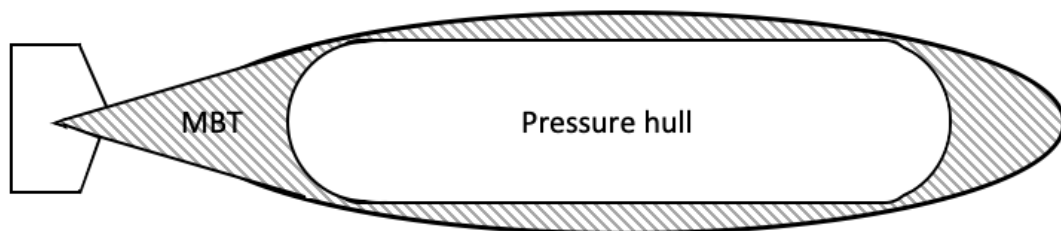
Figure 1.1: Watertight pressure hull surrounded with flooded main ballast tank (MBT).

Critical collapse analysis of underwater vehicles represents one of the most interesting areas to optimise in its structural design. Numerous industrial applications, such as underwater vehicle design, is weight critical. For a fully submerged vehicle, the buoyancy force equals the weight of the liquid displaced by the vehicle. Compared to a surface boat structure, the payload cannot be increased by increasing the volume of an underwater vehicle. Hence, the designers consequently seek maximum strength capacity with minimum weight to increase their payload and its diving depth. According to Liang *et al.* [2], and Burcher *et al.* [3], the pressure hull of underwater vehicle aggregates close to more than one-half of the total structure weight. Burcher *et al.* [3], proposed a proportion of percentage of dry weight devoted to the various functions

of submarines, which means the weight on the surface without variable loads, and is shown in Table 1.1.

Table 1.1: Percentage of dry weight devoted to the various function of submarines (Ref. Burcher *et al.* [3]).

	Weight [%]
Payload	13
Structure	45
Machinery	35
Permanent ballast	7

The payload is considered as weapon stowage, accommodation and launching arrangements. Machinery contributes around one-third of the total dry weight. And about half of the total weight of the submarines in dry weight condition is taken up by the structure. Therefore, it is vital to have an efficient structure as possible to limit this weight to increase the payload.

According to Burcher *et al.* [3], submersibles have mainly been constructed for military purposes, although submarines do exist for non-military use, these are for exploration, oceanographic research, and mineral and oil recovery. The first milestone for submarines history is the John Holland design shown in Figure 1.2a. It was the first underwater vehicle design intended to operate submerged and only surfacing in the beginning and end of a patrol, which the modern submarines can now do. This design lasted for many decades because it is one of the most effective ways of configuring a submersible due to its relatively small length-diameter ratio, and axisymmetric cylinder form which reduced drag force and sound. The outbreak of World War I and World War II progressed submarine design rapidly to achieve better underwater performance to withstand not only hydrostatic pressure but also loads generated by underwater detonations. Additionally, to increase the size to include weapon stowage and launching arrangements. Previous submarine designs had been relatively small and mainly operated on the surface. The *skipjack* class, shown in Figure 1.2b, entered service in 1958, which were considered as a fully operational attack submarine designed with tear-drop shape using modified features from the Holland design. Compared to the Holland design, with a length of 16 meters, the *skipjack* design reached a length of 76 meters. The configuration of

the modern military submarines in the ensuing five decades has not seen any significant changes in the innovative feature of design configurations. However, considerable advances have been taken place in the internal features such as collapse protection of pressure hull to dive deeper, submerged speed, size, and silence due to modern technology.

(a) John Holland design

(b) Skipjack
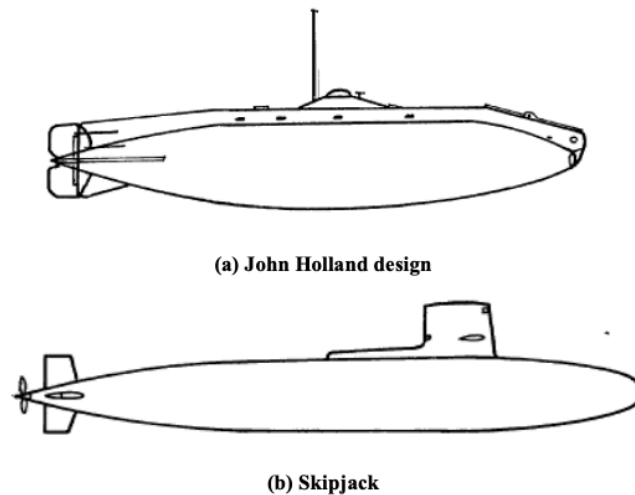
Figure 1.2: Examples of submarine design (Ref. Burcher *et al.* [3]).

The published information of submersible is limited, as the secrecy of military operation cannot be offended. However, the current published studies by authors such as Burcher *et al.* [3], Gabler [4], Friedman [5], Granville [6], Renilson [7], Jones *et al.* [8], and Joubert [9][10], have made known the general design philosophy of underwater vehicles. Especially within the topics of structural design to withstand loading, general internal arrangements to increase volume, hydrostatics stability, hydrodynamics to reduce drag force, and system engineering. These designs also reflect the design philosophy in the DNVGL Naval Ship Rules Part 4 [11]. Gabler [4] and Friedman [5], published studies discussing the existing status of the techniques of a submarine and as a purpose to serve as a handbook for design. Granville [6], studied the shape and size as the two principal geometric parameters as well as other hydrodynamic characteristics of underwater vehicles to eliminate the resisting drag force. Renilson [7] and Jones [8], studied the hydrodynamics aspects of submarines. Renilson [7] also states the principles of submarine geometry. Joubert [9][10] discussed the basis of improved hydrodynamic features and proposed a next-generation submarine by the available knowledge of current submarines, and stated that by altering one piece requires alteration of all the surrounding features to achieve a functional design. It was also concluded that the surface finish of the pressure hull is important to the resistance of a submarine.

The pressure hull of an underwater vehicle is generally designed as a ring-stiffened cylindrical shell, as they have a high strength to weight ratio. However, the shell structure subjected to external hydrostatic load has the potential to buckle and reduce their loading capacity. The buckling of the shell may occur without any warning, which can lead to a sudden catastrophic collapse. This means it is essential to know the science of the shells buckling criteria to be able to produce a solid structure. Ring-stiffeners are applied to the cylindrical shell to prevent buckling from occurring before the onset of yielding in the hull plating (Ref. Mackay *et al.* [1]).

Some researchers have studied the optimisation of the pressure hull. Alvarez *et al.* [12], optimised the pressure hull geometry to reduce the total resistance and Zhou *et al.* [13], studied the optimal structure design of an elliptical pressure hull, by looking at the buoyancy factor which is the total pressure hull weigh and total fluid displacement ratio with various geometrical parameters. Fathallah *et al.* [14][15][16][17] examined the optimum design of a composite elliptical deep submerged pressure hull by reducing the buoyancy factor under failure criteria and the buckling strength constraints to reach maximum depth and minimum weight. Furthermore, an optimisation of a lay-up and multi-object composite material system was investigated to minimise the buoyancy factor and to reduce the weight, as well as to increase the buckling pressure capacity according to the design requirements. Bagheri *et al.* [18], applied the genetic algorithm method to the multi-objective composite to optimise the ring-stiffened cylindrical shells. The result showed that ring-stiffened cylindrical shells yield lower structural weight and higher buckling loads. In addition to this, the stiffener layout played a vital role in the magnitudes of the buckling loads. Liang *et al.* [19], optimised the design of a multilayer composite submersible pressure hulls, taking into consideration the constraints of shell buckling strength, angle-ply laminated facing failure strength and the low-density isotropic core yielding. The thickness of the facings and the core expanded with the increased operational depth.

In the engineering design process, it is essential to understand what and how many design parameters are contributing factors to the output variables such as buckling load and weight. It is an elongated process before the optimisation is completed as to which input parameters play a role in influencing the design, and the uncertainty in the output variables. Due to these uncertainties in the design parameters, the reliability issue of critical buckling pressure for the pressure hull has been studied by some authors using a probabilistic approach. Cai *et al.* [20] studied the influence of uncertainties regarding material properties and geometrical dimensions

on the critical buckling pressure of a composite pressure vessel. Their study showed that longitudinal modulus of composite material and layer thickness has a significant influence on the performance. Furthermore, other parameters, such as unsupported length had a small influence on the performance. Liu *et al.* [21] investigated the strength reliability of a composite laminated vessel using Monte Carlo simulation and response surface method. The results showed that the strength reliability of composite vessels increased with the expansion of composite layer thickness and a slight decrease with increasing radius.

1.2   Objectives

The aim of this thesis is to study the collapse design optimisation by investigating the design influence of collapse performance using the finite element method and probabilistic design system. Simulation of ring-stiffened cylindrical pressure hull subjected to uniform external hydrostatic pressure is performed using ANSYS software. The following sub-objectives are carried out to achieve the main objectives:

- Investigate previously studied collapse design methods.
- Develop a finite element model of a ring-stiffened cylindrical pressure hull in ANSYS.
- Investigate the correlation between the input parameters and the design performance of the ring-stiffened cylindrical pressure hull.
- Investigate how the design influences the critical buckling pressure and the corresponding weight of the pressure hull.
- Perform Six Sigma analysis in ANSYS probabilistic design system to investigate the influence of the parameter uncertainties on the critical buckling pressure.

The geometrical configurations such as the cylindrical shell thickness (t_s), Diameter (D) stiffener spacing (S), stiffener thickness (t_r), and stiffener height (h_r) are significant parameters in the previous studied. Therefore, those parameters are selected as design variables in this thesis.

1.3   Thesis Outline

This thesis is divided into seven chapters and is structures as followed:

- Chapter 2 gives an introduction of the fundamental theories applied in the thesis, such as the structural buckling and cylindrical shell. The collapsing design and stress theories are also investigating.
- Chapter 3 presents the relevant methods used in this thesis to do a buckling collapse assessment of a pressure hull using eigenvalue buckling analysis, and probabilistic approach is presented.
- Chapter 4 contains a parameter correlation study to determine which design variables are co-related to each other or the performance variables of critical buckling pressure or weight.
- Chapter 5 contains eigenvalue buckling analysis to find the parameter influencing the design of critical buckling pressure and its corresponding pressure hull weight. The results are presented.
- Chapter 6 presents a probabilistic design approach, performed to find the probability of failure of the critical buckling pressure.
- Chapter 7 contains a summary and conclusion of the findings in this thesis from eigenvalue buckling analysis, probabilistic approach and correlation study. Recommendations for future work are finally proposed.

CHAPTER 2   THEORY

When studying the theory of buckling collapse of a thin ring-stiffened cylindrical shell, the understanding of the fundamental equation of elasticity and energy stored is needed. This chapter contains a general view of structural buckling and cylindrical shell. Assessment methods for collapse design and equivalent stress theories, a material model used in the finite element method and probabilistic design are covered.

2.1   Elasticity Theory

When external forces alter a solid body, it produces internal stresses and strain, leading to deformation. This deformation depends on its geometrical configuration, boundary conditions, and the mechanical properties of the material (Ref. Ventsel *et al.* [22]). A material is said to be ideally elastic when the deformation caused by force is absolutely reversible, and the relationship between the stresses and strain are linear. Hence, the body has perfect elasticity if it recovers completely. The classical theory of linear elasticity assumes the material to be homogenous and isotropic, i.e., its mechanical properties are identical in all directions (Ref. Prescott [23]).

The linear elastic material is a frequently used material model in solid mechanics. The model is assumed a linear behaviour, where the stress in the material is proportional to the strain, commonly known as Hook's law (Ref. Prescott [23]),

$$\sigma = E\varepsilon \tag{2.1}$$

where the stiffness tensor E known as Young's modulus of elasticity is assumed to be constant during the deformations, in this study, it is assumed that the elasticity limit is never to be exceeded in the material. Hence Hook's law is always valid.

For thin cylindrical shells, the stress components are expressed in x and θ coordinates presented in Figure 2.1. The z coordinate measures the distance from the middle surface of the pipe to its outer surface. The displacement is considered positive if the direction corresponds to the coordinate axis. All the strain components normal to the middle surface of the cylindrical shell

can be neglected, which gives, $\sigma_z = \tau_{\theta z} = \tau_{xz} = 0$. Then, Hook's law for thin cylindrical shells is given by the following equations (Ref. Ventsel *et al.* [24]):

$$\sigma_x = \frac{E}{1 - v^2}(\varepsilon_x + v\varepsilon_\theta)$$

$$\sigma_\theta = \frac{E}{1 - v^2}(\varepsilon_\theta + v\varepsilon_x) \qquad (2.2)$$

$$\tau_{x\theta} = \frac{E}{2(1 - v)}\gamma_{x\theta} = G\gamma_{x\theta}$$

where v is the Poisson's ratio and G shear modulus.
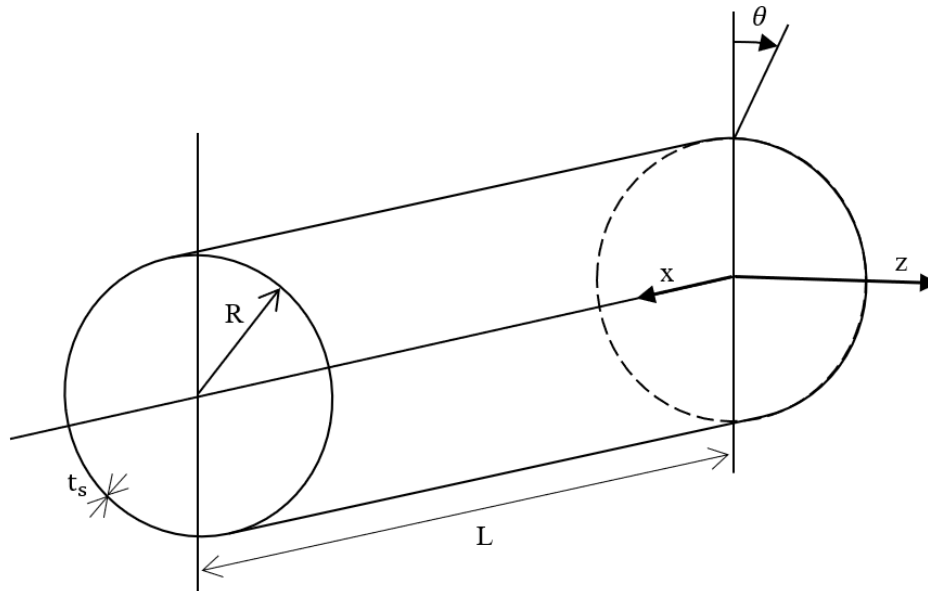
Figure 2.1: The cylindrical coordinate system of a shell.

2.2 Cylindrical Shell Theory

Shells have many structural applications and occupy a leadership position in different fields of engineering because of their intrinsic properties. One great benefit is their high strength to weight ratio, which makes them suitable for a design where low weight is essential and requires large load-carrying capacity (Ref. Kavya *et al.* [25]). Cylinders are common shell configurations within the technology, and they are defined as a body that forms a curved surface in space (Ref. Ramm *et al.* [26]). Geometrically, a cylindrical shell is described by its thickness

t_s, and shape of the cross-sectional surface. The thickness is the distance between the inner and outer surface of the body and is thin compared to its span. The middle surface is at a distance $t_s/2$ from both surfaces (Ref. Cook *et al.* [27]).

There are two different theories for modelling shells, namely thick shells and thin shells theory. It is regarded as a thin shell if the conditions below are satisfied (Ref. Ventsel *et al.* [28]):

$$\max\left(\frac{t_s}{R}\right) \leq \frac{1}{20} \tag{2.3}$$

where R is the middle surface curvature radius, shells with a condition inequal to equation (2.3) are referred to as thick shells.

To be able to describe a cylindrical shell, a coordinate system is applied to the cross-section area of the shell element, as shown in Figure 2.2. The coordinate system gives the longitudinal axis x, circumferential axis θ, and transverse axis z. For a cylindrical shell, its curvature is equal to zero since the radius in the x-direction is infinite. Radius in θ-direction equals to a constant R.
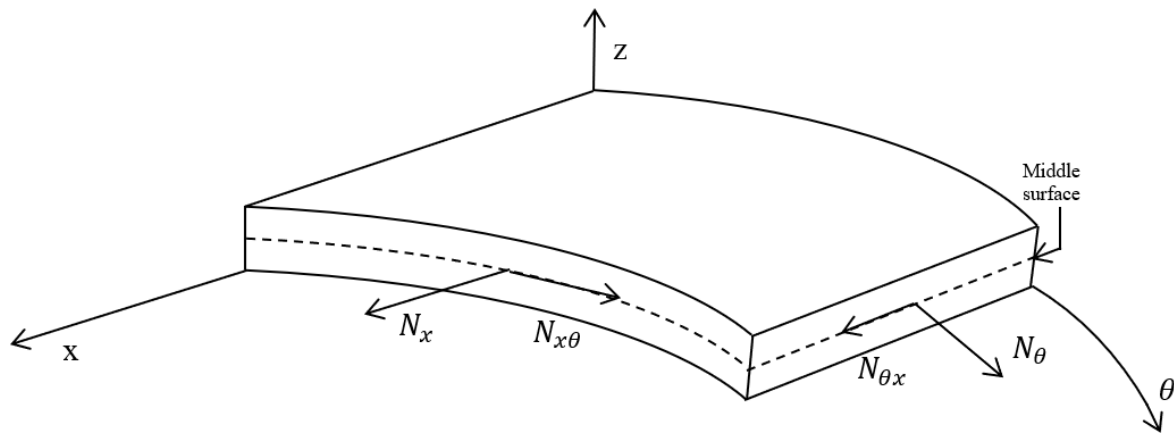
Figure 2.2: Cross-section of a shell element.

In general, a shell displays membrane forces (in-plane forces) and bending forces (out of plane forces) simultaneously in linear thin shells theory, which gives six internal forces, and four moments that characterise the state of stress of the shell completely (Ref. Cook *et al.* [27] and Chen *et al.* [29]). Since the stress components of an elastic cylindrical shell are linearly

10

distributed across the thickness, the internal forces and moments can be expressed by integrating the stress distribution through the thickness of the shell, such as (Ref. Ventsel *et al.* [24]):

$$N_x = \int_{-t_s/2}^{\frac{t_s}{2}} \sigma_x \left(1 - \frac{z}{R}\right) dz \qquad\qquad N_\theta = \int_{-t_s/2}^{\frac{t_s}{2}} \sigma_\theta \left(1 - \frac{z}{R}\right) dz$$

$$N_{x\theta} = \int_{-t_s/2}^{\frac{t_s}{2}} \tau_{x\theta} \left(1 - \frac{z}{R}\right) dz \qquad\qquad N_{\theta x} = \int_{-t_s/2}^{\frac{t_s}{2}} \tau_{\theta x} \left(1 - \frac{z}{R}\right) dz$$

$$Q_x = \int_{-t_s/2}^{\frac{t_s}{2}} \tau_{xz} \left(1 - \frac{z}{R}\right) dz \qquad\qquad Q_\theta = \int_{-t_s/2}^{\frac{t_s}{2}} \tau_{\theta z} \left(1 - \frac{z}{R}\right) dz \qquad (2.4)$$

$$M_x = \int_{-t_s/2}^{\frac{t_s}{2}} \sigma_x z \left(1 - \frac{z}{R}\right) dz \qquad\qquad M_\theta = \int_{-t_s/2}^{\frac{t_s}{2}} \sigma_\theta z \left(1 - \frac{z}{R}\right) dz$$

$$M_{x\theta} = \int_{-t_s/2}^{\frac{t_s}{2}} \tau_{x\theta} z \left(1 - \frac{z}{R}\right) dz \qquad\qquad M_{\theta x} = \int_{-t_s/2}^{\frac{t_s}{2}} \tau_{\theta x} z \left(1 - \frac{z}{R}\right) dz$$

The in-plane normal and shear forces are defined by N_x, $N_{x\theta}$, N_θ, $N_{\theta x}$, and transverse shear forces are defined as Q_x, Q_θ, all measured in N/mm. The bending moments is given by M_x, M_θ, and twisting moments are given as $M_{x\theta}$ and $M_{\theta x}$, all are given to per unit length of the element, Nmm/mm. Stress components at an arbitrary point through the shell thickness are given by σ_x, σ_θ, $\tau_{x\theta}$, $\tau_{\theta x}$, τ_{xz}, and $\tau_{\theta z}$. For a thin cylindrical shell, the terms of order z/R can be neglected when determining stresses in equation (2.4). And for any orthogonal coordinates, $\tau_{xz} = \tau_{\theta x}$ gives the condition of equilibrium of moments. Hence, $N_{x\theta} = N_{\theta x}$ and $M_{x\theta} = M_{\theta x}$. The transverse shear forces are equal to zero, $Q_x = Q_\theta = 0$, due to plane stress conditions assumed for thin shells.

For the expression of normal and shear strain components at any point across the shell thickness, the Kirchhoff-Love hypothesis for shell developed by Love [30], is invoked. As of approximation and neglecting of the stress states, the principal results are that the normal and shear strain components at an arbitrary point across the shell thickness vary linearly through the thickness of the shell. The principal results include the twist, where both types of strains are given in terms of the middle surface displacement, and the in-plane strain components at the

mid surface and the change in curvature. The expression of the strain components at an arbitrary point can be written as (Ref. Jones [31]):

$$\varepsilon_x = \bar{\varepsilon}_x + z\chi_x$$
$$\varepsilon_\theta = \bar{\varepsilon}_\theta + z\chi_\theta \qquad (2.5)$$
$$\gamma_{x,\theta} = \bar{\gamma}_{x,\theta} + z\chi_{x,\theta}$$

where z represents the thickness coordinate distance from the middle surface, $\bar{\varepsilon}_x, \bar{\varepsilon}_\theta$, and $\bar{\gamma}_{x,\theta}$ are the strains at the middle surface, and χ_x, χ_θ, and $\chi_{x,\theta}$ are the changes in the curvature of the middle surface. Donnell [32], was the first to derive the theory of the Kinematic relations of the middle surface of circular cylindrical shells in the early 1903s. This is given as:

$$\varepsilon_x = \frac{\partial u}{\partial x} + \frac{1}{2}\left(\frac{\partial w}{\partial x}\right)^2 \qquad\qquad \chi_x = -\frac{\partial^2 w}{\partial x^2}$$

$$\varepsilon_\theta = \frac{\partial v}{\partial \theta} + \frac{w}{R} + \frac{1}{2}\left(\frac{\partial w}{\partial \theta}\right)^2 \qquad\qquad \chi_\theta = -\frac{\partial^2 w}{\partial \theta^2} \qquad (2.6)$$

$$\gamma_{x,\theta} = \frac{\partial u}{\partial \theta} + \frac{\partial v}{\partial x} + \frac{\partial w}{\partial x}\frac{\partial w}{\partial \theta} \qquad\qquad \chi_{x,\theta} = -2\frac{\partial^2 w}{\partial_x \partial_\theta}$$

where R is the cylindrical radius and u, v, and w are the additional displacements induced by buckling. The equation (2.6) is valid for moderately large deflections (ref. Jones [31]). However, additional terms in the circumferential strain are required for more considerable deflections. In comparison to plates, the circumferential strain ε_θ in equation (2.6) has an additional term. This term, w/R, arises from a large circumference of the cylindrical shell caused by a uniform radial expansion w shown in Figure 2.3. The diameter before the deformation is given as $2R$ and after deformation $2(R + w)$. Thus, the additional circumferential strain term is obtained by the following:

$$\bar{\varepsilon}_\theta = \frac{\Delta\ circumference}{circumference} = \frac{2\pi(R + w) - 2\pi R}{2\pi R} = \frac{w}{R} \qquad (2.7)$$
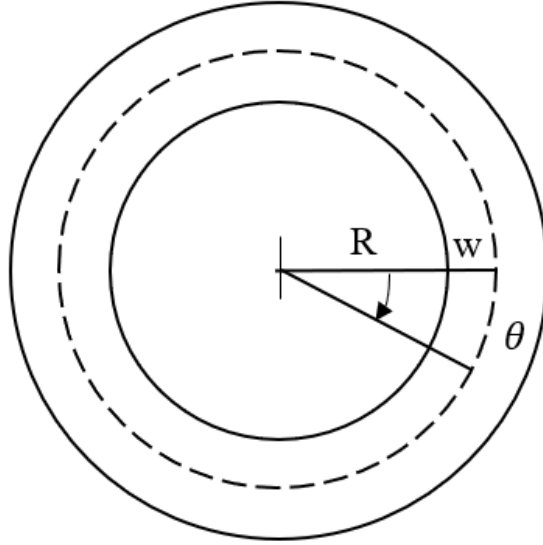
Figure 2.3: Radial expansion w of a cylindrical shell subjected to a load.

By integrating the internal forces N_x, N_θ, and $N_{x\theta}$, and the bending moments M_x, M_θ and $M_{x\theta}$ from equation (2.4), an expression with the six quantities such as the three strain components $\bar{\varepsilon}_x, \bar{\varepsilon}_\theta$, and $\bar{\gamma}_{x,\theta}$ of the middle surface, and the three curvature changes χ_x, χ_θ and $\chi_{x,\theta}$ of the middle surface is obtained. Furthermore, a constitutive equation for a thin-walled cylindrical shell is obtained:

$$
\begin{aligned}
N_x &= C(\varepsilon_x + \nu\varepsilon_\theta) & M_x &= B(\chi_x + \nu\chi_\theta) \\
N_\theta &= C(\varepsilon_\theta + \nu\varepsilon_x) & M_\theta &= B(\chi_\theta + \nu\chi_x) \\
N_{x,\theta} &= K\gamma_{x,\theta} & M_{x,\theta} &= B(1-\nu)\chi_{x,\theta}
\end{aligned}
\tag{2.8}
$$

Where $B = \frac{Et_s^3}{12(1-\nu^2)}$ expressed the bending stiffness of the shell, $C = \frac{Et_s}{1-\nu^2}$ is the extensional stiffness parameter, and $K = \frac{Et_s}{2(1+\nu)}$, in which E is the elastic Young's modulus and ν is Poisson's ratio (Ref. Ventsel *et al.* [24]).

2.3   Ring-Stiffeners

Ring-stiffeners are added to the cylindrical shell, which was described in section 1.2. With stiffener support, the buckling strength and rigidity will improve by only a small increase in weight, without changing the geometry of the pressure hulls. Excluding the ring-stiffeners support, the cross-section or thickness of the cylindrical has to increase to improve buckling strength, which would also lead to a heavier structural weight. Moreover, ring-stiffeners will improve the buckling resistance such that the critical value of applied pressure for the stiffened cylindrical shell is closer to the theoretically determined value, that is predicted by the linear stability theory (Ref. Kavya *et al.* [25]).

The ring-stiffeners may be assumed as a pinned beam element, where the strain relations can be written as:

$$\varepsilon_\theta^r = \varepsilon_\theta + z\chi_\theta \qquad (2.9)$$

It is assumed that the ring-stiffener remains plane during deformation. The bending moment of the cross-section areas of the stiffeners is defined as (Ref. Leontev *et al.* [33]):

$$M_\theta = \int \sigma z dA \qquad (2.10)$$

The hoop stress $\sigma = E\varepsilon$ as given by Hooke's law, equation (2.1), defines the normal stresses in the orthogonal direction, where ε is hoop strain. By integrating equation (2.10) and including the strain displacement and the curvature, the constitutive relation for a ring-stiffener is:

$$M = EI\chi_\theta \qquad (2.11)$$

The curvature of the ring is given by:

$$\chi_\theta = -\frac{1}{R^2}\frac{d^2w}{d\theta^2} \qquad (2.12)$$

2.4   Buckling Theory

The buckling problem has had much interest among researchers for many years because it frequently encounters engineering applications. Buckling is defined as a sudden transformation in the shape of a structural component under loading. The spectral problem can be formulated as a solution related to the limit of elastic stability of the shell (Ref. Millar *et al.* [34]). The design of structures should be based on the buckling criteria. It is particularly crucial in shell structures as it often occurs without apparent warnings, leading to catastrophic effects (Ref. Calladine *et al.* [35]). Its curvature primarily governs the behaviour of a cylindrical shell under external uniform pressure. Bending in shells cannot be separated from stretching, due to its curvature. Hence, they are more complicated than flat plates (Ref. Jones [31]).

In general, the magnitude of membrane stiffness of a shell is several orders greater than the bending stiffness. Hence, a thin cylindrical shell can absorb a substantial amount of membrane strain energy without significant deformations. (Ref. Calladine [35]). However, if a thin cylindrical shell is loaded such that most of its strain energy is stored as membrane compression, and at the same time this membrane strain energy converts to strain energy of bending, the shell may buckle. The loss in membrane strain energy numerically equals the gain in strain energy of bending without any changes off applied load. Large deformation is required to convert such membrane strain energy to strain energy of bending (Ref. Ramm *et al.* [26], Cook *et al.* [36], and Schneider *et al.* [37]). The way buckling occurs on a shell structure depend on the boundary conditions. Especially for shell structures subjected to uniform external pressure. This load case is significantly more dependent on the boundary conditions of the shell than other load cases such as axial compression and shear stress. However, it is shown by experimental results, that shell structure applied external pressure has a smaller sensitivity to imperfection than the other load cases (Ref. Schneider *et al.* [37]).

According to Bushnell [38], there are two types of buckling problems, one is nonlinear collapse, and the other is bifurcation buckling. Nonlinear collapse is predicted through nonlinear stress analysis, where structural stiffness, or the slope of the equilibrium curve, decreases with increasing load. If the pressure is constant as the structure deforms, failure of the material structure is usually dramatic and almost immediate. This type of buckling failure is often called snap-through. The term bifurcation buckling, often called classical buckling, refers to a different kind of failure, predicted through eigenvalue analysis, and is represented in terms of three equilibrium paths:

- Pre-critical equilibrium path, often a linear equilibrium problem.
- Equilibrium state.
- Post-critical or secondary equilibrium path.

Bifurcation buckling is a failure mode with a single application, where the initial stable deformation pattern becomes unstable, and the structure seeks to another stable deformation mode, which differs both quantitatively and qualitatively from the initial mode. The buckling problem can be divided into two categories: axisymmetric and nonaxisymmetric. Furthermore, these two categories can be divided into stable, which is not sensitive to imperfection and unstable, which is imperfection sensitive (Ref. Bushnell [38]). Figure 2.4 shows the equilibrium path OABC that corresponds to an axisymmetric deformation mode called the primary path, where the structure with applied load passes from its unbuckle state continuously to a close buckling state. For action close to the critical load B, more than one equilibrium path exists that corresponds to the equilibrium state of the structure. The post bifurcation equilibrium path BD is a secondary path and corresponds to a nonaxisymmetric deformation mode, which implies that the equilibrium is unstable for the structure (Ref. Zeman *et al.* [39]). For perfect cylindrical shells without ring-stiffeners, the buckling resistance is poor and will buckle non symmetrically (Ref. Prabu *et al.* [40]).
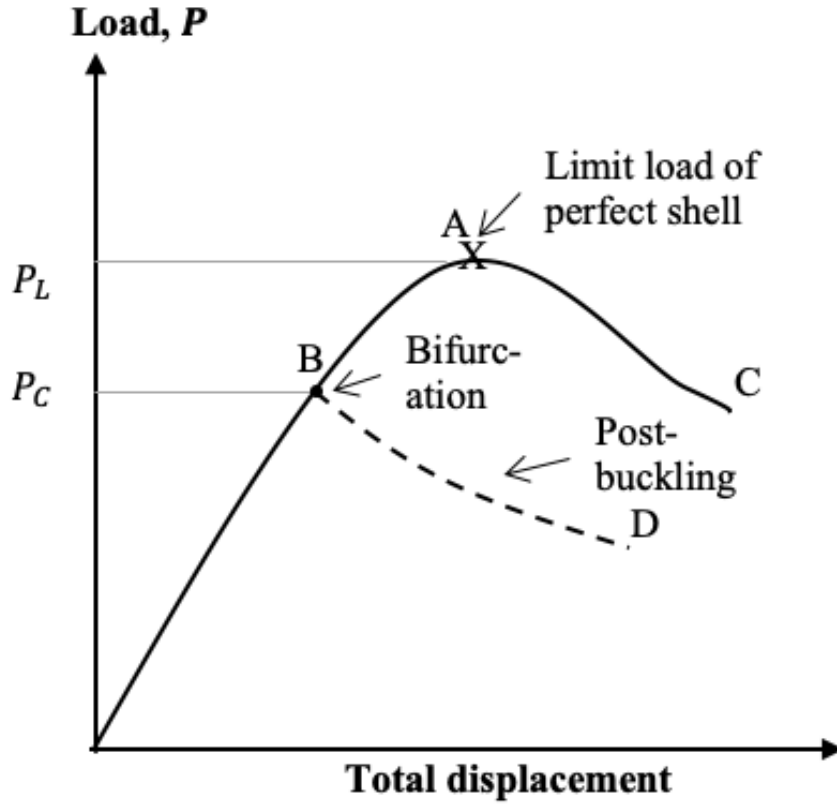
Figure 2.4: Equilibrium paths with critical load A, bifurcation point B, and post-bifurcation equilibrium path, BD.

Many researchers have studied the related buckling equations for the past decade. However, the Von Mises, firstly given by Timoshenko *et al.* [41], is usually used in engineering. The buckling equation for stiffened pipe with radius R, shell thickness t_s and unsupported spacing S is given in equation (2.13), and the approximate wave number can be determined by equation (2.14).

$$P_{cr} = \frac{Et_s}{R} \frac{1}{(n^2-1)\left(\dfrac{n^2}{\left(\frac{\pi R}{S}\right)^2 + 1}\right)^2} + \frac{Et_s^3}{12(1-v^2)R^3}\left[(n^2-1) + \frac{2n^2-1-v}{\left(\frac{\pi R}{S}\right)^2 + 1}\right] \tag{2.13}$$

$$\bar{\varepsilon}_\theta = \sqrt[8]{\frac{3\left(\frac{\pi R}{S}\right)^4}{t_s^2/(12(1-v^2)R^2)}}$$ (2.14)

A classical bifurcation buckling analysis reaches for the load at which the equilibrium of the structure is stable. However, for the shell under identical applied external load and boundary conditions, the possible equilibrium configuration may vary. In some cases, the bifurcation load may falter from the maximum structural load. In other cases, the bifurcation load may never be reached in simulation experiments. From research, the maximum load for thin-walled cylindrical shells, is much less than the theoretical load, as the geometrical imperfection sensitivity has an impact, and can make it less engineering significance (Ref. Bushnell [42]).

2.5   Buckling Modes

When a stiffened cylindrical shell is exposed to a critical load, buckling occurs in a particular mode. Several properties influence the buckling mode, among them, are the type of pressure, the bending stiffness of stiffeners and shells, and the type of stiffeners, such as longitudinal, ring or combinations of these two stiffeners. The various types of buckling modes for ring-stiffened cylindrical shells can be divided into two main groups: local buckling mode, and global buckling modes, which will be introduced in section 2.5.1 and 2.5.2, respectively. Additionally, a less common buckling mode is the tripping of stiffeners. This happens when the geometrical dimension of the stiffeners is not strong enough to support the shell cylinder, and buckles first (Ref. Hu *et al.* [43]).

2.5.1   Local Buckling

The most significant contribution to the cylindrical shells bending stiffness is the magnitude of the second moment of area of the ring-stiffeners. This magnitude depends on the shape and dimension parameters of the ring-stiffeners. If the ring-stiffeners bending stiffness is in such a degree that they do not buckle when the shell is subjected to a critical load, the unsupported spacing between the stiffeners will buckle (Ref. Kavya *et al.* [25]). The ring-stiffened cylindrical shell in Figure 2.5 is exposed to local buckling.
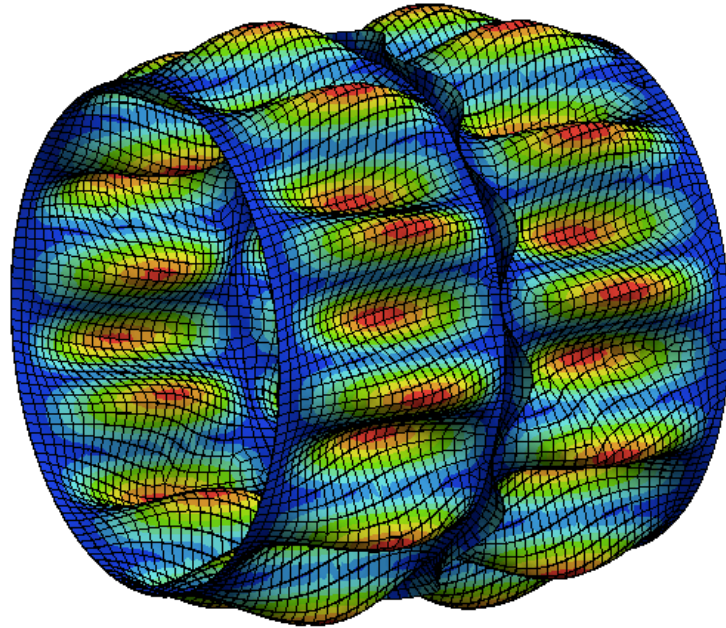
Figure 2.5: Screenshot from ANSYS of local buckling of stiffener for a ring-stiffened cylindrical shell.

2.5.2 Global Buckling

A ring-shell combination may buckle if the ring-stiffeners do not have enough bending stiffness strength to preventing shell displacement (Ref. Kavya *et al.* [25]). This failure mode is referred to as global buckling. This buckling mode does not acknowledge the stiffeners in the structure. Consequently, the shell is carrying most of the load. Global buckling is an overall stiffened pipe collapse accompanied by its stiffeners and deformers in the same waves, which is presented with an ANSYS model in Figure 2.6.
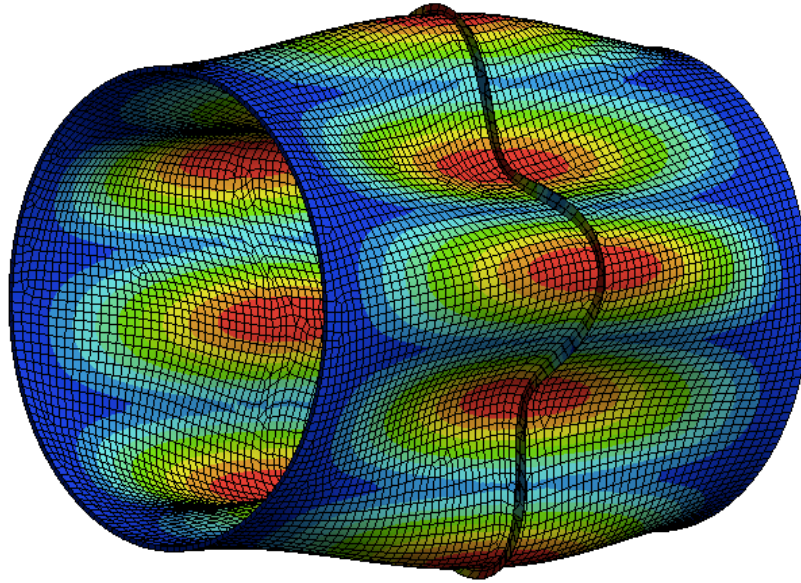
Figure 2.6: Screenshot from ANSYS of global buckling of stiffener for a ring stiffened cylindrical shell.

2.6 Imperfection and Uncertainties in Parameters

When designing a shell structure, the shape of a shell will not achieve a constant curvature or coordinate geometry. Due to the production size and scale of shell structures, they are subjected to unfavourable imperfection and geometrical uncertainties that can give different in load-carrying capacity for large construction. Any geometrical errors, such as variations from circularity or deviation from straightness of the stiffeners, can lead to precipitation of collapse. The design of a pressure hull structure has to take account of such imperfections and uncertainties. Bushnell [38], expressed the term imperfection by the sensitivity of the load at which the shell buckles to defects in the shape of a shell. Compared to the bifurcation buckling described in the section (2.4), the actual structure with imperfection will follow an original equilibrium path OEF in Figure 2.7, with a failure corresponding to a nonaxisymmetric deformation such as to snap-through at point E, at the collapse load S.
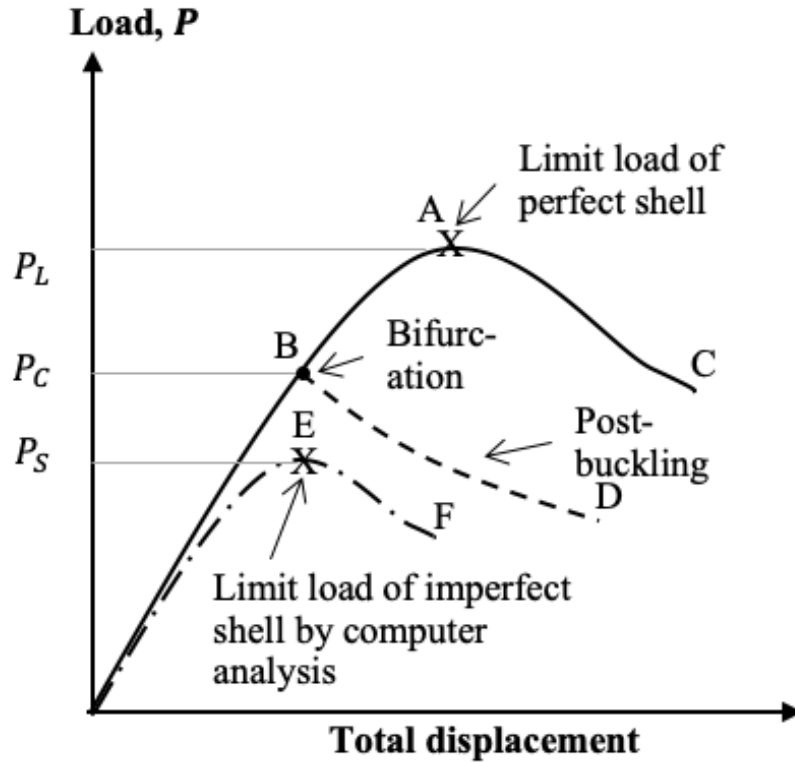
Figure 2.7: Equilibrium paths for perfect shell, and imperfect equilibrium path OEF with collapse load at E.

It is impossible to eliminate all imperfection and uncertainties in a structural component. However, even though the true bifurcation buckling is fictitious, the analytical model of the bifurcation buckling is valid for a good approximation of the actual failure load. Although imperfection is arbitrary by nature, there have been efforts to study and classify geometrical imperfection to include the uncertainties in the analytical model.

Calladine [44], stated in his paper "Understanding imperfection-sensitivity in the buckling of thin-walled shells" in 1995 that imperfection in a structure could be categorised into three categories.

- The buckling load fall shorter than what is predicted by classical theory.
- Experimental buckling load is unpredictable and distributes over a wide range.
- Unstable buckling leads to catastrophic failures.

However, he also states that shell-buckling behaviour does not always fall into these categories.

21

Kármán *et al.* [45], took the first significant step in 1940 to attempt a theory to predict the buckling load of shell imperfection. He argued that shells behave similarly to a sort of longitudinal beams supported by nonlinear springs. This argument led to both theoretical and numerical studies of simple columns, and the presence of small misalignment of the columns lead to the three behaviours above.

Meanwhile, Koiters formula was developed. The fundamental theory imposes that the imperfection is solely in the shape of the buckling modes and that the sensitivity of the buckling load influence shells imperfection. The approach introduced geometrical imperfection utilising simple scheme of disturbance (Ref. Calladine [44], and Godoy *et al.* [46]). This formula gave an explicit reduction factor for the buckling load of the shell on account of imperfection having various forms written as:

$$P/P_{cr} = 1 + \sqrt{12\alpha/t_s} \qquad (2.15)$$

where P_{cr} is the classical critical buckling load, α is the amplitude of the initial imperfection and t_s is the thickness of the cylindrical shell.

Cederbaum *et al.* [47], applied probabilistic methods to the Koiter formula to derive the reliability of shells imperfection by taking account of the randomness of two parameters into the equation: the initial imperfection and the allowable load. By including the loading randomness, the reliability was reduced as this only considers the randomness of initial imperfection.

A study done by Arbocz *et al.* [48], used a characteristic imperfection spectrum classified by the fabrication. Research from Hilburger *et al.* [49], states that measured initial geometrical imperfection from produced shells can be used as an imperfection signature input for finite element analysis. Results indicated a good representation of preliminary design data for less conservative buckling load and reduction in weight.

For any loaded cylindrical shells, the geometrical imperfection and uncertainties should be assumed as the worst case when the imperfection cannot be known, (e.g., the structure is not built, and the contractor cannot give construction tolerance) to be assured that the imperfection

or geometrical uncertainty investigation can be an appropriate knock-down factor or design factor.

2.7   Finite Element Analysis

Finite element analysis is a numerical procedure that is a leading computational method in science and engineering. This procedure can be applied to gather solutions to a variety of physical phenomena in engineering, a way of virtually testing design to help implement appropriate changes. The idea of finite element analysis is to divide a complicated body into simple finite elements, where each individual element is connected by global nodes. The division of geometry allows for a representation of the behaviour over individual elements. This particular arrangement of finite elements is called mesh. The number of such element is increased to improve the accuracy of the numerical model, and such process is commonly known as meshing. Loads and boundary conditions are applied at the global nodes. Since each element is connected to a node, the solution from elements must have the same value at that node (Ref. Chakrabarty *et al.* [50]).

The mathematical formulation of a finite element method consists of coupling the absolute equation of each of the individual elements to form a complete solution for the domain that satisfies the boundary conditions (Ref. Jawad [51]). The basic concept of the finite element formulation is based on assuming a general displacement field $[\delta]$, depending on the nodal displacement vector of an element $[q]$ and shape function matrix [N], written as:

$$[\delta] = [N][q] \tag{2.16}$$

The shape function depends on the type of element and the number of nodes. The strain displacement relation can be expressed as:

$$[\varepsilon] = [d][\delta] \tag{2.17}$$

where [d] is a partial derivative matrix and $[\varepsilon]$ the total strain in an element. By coupling equation (2.16) with equation (2.17), the strain in an element can be expressed in terms of the deflection of the nodal points:

$$[\varepsilon] = [d][N][q] = [B][q] \tag{2.18}$$

where

$$[B] = [d][N] \tag{2.19}$$

Now the total strain energy in an element is given by:

$$U = \frac{1}{2} \int_V [\varepsilon]^T [\sigma] - [\varepsilon_0]^T [\sigma] \ dV \tag{2.20}$$

where $[\varepsilon_0]$ is the initial strain in a domain, and the stress-strain relation is given by $[\sigma]$, and is obtained by:

$$[\sigma] = [D][B][q] - [D][\varepsilon_0] \tag{2.21}$$

The external work done by the nodal force is obtained by:

$$W_F = [F]^T [q] \tag{2.22}$$

And the external work due to surface pressure:

$$W_P = \int_S [\delta][q] \ dS \tag{2.23}$$

Hence, the potential energy in a body is given by the difference between the strain energy within the element and the work done on the element:

$$\Pi = U - (W_F + W_P) \tag{2.24}$$

The material stiffness matrix for an element is written as:

$$[K_e] = \int_V [B_e]^T [D_e][\, B_e]\, dV \qquad\qquad (2.25)$$

Hence, the finite element equitation with applied load [F] is given:

$$[F] = [K_e][q] \qquad\qquad (2.26)$$

2.8 Collapse from Buckling Design

Pressure vessel design for protection against collapse from buckling is currently available in several codes, with different design methodologies and requirements. For the state of stability of a pressure vessel, a sufficient design factor is required with respect to the particular concerned form of failure. The main contributors for such codes are the American Society of Mechanical Engineers Providing the ASME VIII code [52][53], the Technical Committee in Brussels, providing the European Standard NS-EN 13445 [54], and the British Standards institution, providing BS PD 5500 [55]. Design methods provided by the different codes are presented in Figure 2.8.

The different codes available can provide two methods for the design of pressure containing components. These two methods listed below determine the required geometrical dimensions, such as cylindrical shell wall thickness to withstand external loads or internal pressure. This thesis will focus on external load approaches.

- Design by Rules
    - o   Specify the overall load and dimensions.
    - o   Calculate the wall thickness using formulas, charts, and predefined procedures.
- Design by Analysis
    - o   Defines the overall dimensions and geometry.
    - o   Evaluation of allowable loads through detailed structural analysis.
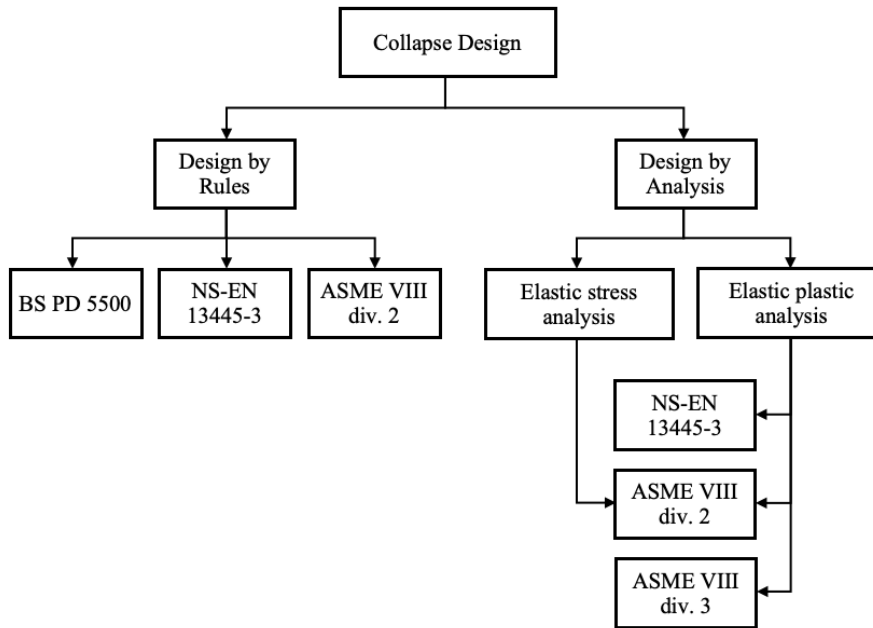
Figure 2.8: Collapse design for buckling from different codes for two different design methods.

2.8.1   Design by Rules

Design by Rules (DBR) approach provides formulas to determine the required cylindrical shell wall thickness and unsupported length based on design pressure, allowable stress, and geometry parameters. The requirements for specific configurations are determined by formulas and several diagrams provided in the codes.

By following the DBR method, each standard has different approaches and formulas to use. However, the codes providing DBR given in Figure 2.8 has a clear step by step approach to follow, which is shown in Table 2.1. In contrast, ASME VIII div. 2 [52], provides formulas to calculate elastic buckling stress and predicted buckling stress in their steps, while formulas to calculate the pressure that reaches yield point between stiffeners and elastic instability pressure are provided in NS-EN 13445-3 [54]. The rules for external pressure design in NS-EN 13445-3 are based almost entirely on the rules in the published document BS 5500 [56].

Although the rules are said to be rules for design, for all codes, the first step requires the user to choose the cylindrical shell thickness and dimension for stiffeners for all cases. Furthermore, the application of the rules will show whether the proposed dimensions are adequate for allowable pressure. The allowable external pressure has to be equal to or more than the external

design pressure. If not, both ASME VIII div. 2 and NS-EN 13445-3 suggest that the assumed shell thickness shall be adjusted, or the unsupported length of the shell shall be reduced.

Table 2.1: Step by step approach to determine the allowable external pressure for cylindrical shell using the design by rules approach with external pressure for ASME VIII div. 2 and NS-EN 13445-3 codes.

Steps	ASME VIII div.2	NS-EN 13445-3
1	Assume the shell thickness and unsupported length	Assume the shell thickness and calculate the pressure midway between reaches yield point, $$P_y = \frac{sf_s}{R(1-\beta Y)}$$
2	Calculate predicted elastic buckling stress $$F_{he} = \frac{1.6c_h E t_s}{D}$$	Calculate elastic instability pressure $$P_m = \frac{E\varepsilon}{R}$$
3	Calculate predicted buckling stress depending on the magnitude of F_{he}, and apply a safety factor	Calculate $\frac{P_m}{P_y}$ and determine $\frac{P_a}{P_y}$
4	Calculate the allowable external pressure, $$P_a = 2F_{ha}\left(\frac{t_s}{D}\right)$$	Allowable external pressure is less or equal to design external pressure $$P_a \leq P$$
5	Allowable external pressure is less or equal to design external pressure $$P_a \leq P$$	

To be able to ensure the lateral stability of the stiffeners, and prevent stiffeners from tripping, the design by rules requires the configurations to be within a range. Formulas to be used are individual in for different types of stiffeners. For pinned beam stiffener used in this thesis, the DBR approach requires the configurations to be within the range as follows for ASME VIII div. 2:

$$\frac{h_r}{t_r} = 0.375 \sqrt{\frac{E}{\sigma_{all}}} \tag{2.27}$$

where σ_{all} is the allowable stress. For NS-EN 13445-3 the required configuration is as follows:

$$\frac{h_r}{t_r} = 0.5 \sqrt{\frac{E}{sf_s}} \tag{2.28}$$

where s is the factor relating to the effective yield point, and the magnitude to steel it 1.1. The design stresses for a stiffener are presented as f_s.

These configuration requirements give a limitation of the design, while design by analysis method, which will be introduced in section 2.8.2, gives no limitation of the design configurations before the analysis.

2.8.2   Design by Analysis

With a Design by Analysis (DBA) method, a pressure containing component is evaluated based on results obtained from numerical analysis. DBA may be used within the scope of the formulae specified in the DBR method, as a complement or in all cases outside the scope and in all the cases, not covered within the design formulas (Ref. Zeman *et al.* [39]).

The computer software available today makes it easy to obtain finite element results, but achieving reasonable correct results is not. The process of establishing the model and defining the relevant boundary conditions that are according to the use of standards design factor requires knowledge.

The codes provide different analysis setup and acceptance criteria to determine if the component is safe depending on what type of analysis being used or pressure applied. The ASME VIII code covers different pressure ranges divided into divisions. Division two contains the pressure range in general, whereas division three is covering high-pressure vessels. As ASME VIII div. 3 and NS-EN 13445-3 only provides an elastic-plastic analysis (Figure 2.8), they will not be further described. ASME VIII div. 2 is the only design code to be used in this thesis.

For protection against collapse from buckling, there are three alternative analysis methods provided in ASME VIII div. 2 [52], and the different methods are such:

- **Elastic stress analysis**
- Limit load analysis
- Elastic-plastic analysis

From the analysis procedure listed above, the most common analysis is elastic stress analysis and elastic-plastic analysis. Elastic stress analysis approximates the protection against collapse from buckling. Furthermore, a developing analysis method for protection against buckling is an elastic-plastic stress analysis which uses a material model that includes softening and hardening. ASME VIII div. 2, has an additional limit load analysis method, which involves determining the lower bound limit load of a component. The limit load analysis and elastic-plastic analysis will not be future considered in this thesis.

Elastic stress analysis has been a part of the industry for many years and extensively used in the design of a pressure vessel. In this analysis method, stresses are computed using a linear-elastic material model. Hence the plastic hardening is not considered in the material. The stresses have been established and classified into categories and compared to the allowable values, such that plastic collapse does not occur. The collapse load is determined considering both loading and deformation characteristics of the structure where the design factor is added from the calculated collapse load. The design code provides a margin of safety, which takes care of the inaccuracy of calculations of strength, such as departure from design shape, stress concentrations causing fatigue and imperfect factory production of the indeterminate structure.

ASME VIII div. 2 [52], provides several parts of standards, and they are interdependent, such that to be able to use the design code for the numerical analysis, the specified requirements in all the parts have to be fulfilled. For material, the code provides a precise specification of approved materials to be used in the analysis, depending on anticipated material behaviour for elastic analysis. Additionally, the quality requirements for materials and weld are specified to ensure a safe structure. The code also specifies that all the loads applied to a component shall be considered to act as individual and combination and to consider the most unfavourable load.

The requirements to use the design factor of 2.5 for elastic stress analysis for protection against collapse from buckling is summarised in Table 2.2.

Table 2.2: Requirements for loading, quality assurance and quality control (Qa/Qc), and material to use design factor from ASME in an elastic stress analysis.

Analysis	Design factor	Loading	Qa/Qc	Material
Elastic stress analysis without geometric non-linearities	$\varphi_\beta = 2.5$	▪ The load shall be considered individual and combinations. ▪ Whichever load combination produces the most unfavourable effect being considered.	▪ Strict requirements for material and weld quality. ▪ The nominal pipe wall shall be less than or equal to 50 mm	The code describes the acceptance material formerly.

2.9   Probabilistic Design

2.9.1   Deterministic vs Probabilistic Design

The deterministic design approach gives an algorithmic relationship between the input parameters and the output variables using a finite element software. Such as geometric dimension and critical buckling pressure and weigh of the pressure hull. Moreover, the approach assumes certainty in all aspects. Hence, for it to serve, it requires the appropriate use of extreme values or a worst-case scenario to quantify the safety of the design (Ref. Reh *et al.* [57]). The approach applies an uncertainty factor, also known as the design factor, to account for the uncertainties to achieve a conservative structural design. The concept of this design factor is to provide a safe margin between an operational level and design strength. Hence, it accounts for the possibility that an actual load exceeds the predicted load, or that the actual design strength is less than the expected strength. In the 1930s, a design factor of 1.5 was derived and became a formal requirement for the aerospace industry, which has been later accepted and evolved for many engineering applications. For this study, the design factor for protection against buckling collapse of 2.5 is used as described in section 2.8.2. However, it is unknown exactly how safe it is due to the uncertainties in many aspects, such as structural loads, design analysis, material, and environment (Ref. Heitzmann *et al.* [58]). The design factor may be too large or too small, depending on the variability in design, manufacturing, and operating environments. If the variability is reduced, a reduction of the design factor could be justified. However, an increase of the variability with, for example, a new material, the magnitude of the design factor may be unconservative and have to be improved. Hence, there is no guarantee that the design factor is viable for a problem, even if the same problem has been successful in the past.

According to Heitzmann *et al.* [58], the probabilistic design approach accounts for the uncertainties in the definition of geometry, load, manufacturing processing, material properties, and the uncertainties of testing in an engineering problem. Knowing the inherent risk of design failure is becoming increasingly important to both the customer and the manufacturer. Long *et al.* [59], summarized the foundation of the probabilistic approach as the statistical definition of all input parameters required for structural analysis methods, and its resulting stress and strength by evaluation of the resulting probability of failure or risk. With the probabilistic approach, each variable is no longer a single value but rather a probabilistic distribution of

failure, predicted through an engineering system. By considering this distribution, the designer can constrain the flow of random variability and improve quality without using a design factor. A powerful attribute of this approach is the information gained in understanding the interactions and sensitivity of design variables. Hence, this information can be used to improve the design or manufacturing tolerances. For instance, if one parameter shows that minor variation had a significant effect on the resultant strength.

2.9.2 Six Sigma

Six Sigma, first developed in the early 1980s by Motorola, is a well-accepted definition of a failure probability. The Six Sigma methodology seeks to bring the operation to a Six Sigma level of quality, which essentially means limiting the defective performance of the design requirements to a probability of 3.4 for every one million opportunities. Hence, if a parameter is defined by specific limits separation from adverse outcomes of a process, then a Six Sigma analysis has a mean that is six standard deviation from the nearest specification limit, as shown in Figure 2.9. This means, if a book contained one million words, the Six Sigma quality would give a probability that 3.4 word was to be wrongly written. Compared to a mean value that is three standard deviations from the nearest specification limit, which would give a probability that 1350 words of one million are wrongly written. Hence, a Six Sigma level of quality would nearly mean defect-free (Ref. Montes *et al.* [60]).
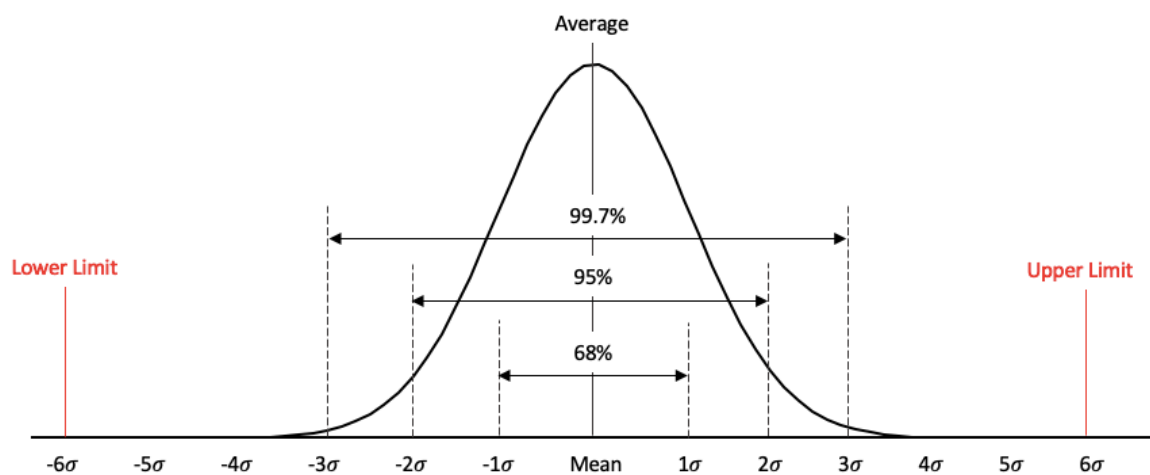

Figure 2.9: Six Sigma Gaussian distribution.

Sigma outlines the population standard deviation, a measure of the dispersion from the mean of a data set collected about the process. The standard deviation of n observation and mean μ is defined as follows (Ref. ANSYS [61]):

$$\sigma_{SD} = \sqrt{\frac{1}{(n-1)} \sum_{i=1}^{n} (y_i - \mu)^2} \tag{2.29}$$

where the mean μ is defined as:

$$\mu = \frac{1}{n} \sum_{i=1}^{n} y_i \tag{2.30}$$

Six Sigma analysis uses statistical distribution functions such as Gaussian or normal distribution to describe uncertain parameters. However, an output parameter rarely follows a gaussian distribution. The nonconformance probability can be calculated for any distribution the output parameter follows. For other distribution than gaussian, the Six Sigma level is not precisely six standard deviation away from the mean value. However, it does represent a probability of 3.4 defaults per million, which is consistent with the definition of Six Sigma quality. A cumulative distribution function is a review tool to assess the reliability or the failure probability of the chosen random variable (Ref. ANSYS [61]).

2.9.3 Response Surface

According to Yang *et al.* [62] and An *et al.* [63], the response surface methodology, proposed by Box and Wilson in 1951, is a widely adopted statistical design tool to investigate the coupled impact between different parameters. The method performs a series of numerical analysis for a given set of design point and generates a response surface as a function of the given input parameters over the design space. It defines the influence of the independent parameters, alone or in combination, of the process (Ref. Rout *et al.* [64]). Response surface in this thesis is created using generic aggregation, where the prediction of the response surface area defined by $\hat{y}_i$, and w_i is the weight factor of the response surface. The Generic aggregation response surface is written as follows (Ref. ANSYS [61]):

$$\hat{y}_{ens}(x) = \sum_{i=1}^{N_M} w_i \hat{y}_i(x) \tag{2.31}$$

CHAPTER 3 NUMERICAL ANALYSIS METHODS

This chapter explains the procedure of collapse from buckling assessment made for a pressure hull with the use of eigenvalue buckling analysis and probabilistic approach.

3.1 Eigenvalue Buckling Analysis

Eigenvalue buckling analysis predicts the theoretical critical buckling load on an ideal linear elastic structure (Ref. Ellobody *et al.* [65]). The initial imperfection of the structure is assumed to be neglected. Hence, the analysis is limited to symmetric bifurcation buckling. This analysis is used to anticipate the bifurcation point by using a linearized model of an elastic structure (Ref. Prabu *et al.* [40]). A full 360-degree model is required because the deformation of the structure is no longer axisymmetric after buckling occurs (Ref. Kavya *et al.* [25]).

The membrane stresses acting tangent to the middle surface of a shell has an influence on the lateral deflection. These internal membrane stresses cause a second-order strain stiffening and are significantly large than the elastic bending stiffness in the shell, and must be included in the total stiffness matrix. Hence, the effects of the internal membrane forces are accounted for by the geometrical stiffness matrix $[K_G]$. The geometrical stiffness is a function of stress and directly proportional to the load. Additionally, it is independent of elastic properties. (Ref. Cook *et al.* [36]).

When a structure is applied a reference level of external loading $\{P\}_{ref}$, the membrane stresses in elements can be obtained by carrying out a standard linear static analysis. Hence, a geometric stiffness matrix $[K_G]$ appropriated to $\{P\}_{ref}$ is generated. For another load level, the geometric stiffness matrix can be expressed in terms of a reference geometric stiffness matrix, with a scale multiplier, λ (Ref. Cook *et al.* [36] and He *et al.* [66]):

$$[K_G] = \lambda[K_G]_{ref} \qquad \text{when} \qquad \{P\} = \lambda\{P\}_{ref} \qquad (3.1)$$

The geometrical stiffness matrix $[K_G]$ is independent on the applied reference load while the reference geometrical stiffness matrix $[K_G]_{ref}$ denotes the variation of the stiffness matrix, and depends on the stress induced by the applied load. The equilibrium equation for the structure is written as:

$$([K_e] + \lambda_{cr}[K_G]_{ref})\{D\} = \lambda\{P\}_{ref} \qquad (3.2)$$

where $\{D\}$ are displacement vector induced by the applied reference external load $\{P\}_{ref}$ and $[K_e]$ the material stiffness matrix, respectively. Since the external load does not change at the bifurcation point, the equilibrium equation for a structure may be written as:

$$([K_e] + \lambda_{cr}[K_G]_{ref})\{dD\} = \{0\} \qquad (3.3)$$

where $\{dD\}$ is the eigenvector, and the critical eigenvalue is given by λ_{cr}. Equation (3.3) defines the eigenvalue problem for the lowest critical eigenvalue λ_{cr} associated with buckling. Hence, when the load factor equals the lowest eigenvalue, the structure buckles. The critical buckling load is then found from:

$$\{P\}_{cr} = \lambda_{cr}\{P\}_{ref} \qquad (3.4)$$

The eigenvector $\{dD\}$ associated with critical eigenvalue λ_{cr} represents the buckling mode characteristic for the corresponding critical buckling load. However, since the magnitude of the eigenvector is indeterminant, it only defines the shape and not the amplitude.

3.2   Software

ANSYS Workbench 19 software is used to produce the model and obtain the result of the collapse design optimisation. This is a finite element analysis software, and the simulation process consists of separate systems involving a flow chart model. The flow chart designates the order in which the system is processed. ANSYS provides different types of analysis systems. For the case of buckling analysis, the combination of two separate systems is necessary, namely static structure and eigenvalue buckling. Both analyses consist of the following cells:

- Engineering data
- Geometry
- Model
- Setup
- Solution
- Results

The *engineering data* provides the material properties for the model. The *geometry* cell is used to set up the geometrical model for the analysis. The *model* and *setup* cells provide modelling of the structure, including the boundary condition and loads. The mesh element is also generated in this cell. The *solution* cells show the deformation model after every pre-processing and processing feature has been applied. The *results* can be shown in terms of different parameters calculated by the solution process.

The difference between static structural analysis and the eigenvalue buckling analysis is the analysis procedure. Static structural solves the static equilibrium, and the eigenvalue buckling estimates the eigenvalues problem and corresponding eigenvectors.

The two described systems and the parameter correlation analysis are connected within the flowchart shown in Figure 3.1, allowing the information and solution from the static structural system to flow to the eigenvalue buckling system to achieve the collapse buckling pressure. In this way, the static structural analysis acts as a preliminary process for the buckling analysis. For the parameter correlation analysis, both structural analysis and buckling analysis acts as post-process through the parameter setup.
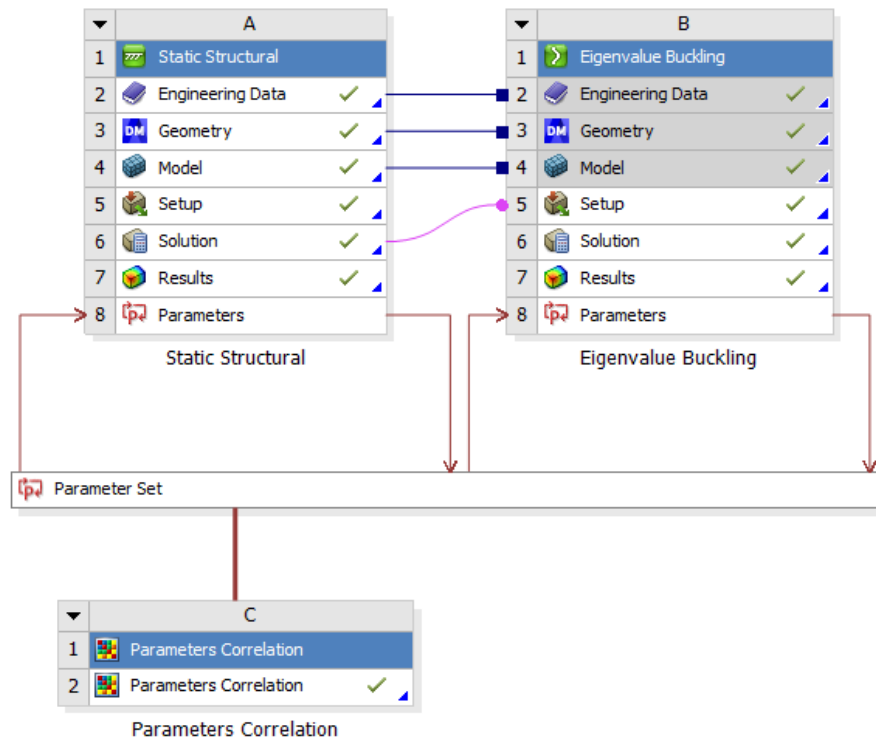
Figure 3.1: Screenshot of flowchart from ANSYS. System A the static structural system B the eigenvalue buckling system and system C the parameters correlation.

3.2.1   Probabilistic Design Setup

The probabilistic approach of the pressure hull is delivered from ANSYS design explorer. The probabilistic design system allows extracting characteristic results parameters such as the critical buckling pressure from the finite element analysis model. This means that the structural analysis and buckling analysis are preliminary processors for the Six Sigma analysis through the parameter set, as shown in Figure 3.2.
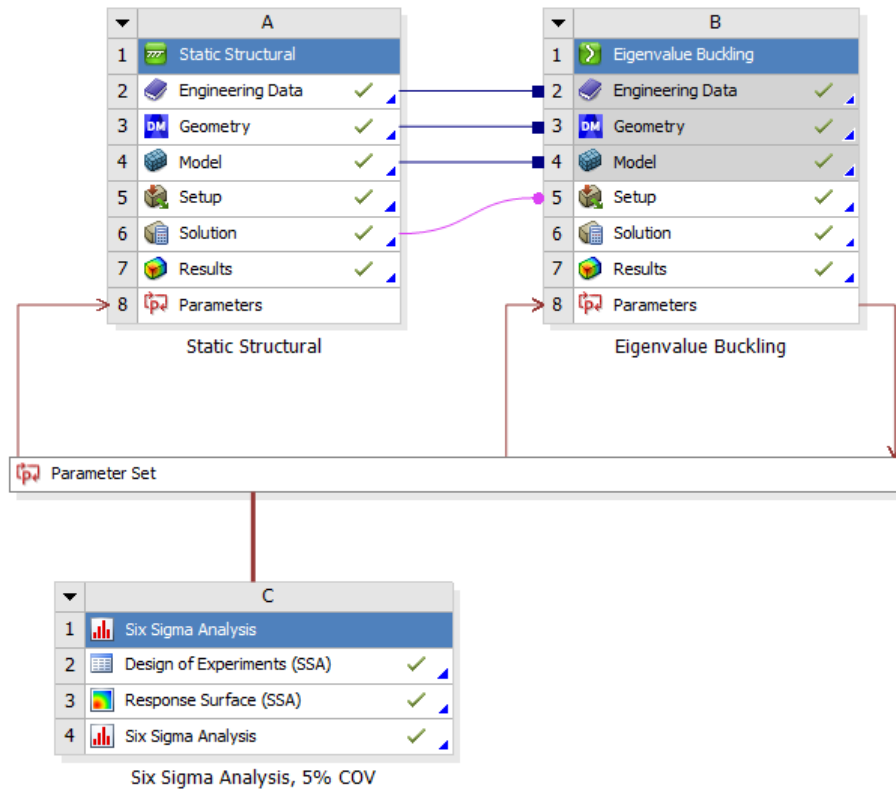
Figure 3.2: Screenshot of flowchart from ANSYS. System A the static structural system B the eigenvalue buckling system and system C the Six Sigma analysis.

Six Sigma analysis in ANSYS design explorer consists of three different analysis cells:

- Design of experiments
- Response surface
- Six Sigma analysis

The *design of experiments* uses a deterministic method which provides a matrix with large numbers of design points, with parameters as its fundamental components with a fixed mean and covariance (COV). In this thesis, the composite control design is used as the investigation type. This means that the parameters keep the same distance between each other. *Response surface* is built from the values of the design plots produced in the design of experiments cell. This tool uses the correlated parameters from the matrix generated in the *design of experiments* to produce a large size of measured values. The response surface type used in this study is generic aggregations, which gives a smooth connection between the infinite interpolated design point. *Six Sigma analysis* generates a fixed number of samples of uncertainty parameters in a

chosen statistical distribution function which describes the randomness. In this case, ten thousand samples are chosen, and normal distribution is used.

3.3 Geometry

In this study, a simple generic model was considered adequate. Figure 3.3 presents the geometry of a ring-stiffened cylindrical pressure hull, including its coordinate system.
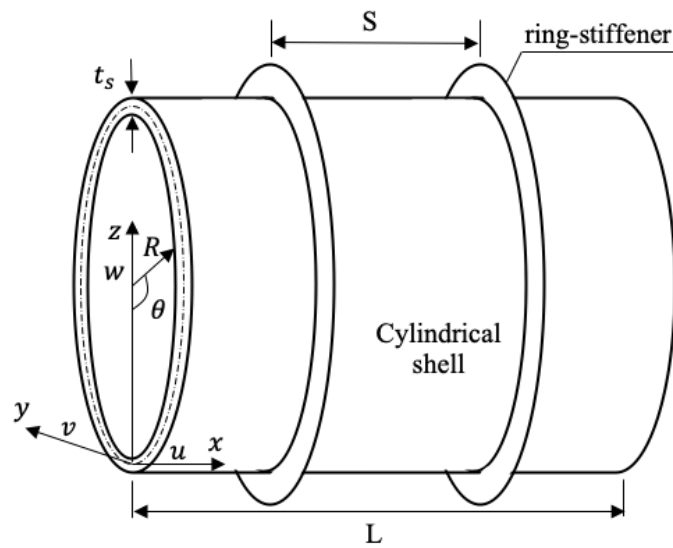

Figure 3.3: Geometry and coordinate system of a ring-stiffened cylindrical pressure hull analysis model.

Dimension L represents the length of the circular cylinder, S the unsupported spacing between the ring-stiffeners, t_s the shell thickness, and R_i the internal radius (Figure 3.3). The orthogonal coordinate system is represented by $u, v,$ and w.

The effective cross-section showed in Figure 3.4, represents the stiffness of the ring-stiffeners on the pressure hull. L_e is the effective length of the cylindrical shell found in ASME VIII div. 2 [52], h_r represents the height of the stiffener, and t_r the thickness.
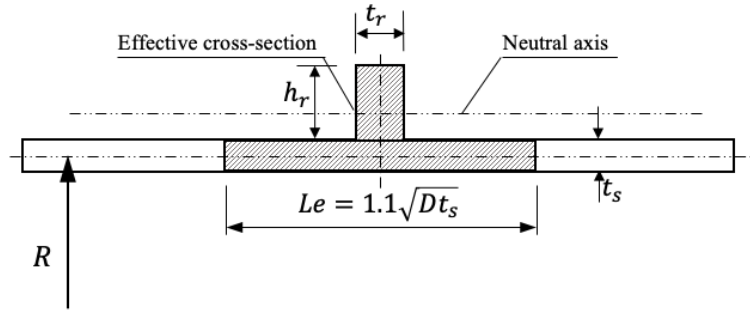
Figure 3.4: Effective cross-section of ring-stiffeners.

The cylindrical shell thickness, ring-stiffener thickness, and the unsupported spacing between the stiffeners and the stiffener height are selected as design variables for the steel cylindrical model in this study. The second moment of area varies as the stiffener height increases. Table 3.1 shows the variables parameters to study. The radii of the eigenvalue analysis are constant. To achieve symmetry of the spacing between the ring-stiffeners, two different length-diameter ratios are selected. The ANSYS model of the pressure hull is presented in Figure 3.5.

Table 3.1: Dimensions of the cylinder with ring-stiffener.

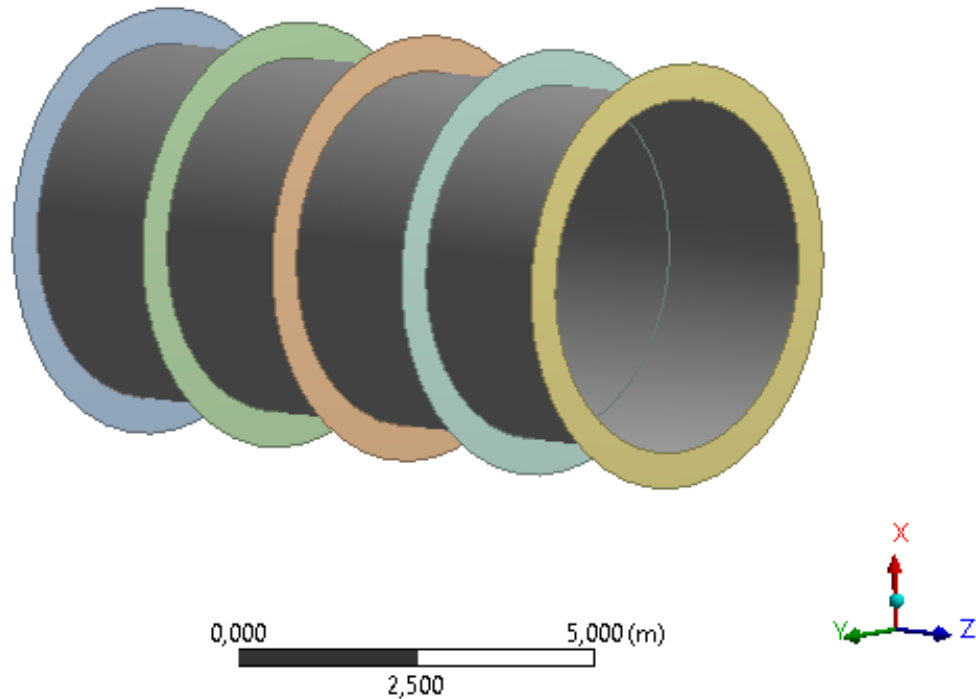| Ring-Stiffener thickness, t_r [mm]	Ratio of radius to shell thickness, R/t_s	Ratio of spacing and length, S/L	Second moment of area, I_r [cm⁴]
8	125	0.1	
10	156.25	0.17	
13	200	0.2	I_r
15	250	0.25	

Figure 3.5: Screenshot of the geometry of the pressure hull from ANSYS.

3.4   Material Properties

The material employed in the finite element analyses is linear-elastic steel for both the cylindrical shell and the ring-stiffeners. Table 3.2 hold the material properties.

Table 3.2: Material properties of the model.

Young's modulus, E [N/mm²]	Poisson's ratio, ν	Yield Strength σ_y [N/mm²]	Density ρ [kg/mm³]
2.0e +05	0.30	250	7.85e -06

3.5   Mesh Details

In finite element analysis, the mesh represents a system of algebraic equations that are used to solve the structural system numerically (Ref. Wang *et al.* [67]). As the cylindrical shell buckles both in the longitudinal and circumferential direction, and the deformation is no longer axisymmetric after buckling occurs, as mention in section 3.1, the mesh quality plays a significant role in the accuracy and stability of numerical computation (Ref. ANSYS [68]). For 2D plane problems, triangular and quadrilateral plane elements can be used because they represent both planar and axisymmetric solids, as shown in Figure 3.6 (Ref. ANSYS [69]).

a) 3 Node Triangle   b) 4 Node Triangle   c) 6 Node Triangle   d) 8 Node Triangle
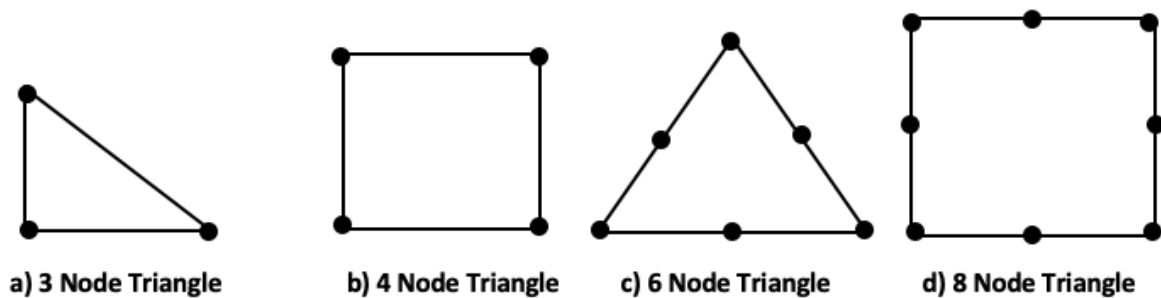
Figure 3.6: Mesh element types for 2D problems.

To be able to obtain an element size sufficient enough to produce converged results, a mesh refinement study is performed. Due to a significantly longer run time with finer element size, the ultimate element size is the one with the largest mesh size that gives an accurate description and a reasonable buckling load of associated buckling mode. The results of the mesh refinement study for a 5000 mm diameter ring-stiffened cylindrical shell is found in Table 3.3 and Figure 3.7. Additionally, Figure 3.8 shows the percentage error of the mesh refinement.

Table 3.3: Results from mesh refinement study, 5000 mm diameter ring-stiffened cylindrical shell.

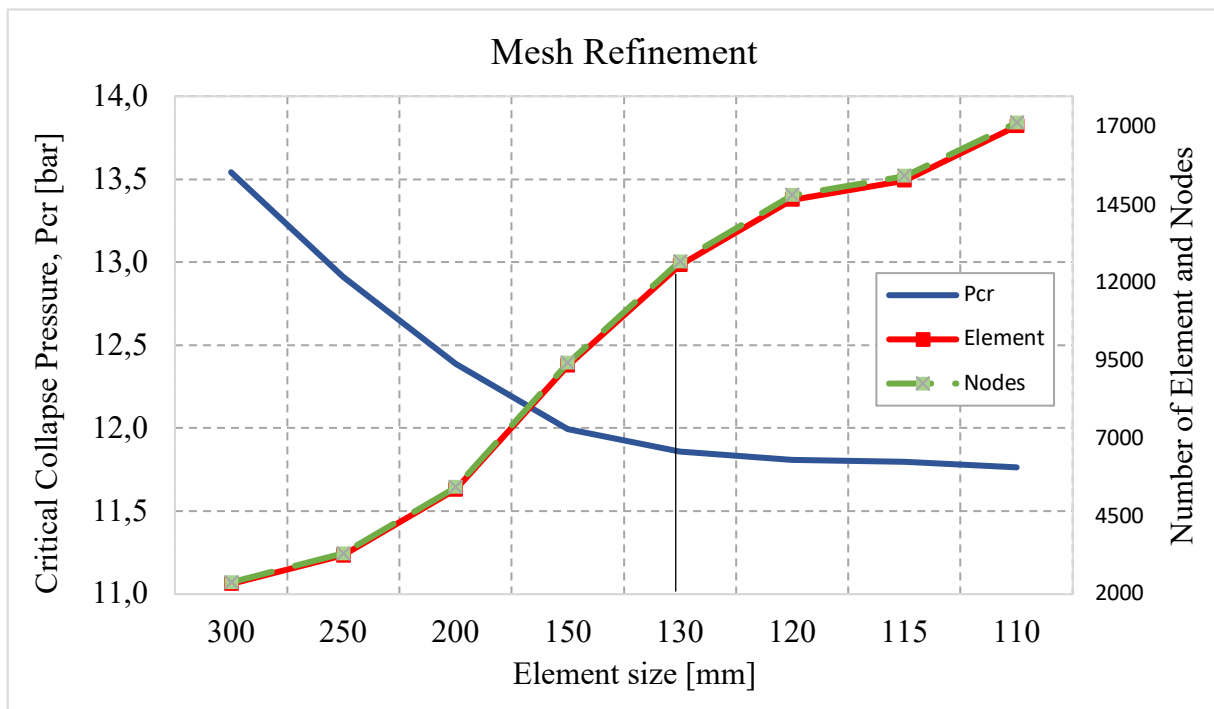| Element size [mm]	Number of elements	Number of nodes	Elastic collapse pressure [bar]
300	2329	2380	13.54
250	3246	3303	12.91
200	5367	5437	12.39
150	9342	9424	11.95
130	12,574	12,689	11.86
120	14,677	14,814	11.81
115	15,293	15,432	11.80
110	17,039	17,149	11.76

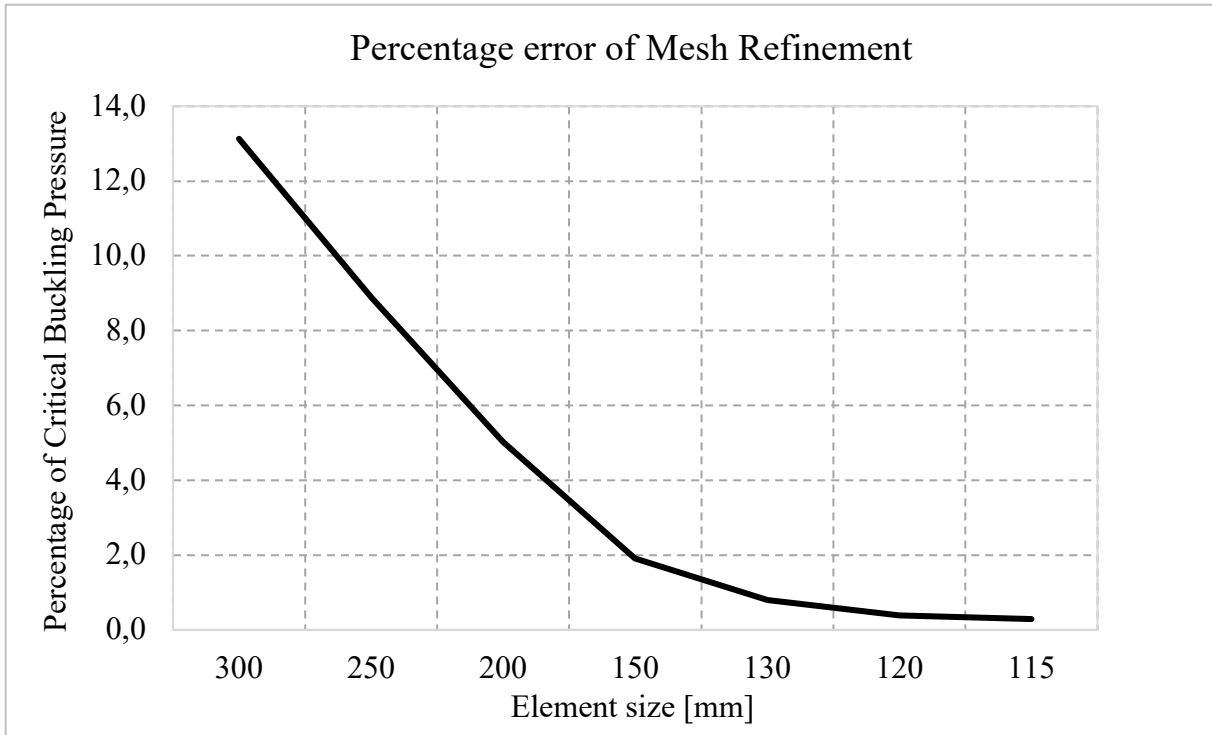Figure 3.7: Result of mesh refinement study.

Figure 3.8: Percentage error of the mesh refinement study result.

For the mesh refinement, the critical buckling pressure seemed to stabilise at an element size of 130 mm. An element size of 130 mm is sufficiently small to produce a converged solution for the elastic collapse pressure and was chosen for the analysis. This corresponded to a total count of 12,574 elements and 12,689 nodes of the cylindrical shell model with five stiffeners. Figure 3.9 shows the visualized mesh details of the pressure hull model.
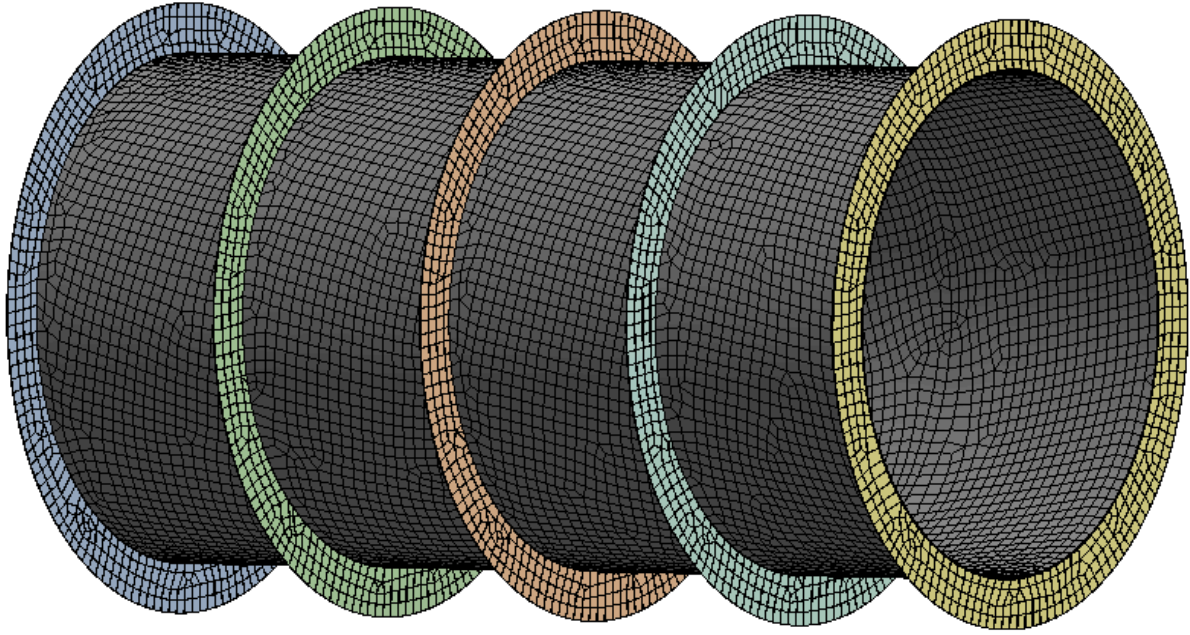
Figure 3.9: ANSYS model showing the visualised mesh details of 130mm element size.

3.6   Load and Boundary Conditions

The load and boundary condition for the ANSYS model is presented in Table 3.4. Furthermore, the boundary conditions and design values with its designated direction for the imposed action are presented in Figure 3.10. The face boundary conditions considered in this case study are two loads: a compressive load and axial force. The uniform external hydrostatic pressure (B) is applied on the outer surface of the cylindrical shell, and the axial force (A) is applied on the free end. The force acting on the opposite side of the fixed point is to prevent the cylindrical shell from displacing in any other direction than the longitudinal direction. The fixed point (D) at $z = 0$ implies that this region is restrained against translation in all three orthogonal directions. Furthermore, the displacement boundary condition (C) restrains the model against translation in two orthogonal directions, x-axis and y-axis for the free end. Hence, the cylindrical shell can only move in the longitudinal z-direction.

Table 3.4: Load and boundary conditions for the ANSYS model.

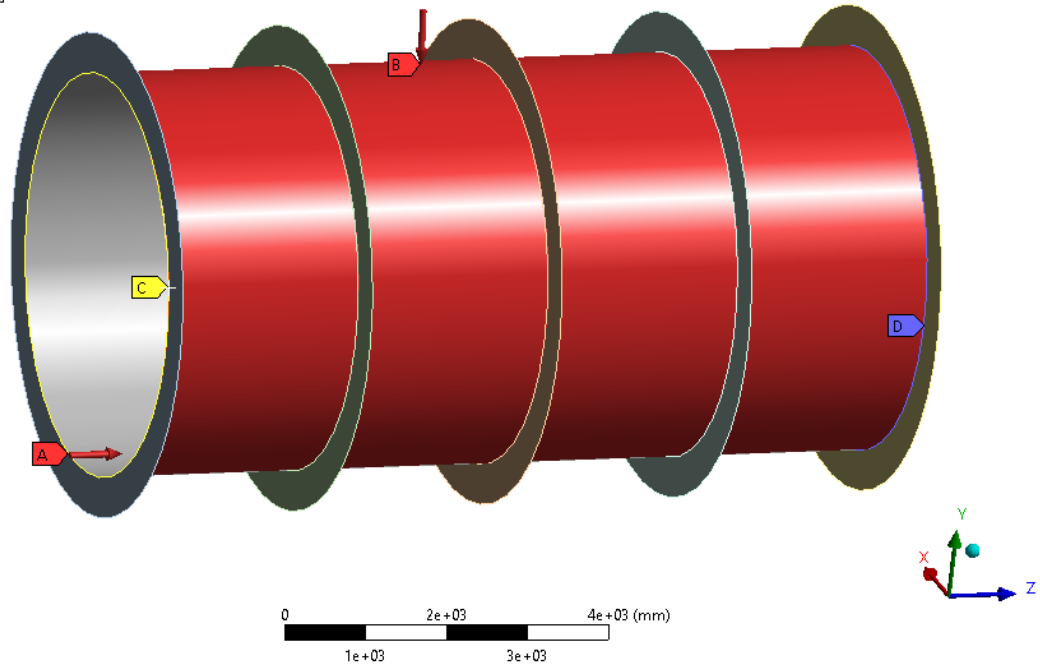| External pressure [bar]	Force [N]	Fixed support	Displacement restriction
1	2.0e+06	$z = 0$	x-0, y-0, z-Free

Figure 3.10: Screenshot of loads and boundary condition on the ring-stiffened cylindrical shell from ANSYS.

CHAPTER 4   PRELIMINARY STUDY

This chapter contains a parameter correlation study to determine which design variables are co-related to each other or the performance output of critical buckling pressure or the weight of the pressure hull.

4.1   Parameter Correlation

The scientific progress of correlation is to determine which variables are co-related and which are independent. This study is valuable for engineering parameters, as it reveals the relationship between design parameters. A coefficient of correlation gives the level of relationship between the variables. This coefficient is a single number that represents to what extent variation in one parameter (P1) goes with a variety of another (P2). A correlative factor is a number between -1 and +1. A positive value indicates that P2 increases with P1, while a negative value indicates that P2 decreases with P1 (Ref. Meissner [70]). The closer the value of correlation is to -1 or +1, the stronger is the correlation between input and output variables. Guilford [71], has provided a classification of the coefficient of correlation quantity, to describe how defined the strength is between the parameters and is presented in Table 4.1.

Table 4.1: Description of the coefficient of correlation strength.

Magnitude of ρ	Degree of relationship
< 0.2	Slight correlation, and almost negligible
0.2 – 0.4	Low correlation, definite but small relationship
0.4 – 0.7	Moderate correlation, substantial relationship
0.70 – 0.90	High correlation, marked relationship
0.90 <	Very high correlation, dependable relationship

The correlation coefficient can be computed by different correlation methods like Pearson correlation and spearman correlation. In this study, the Pearson correlation method is adapted. The linear coefficient of correlation $\rho_{P_1 P_2}$, between the two variable P_1 and P_2 are defined as:

$$\rho_{P_1 P_2} = \frac{\text{cov}(P_1, P_2)}{\sigma_{P_1} \sigma_{P_2}} \tag{4.1}$$

where $cov(P_1, P_2)$ is the covariance, and σ_{P1} and σ_{P2} are the standard deviations (Ref. Pearson [72][73]). The results are given in an $n \times n$ correlation matrix, and correlation scatters where the coefficient factors are collected between n design parameters and given as an overview of the design parameter. This can identify the significant parameters that will critically influence the design.

4.2   Correlation Study of Parameters

Pearson correlation matrix presented in Figure 4.1 shows the correlation of geometrical configuration variables of cylindrical shell thickness (t_s), stiffener spacing (S), stiffener thickness (t_r), and stiffener height (h_r), and the output parameters of the performance considering the weight and critical buckling pressure of the pressure hull, respectively. The correlation matrix is a sample size of 100, and due to $cov(P_1, P_2) = cov(P_2, P_1)$, the correlation matrix is symmetrical.
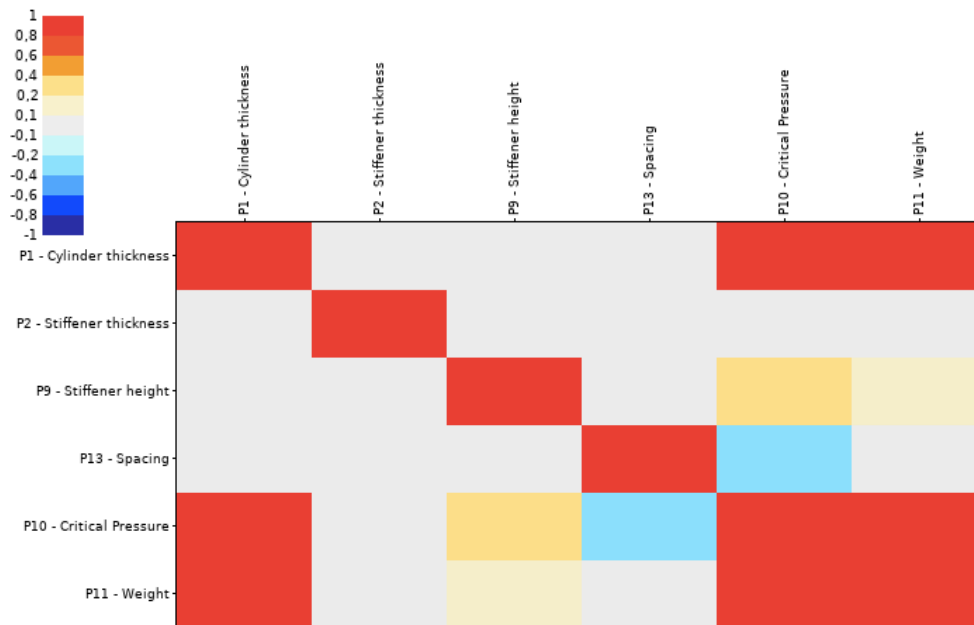

Figure 4.1: Pearson correlation matrix of the design input parameters and output variables of critical buckling pressure and weight of the pressure hull.

The correlation matrix in Figure 4.1 influence some meaningful information about the correlation by a colour-bar and shows some variables which are co-related. Table 4.2 presents the coefficient of correlation of the linear relationship between the parameters.

Table 4.2: Coefficient of correlation from the parameter correlation study.

	t_s	t_r	h_r	S	P_{cr}	W
t_s	1	0.00081	0.02510	-0.00509	0.88144	0.99299
t_r		1	-0.00036	-0.05418	0.01687	0.00622
h_r			1	-0.00068	0.30061	0.14274
S				1	-0.21995	-0.00581
P_{cr}					1	0.90795
W						1

In Table 4.2, the cylindrical shell thickness shows a strong coefficient of correlation with the critical buckling pressure. Whereas the critical buckling pressure of the pressure hull will increase as the thickness of the cylindrical shell increases. Additionally, the thickness of the cylinder has an additional very strong correlation with the weight of the pressure hull. The geometrical variables show a slight and almost negligible correlation with each other. Moreover, all parameters, except cylinder thickness, has an almost negligible correlation to weight. Unsupported spacing and height of ring-stiffeners have defined, but a small coefficient of correlation with the two considered performance variables, weight and critical buckling pressure, which might make a design impact on the pressure hulls performance. However, the correlation with the pressure hulls critical buckling pressure is still low.

A close-up of the coefficient of correlation for cylinder thickness and spacing to the performance variable critical buckling pressure is presented in a scatter diagram as illustrated in Figure 4.2 and Figure 4.3.
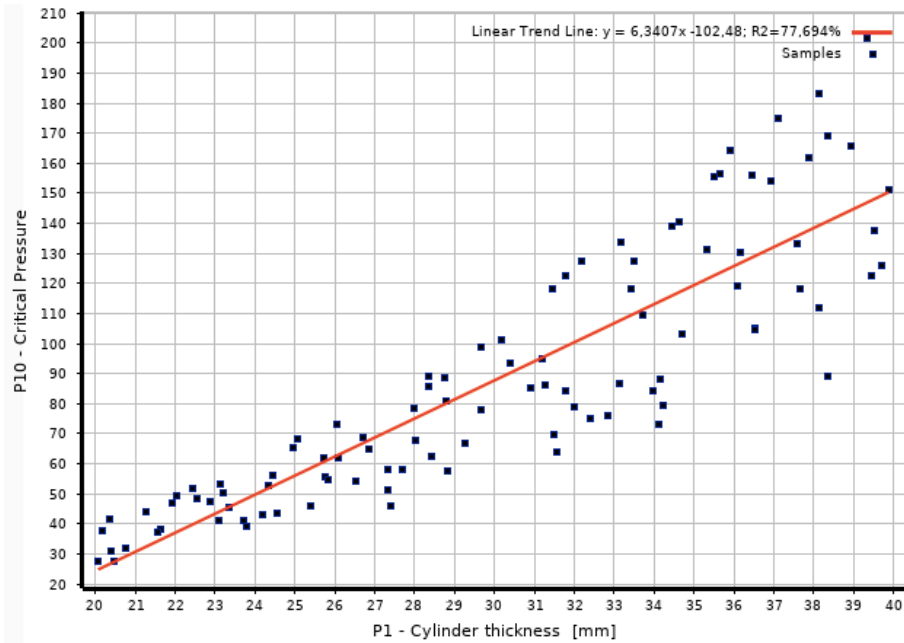
Figure 4.2: Correlation scatter diagram, critical buckling pressure vs cylinder thickness.
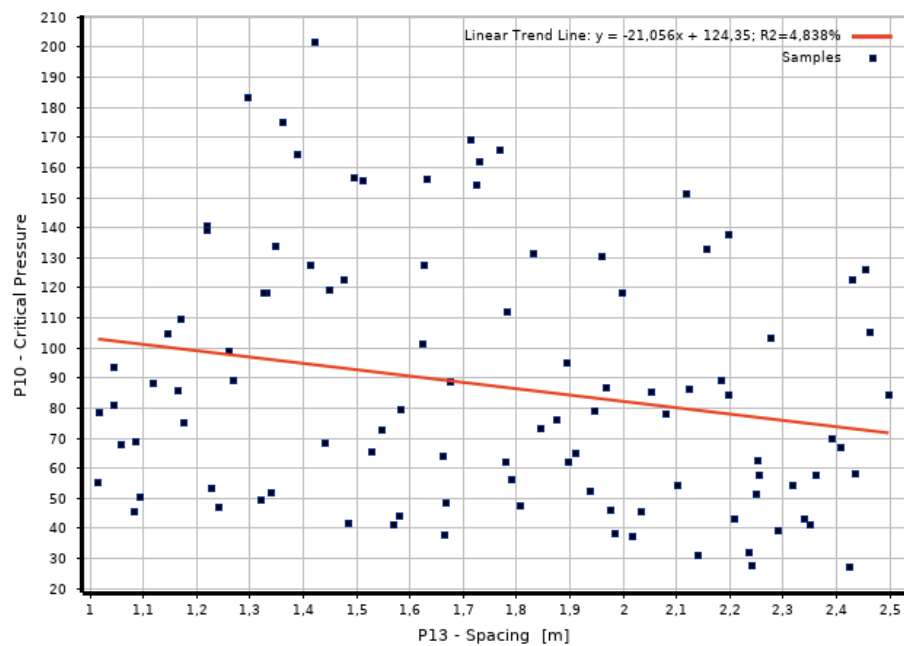

Figure 4.3: Correlation scatter diagram, critical buckling pressure vs spacing.

The scatter diagram between critical buckling pressure and cylinder thickness presented in Figure 4.2, is small, which relates to the strong correlation. Hence, the design parameter might have a larger influence on the design pressure of the pressure hull. Figure 4.3 shows a large scatter diagram between critical buckling pressure and unsupported spacing between the stiffeners and define a low correlation.

In Figure 4.4, the scatter diagram between the two output results, the collapse capacity and the weight of the pressure hull are presented. The scatter diagram is small scattered, which corresponds to a very strong coefficient of correlation between them. Hence, as the weight of the pressure hull increases, the collapse capacity will also increase almost linear to the weight.
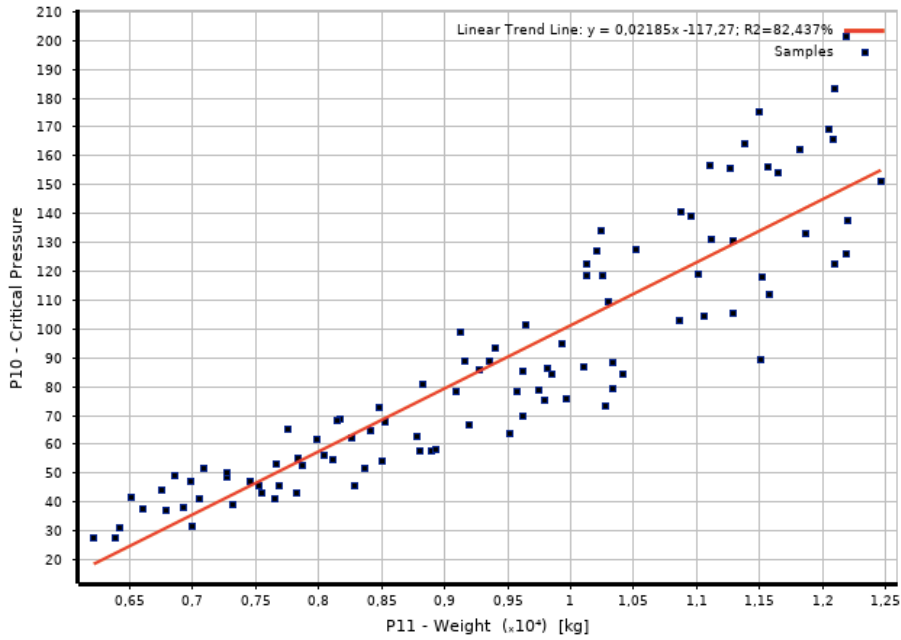

Figure 4.4: Correlation scatter diagram, critical buckling pressure vs the pressure hull weight.

CHAPTER 5   INFLUENCE OF DESIGN

To look at how the design influence the collapse capacity of the pressure hull, linear buckling analysis is conducted by using eigenvalue buckling in ANSYS. This involves finding the theoretical bifurcation buckling load of the giving model with various geometrical configurations. This analysis used the pre-stress analysis solution and carried out the load multiplier of the pressure hull model from the various inputs parameters and recognised the resulting buckling mode shape, which primarily consists of eigenvectors. The resulting critical buckling pressure of the model is found by multiplying the load multiplier with the input pressure. This study uses an input pressure of 1 bar, which means that the load multiplier equals the critical buckling pressure. Common for all the analyses is the boundary condition and loading. When analysing a structural engineering problem concerning failure, the lowest eigenvalue mode should be assumed as a solution to a most conservative design, as it resembles to be the first value to be reached when applying external pressure to a structure.

5.1   Distance Between Stiffener

This analysis looks at the different spacing between stiffeners and its effect on the collapse capacity and the corresponding weight of the pressure hull. The analysis model is done with constant cylinder thickness and ring-stiffener thickness. Figure 5.1 presents the variation of critical buckling pressure, including the buckling mode, as well as the applied design factor of 2.5 for the ratio of spacing and pressure hull length of 0.1.
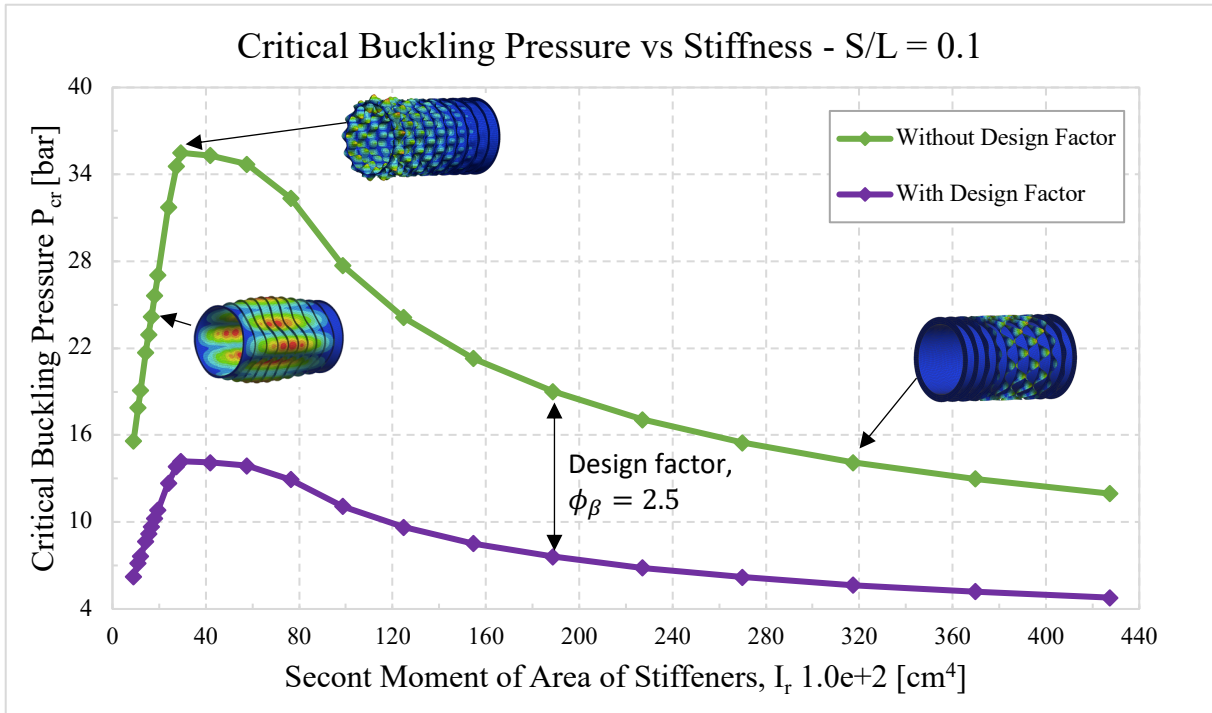
Figure 5.1: Critical buckling pressure vs stiffness including buckling modes and AMSE VIII div.2 design factor of 2.5, for S/L = 0.1.

The close-up view of the spacing and length ratio of 0.1 presented in Figure 5.1, shows that the critical buckling pressure increases linearly to the stiffness of the ring-stiffeners with a corresponding global buckling mode. Furthermore, critical buckling pressure reaches its maximum with a corresponding local buckling mode and following a decline with a buckling mode of stiffener tripping. For all the analysis of the chosen spacing to length ratio, shows the same buckling mode response. Tripping of stiffeners is eliminated in the following results, as this happens when the geometrical dimension is not strong enough to support the shell cylinder. The design factor for protection against collapse from buckling of the pressure hull, given by ASME VIII div. 2 code presented in section 2.8.2 is added to the eigenvalue buckling results. As can be seen in Figure 5.1, the collapse capacity decreases significantly when the design factor of 2.5 is applied. The design factor is applied to all the following results. The buckling modes responds the same for

Figure 5.2 and Figure 5.3 presents the result of the critical buckling pressure with all the chosen design variation of spacing and length ratio, and its corresponding stiffness of ring-stiffeners and pressure hull weight. The second moment of area of the ring-stiffeners increases as the ring-stiffener height increases.
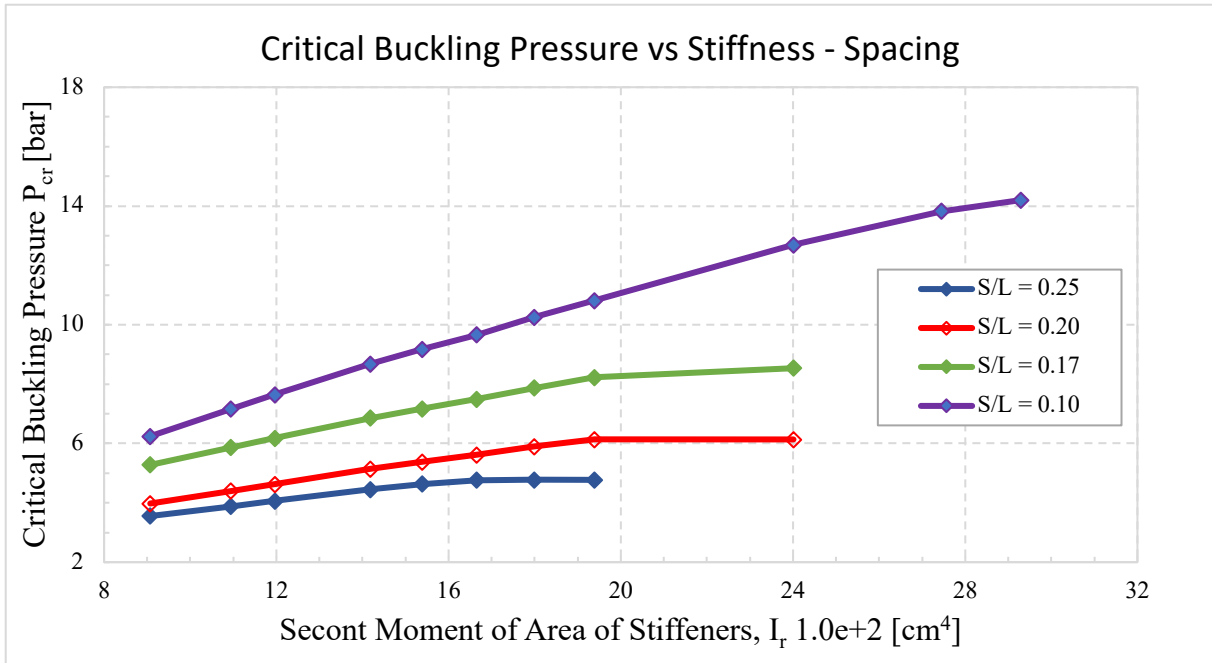
Figure 5.2: Critical buckling pressure vs stiffness for all spacing variations.
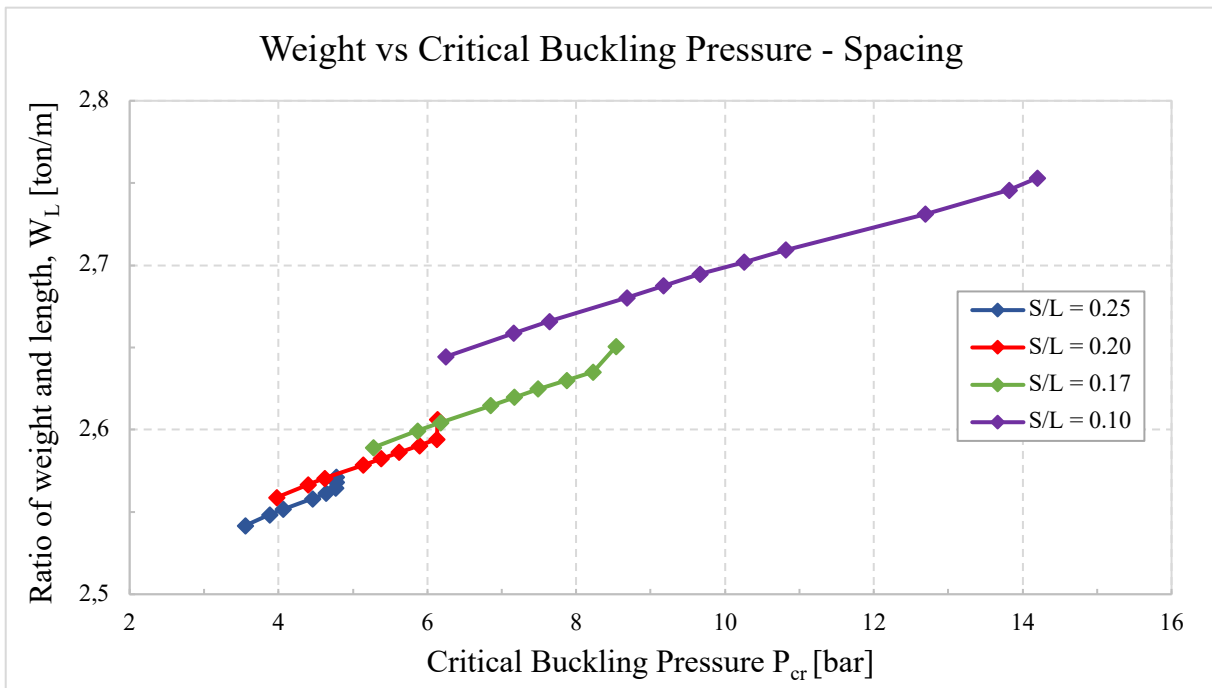

Figure 5.3: Weight of pressure hull vs critical buckling pressure for all spacing variations.

Since the cylinder thickness and the ring-stiffener width is held constant in this analysis, the stiffness is the same for the various spacing choices. The change in critical pressure is all due to the different spacing. Moreover, as seen in Figure 5.2, the critical buckling pressure increases as the distance between the stiffeners are reduced. By comparing the critical buckling pressure

with the weight of the pressure hull in Figure 5.3, there is an increase with a smaller length between the stiffeners, especially from spacing to length ratio between 0.17 and 0.1.

5.2   Thickness of Ring-Stiffener

The following analysis focuses on how the design of ring-stiffener thickness influences the collapse capacity and the corresponding weight of the pressure hull.

Pressure hull dimensions of the analysis model are presented in Table 5.1. Four models are selected with the variation of stiffener thickness, with a combination of various spacing. The results are presented in Figure 5.4 and Figure 5.5, respectively.

Table 5.1: Geometry of the analysis models for design influence of ring-stiffener thickness.

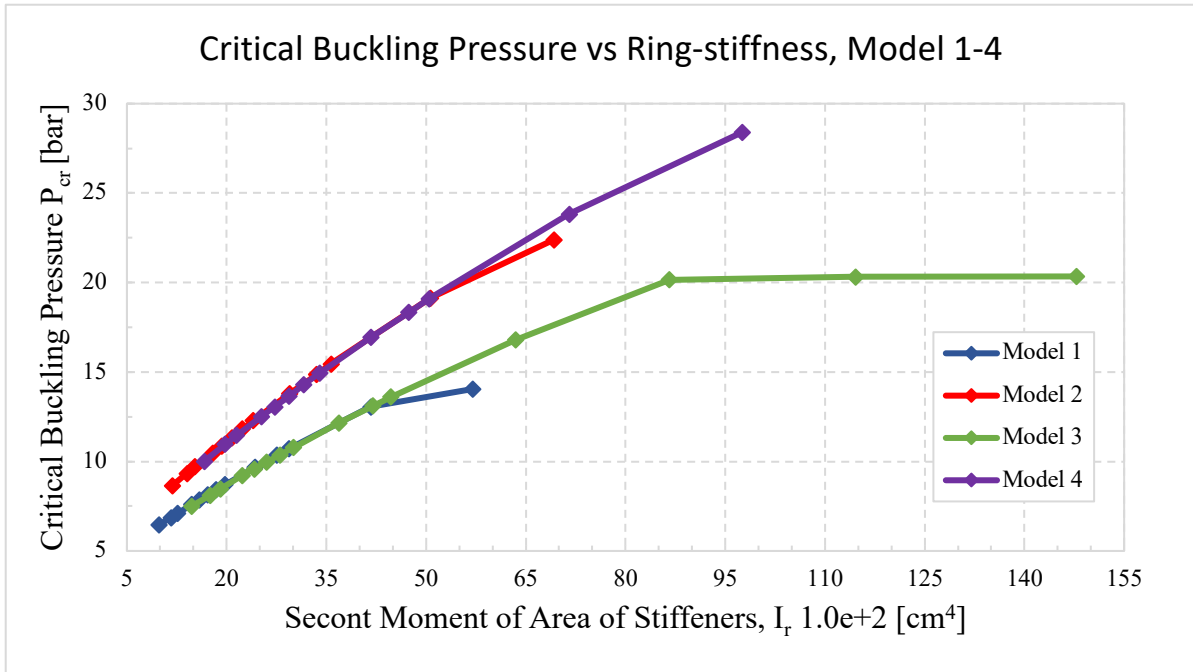| Model	Stiffener thickness, t_r [mm]	Ratio of spacing and length, S/L	Ratio of radius to shell thickness, R/t_s
1	8	0.20	156.25
2	10	0.17	156.25
3	13	0.20	156.25
4	15	0.17	156.25

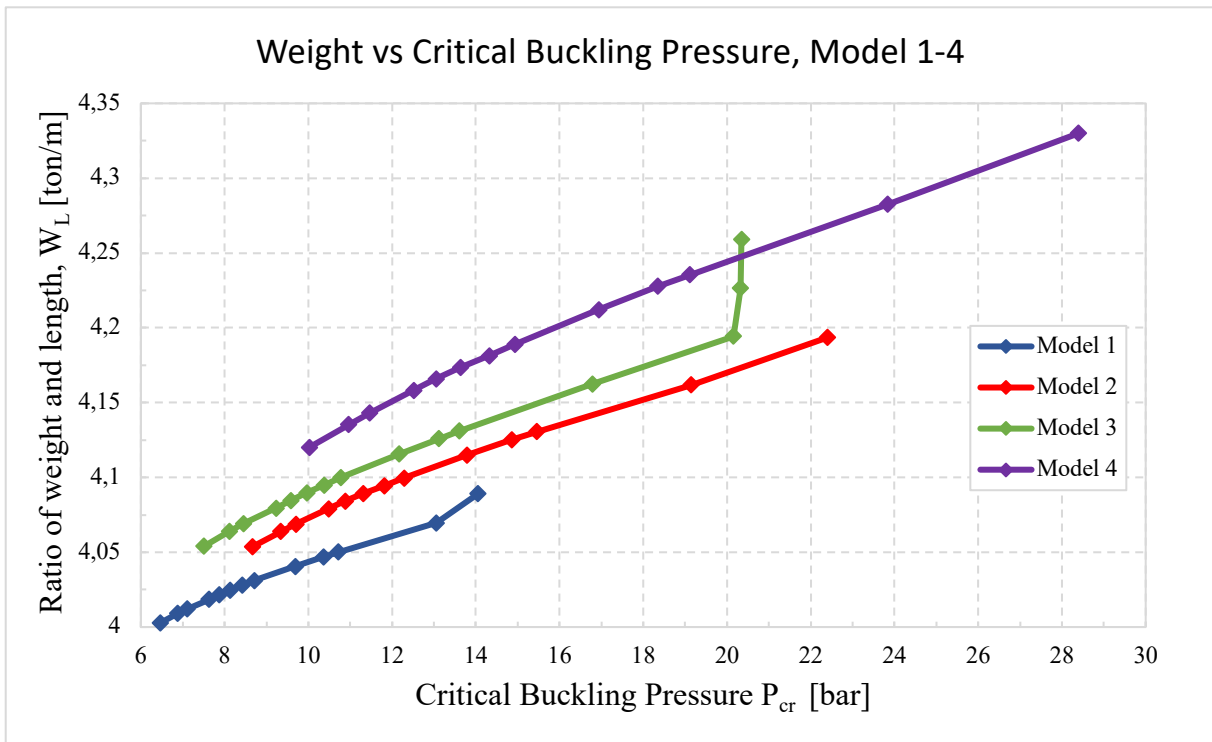Figure 5.4: Critical buckling pressure vs stiffness for Model 1-4.

Figure 5.5: Weight of the pressure hull vs critical buckling pressure for Model 1-4.

Figure 5.4 shows that the models with equal geometrical dimension except for ring-stiffener thickness increase equal to each other. When looking at Model 1 and 3, the only difference is the ring-stiffeners thickness, and this equals for model 2 and 4. As mention, the height of the

stiffeners increases as the second moment of inertia increases. Model 3 can reach a stiffness before stiffener tripping. Hence a higher critical buckling pressure. However, for a long-range of cross-section stiffness, a thicker dimension does not increase the critical buckling pressure. The weight of the different dimensions in Figure 5.5 shows a slight increase with increased thickness. Notice that Model 2 and 3 give the same pressure hull weight but different critical buckling pressure. A close-up view of the two models will be introduced in section 5.4.1.

5.3   Thickness of Cylinder

The following analysis focuses on how the design of cylinder thickness influences the collapse capacity and the corresponding weight of the pressure hull.

Pressure hull dimensions of the analysis model are presented in Table 5.2. Four models are selected with the variation of cylinder thickness, moreover a constant ring-stiffener thickness and spacing. The result of this analysis is shown in Figure 5.6 and Figure 5.7.

Table 5.2: Geometry of analysis models for design influence of cylinder thickness.

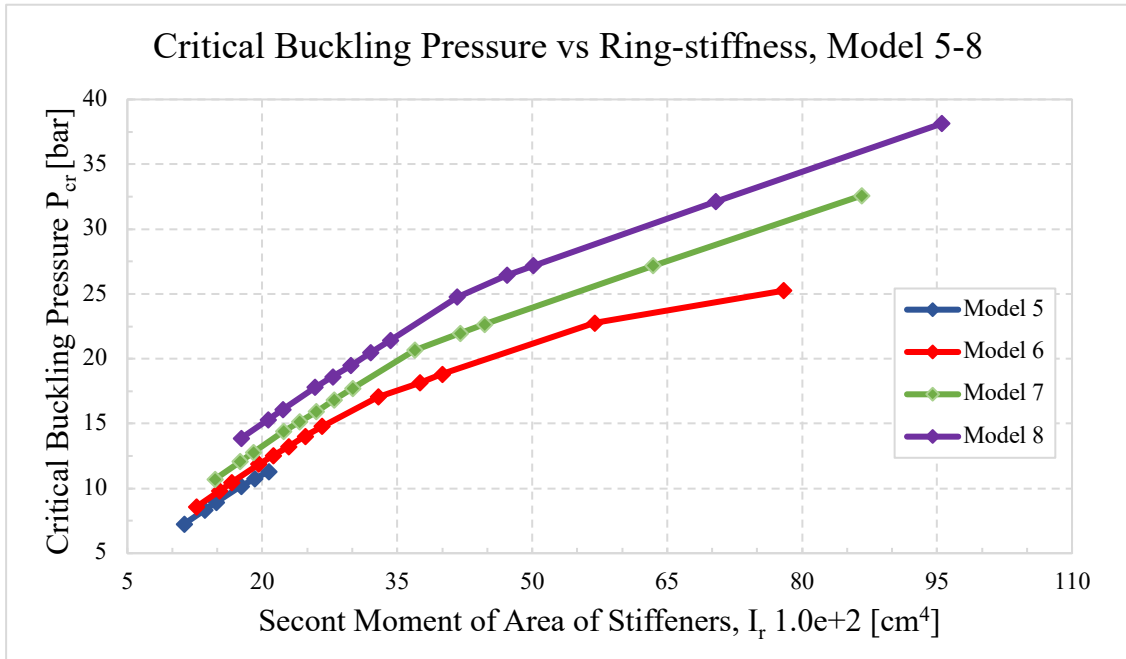| Model	Stiffener thickness, t_r [mm]	Ratio of spacing and length, S/L	Ratio of radius to shell thickness, R/t_s
5	13	0.1	250
6	13	0.1	200
7	13	0.1	156.25
8	13	0.1	125

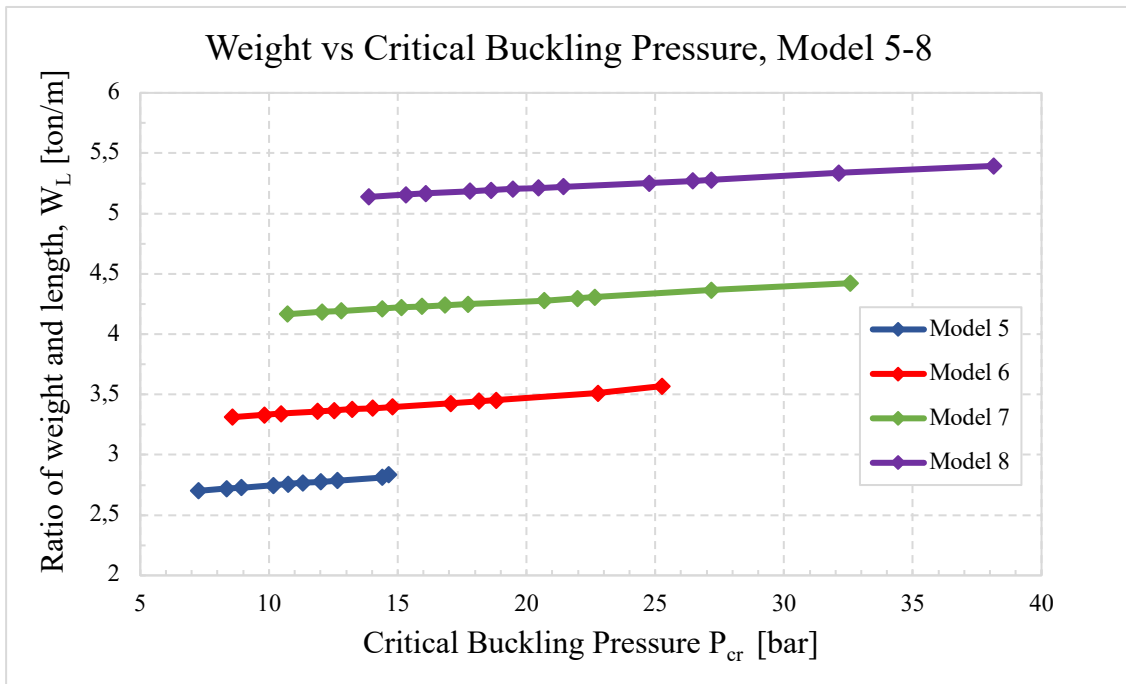Figure 5.6: Critical buckling pressure vs stiffness for model 5-8.

Figure 5.7: Weight of the pressure hull vs critical buckling pressure for model 5-8.

It clearly states in Figure 5.6 that the cylinder thickness of the pressure hull strongly correlates with the reachable collapse capacity. The pressure hull weight presented in Figure 5.7 also indicates a significant increase when the thickness increases. Furthermore, the difference in the rise in the critical buckling pressure from model 5 to model 6 compared to the rest of the models

is notable. As the ratio between radii and cylinder thickness decreases, the responding reached critical buckling pressure gives a moderate rise.

5.4   Design Combinations

The following analysis compares different design dimensions and how the parameters influence the collapse capacity versus the weight. Pressure hull dimensions of the different analysis model are presented in Table 5.3.

Table 5.3: Geometry of analysis models for design influence of different design combinations.

Model	Stiffener thickness, t_r [mm]	Ratio of spacing and length, S/L	Ratio of radius to shell thickness, R/t_s
2	10	0.17	156.25
3	13	0.20	156.25
6	13	0.1	200
7	13	0.1	156.25
9	13	0.2	125
10	10	0.17	125

5.4.1   Combination of Different Stiffener Thickness and Spacing

A close-up view of models 2 and 3 presented in section 5.2, is shown in Figure 5.8 and Figure 5.9. The models approach a slight difference in critical buckling pressure. However, the two models reach the same weight of pressure hull (Figure 5.9). The dimensions of the two different models show that model 2 has a thinner stiffener thickness and a smaller unsupported spacing and model 3 has a thicker stiffener, and a longer unsupported spacing, with equal cylinder thickness for both models (Table 5.3). The comparison of the different dimensions indicates that a shorter unsupported spacing between ring-stiffeners has a more substantial impact on the critical buckling pressure than the thickness of the stiffeners.
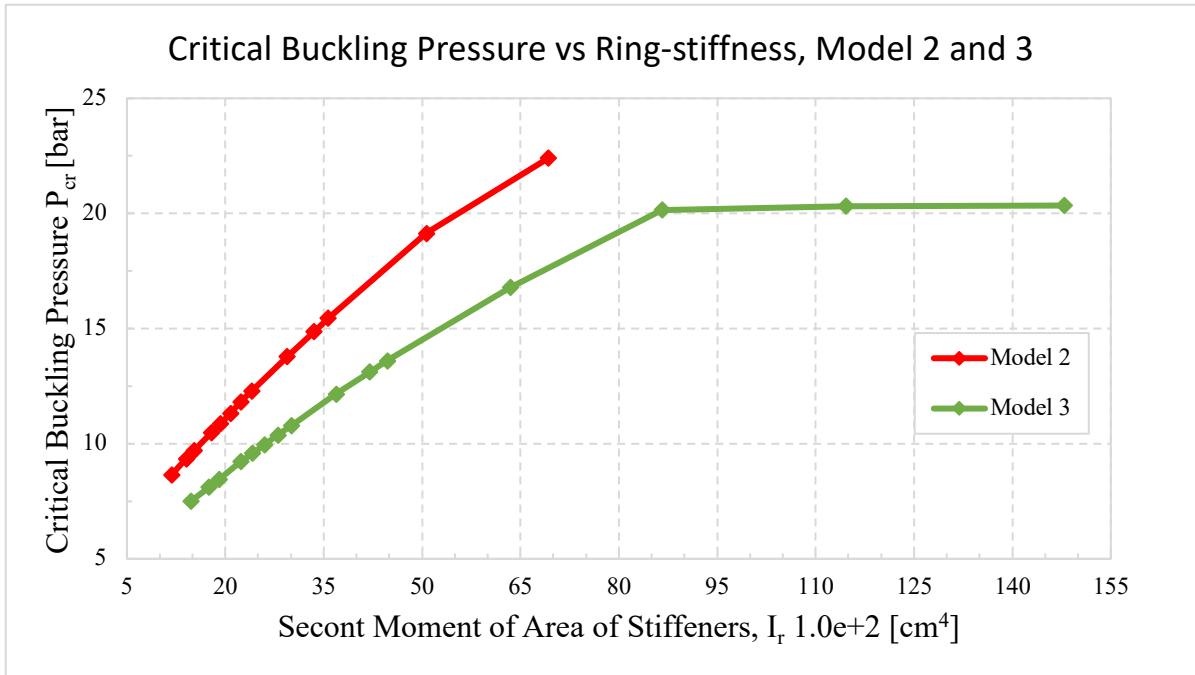
Figure 5.8: Critical buckling pressure vs stiffness of design combination between model 2 and model 3.
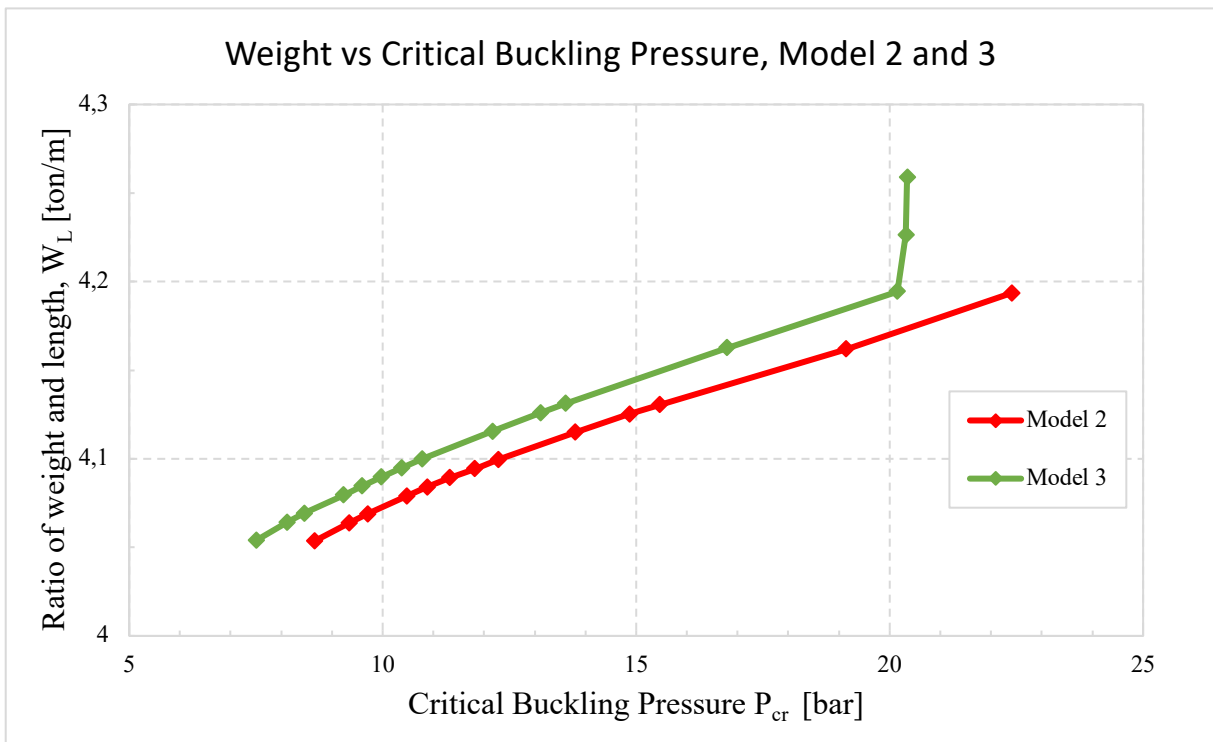

Figure 5.9: Weight of pressure hull vs critical buckling pressure of design combination between model 2 and model 3.

5.4.2 Combination of All Different Input Parameters

The pressure hull dimension for model 6 and 10 are all different (Table 5.3). This analysis of critical pressure and stiffness of the various design dimensions is presented in Figure 5.10. Model 6 offers a higher collapse capacity than model 10 while having a smaller spacing, thicker stiffener, and thinner cylinder thickness, which gives a lighter weight, as shown in Figure 5.11. Whereas, a smaller unsupported length between stiffeners and thicker ring-stiffener increases the weight of the pressure hull. However, in this case, model 6 provides a more considerable critical buckling pressure and a significantly lighter weight of the pressure hull than model 10. Hence, this shows that an increase in cylinder thickness has a larger impact on the weight than both an increase in spacing and ring-stiffener thickness.
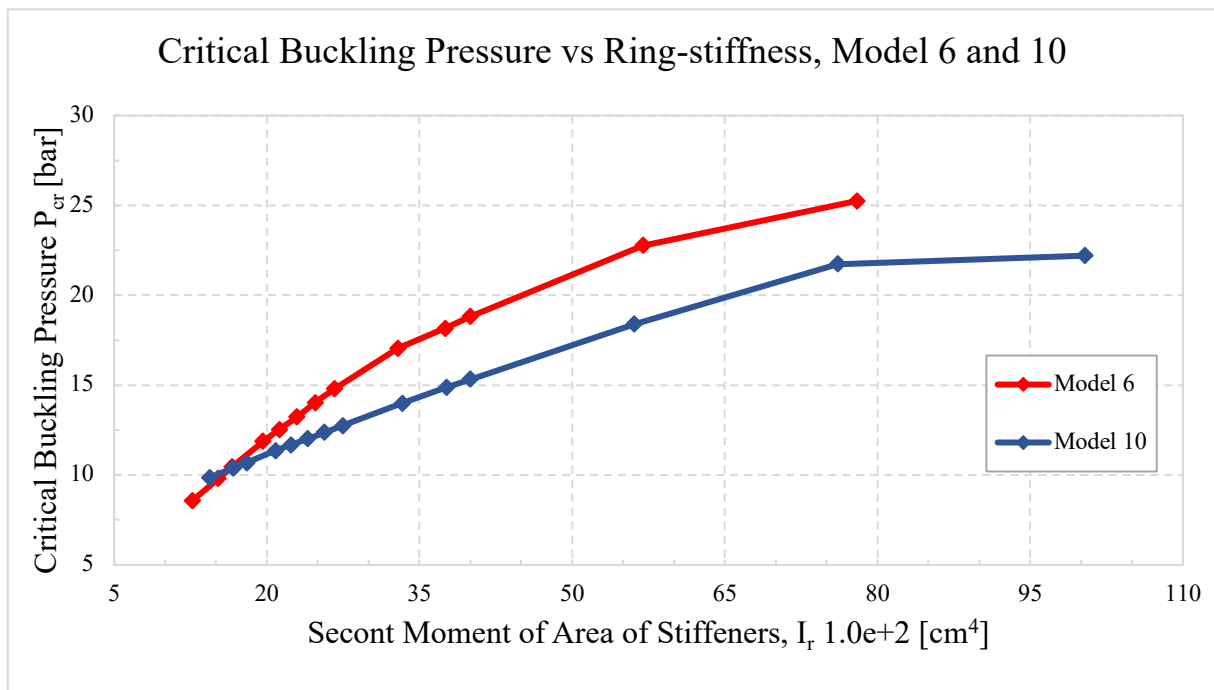

Figure 5.10: Critical buckling pressure vs stiffness of design combination between model 6 and model 10.
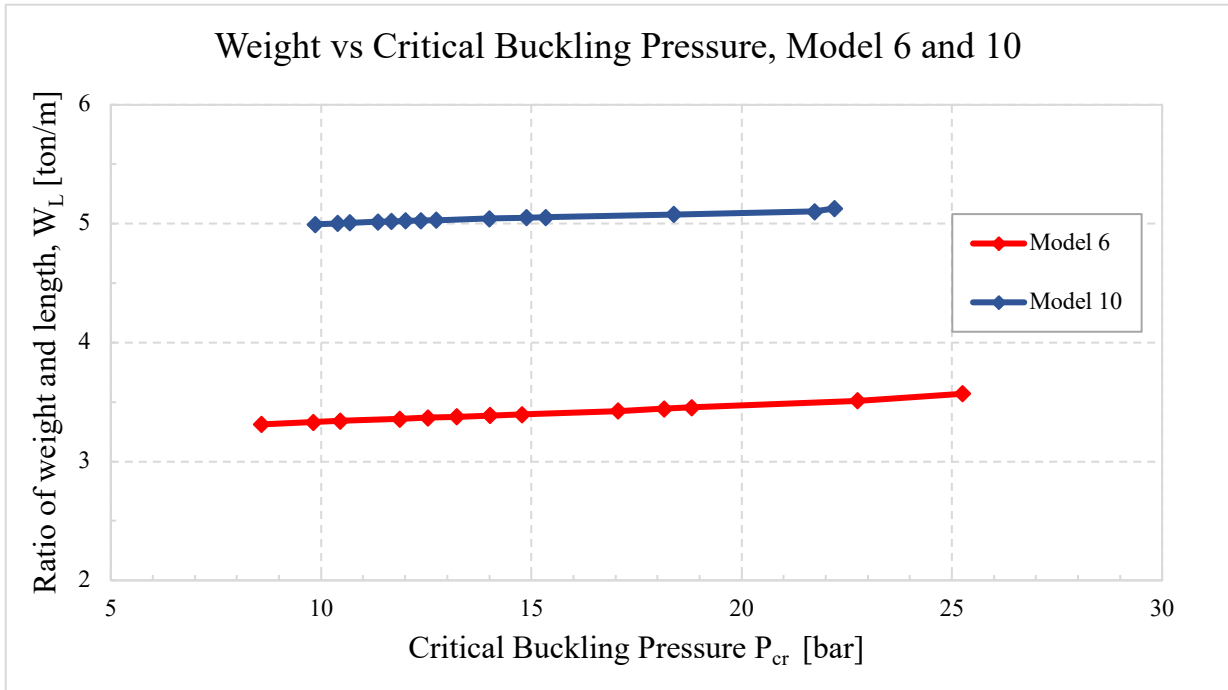
Figure 5.11: Weight of pressure hull vs critical buckling pressure of design combination between model 6 and model 10.

5.4.3 Combination of Different Spacing and Cylinder Thickness

Figure 5.12 presents the critical buckling pressure to the stiffness of the different design combination in model 7 and model 9 with different spacing and cylinder thickness and with the same ring-stiffener thickness (Table 5.3). The two models reach the same critical buckling pressure. However, model 9 has a significantly higher weight of the pressure hull than model 7, which is presented in Figure 5.13. This indicates a stronger correlation between the weight and cylinder thickness than the spacing between the stiffeners. And a considerable equal relationship between the critical buckling pressure and both spacing and cylinder thickness.
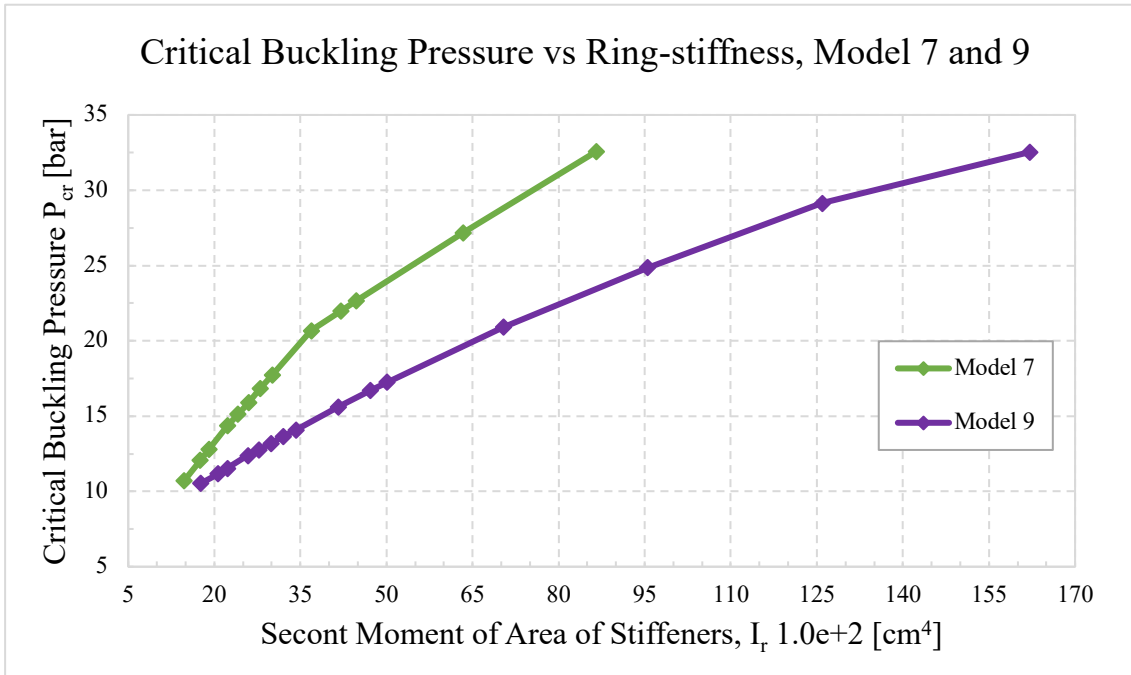
Figure 5.12: Critical buckling pressure vs stiffness of design combination between model 7 and model 9.
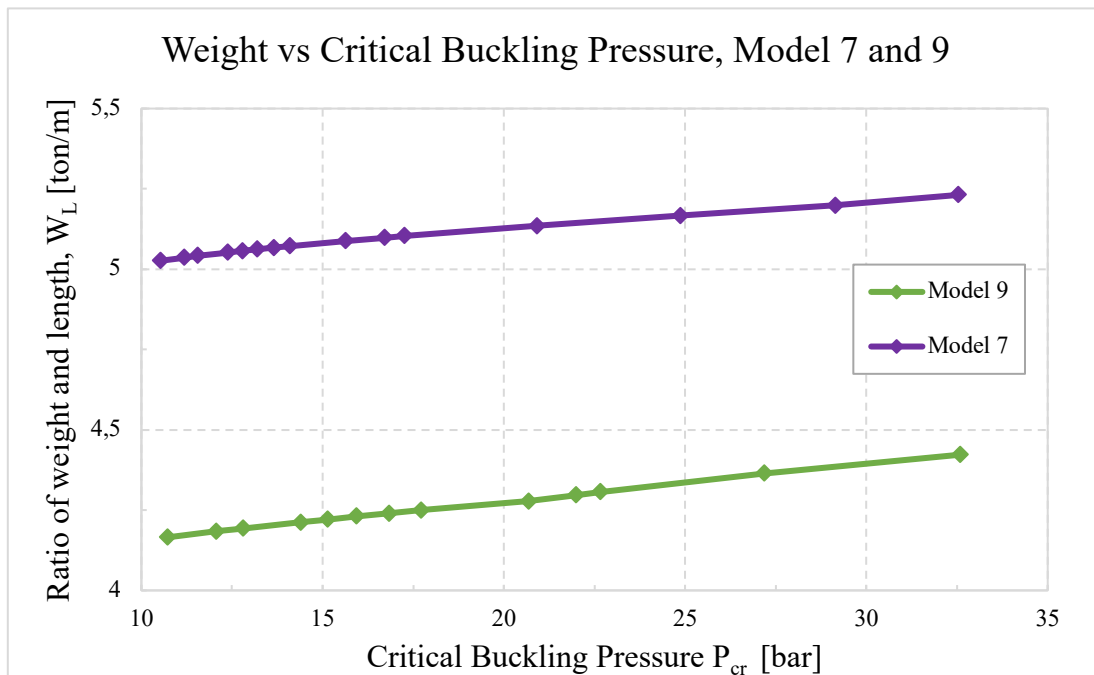

Figure 5.13: Weight of the pressure hull vs critical buckling pressure of design combination between model 7 and model 9.

CHAPTER 6   PROBABILISTIC DESIGN

The probabilistic design approach of Six Sigma analysis was performed in ANSYS design explorer to investigate the uncertainty in the critical buckling pressure of the pressure hull model. This approach involves finding the probability of failure, the mean and the standard deviation of the critical buckling pressure. The spacing, cylinder thickness, diameter, stiffener height and thickness are set as uncertain parameters in the pressure hull model, and the critical buckling pressure is taken as an uncertainty output. Load multiplier is fist found and multiplied with the input pressure of 1 bar. Hence, the load multiplier corresponds to the critical buckling pressure. The Six Sigma analysis of ten thousand samples was performed on the model presented in Figure 5.1 in section 5.1. The maximum critical buckling pressure for this model is 35.50 bar without design factor, hence the nominal critical buckling pressure for the Six Sigma analysis is $P_{cr\_nom} = 35.50$ bar.

6.1   5% COV for All Design Variables

This Six Sigma analysis chose a predicted relative error of 5% for all design variables. The statistical characteristics of pressure hull dimensions are presented in Table 6.1, and the result of the Six Sigma analysis is presented as a distribution function of the critical buckling pressure and shown in Figure 6.1.

Table 6.1: Statistical characteristics dimension for pressure hull with 5% COV.

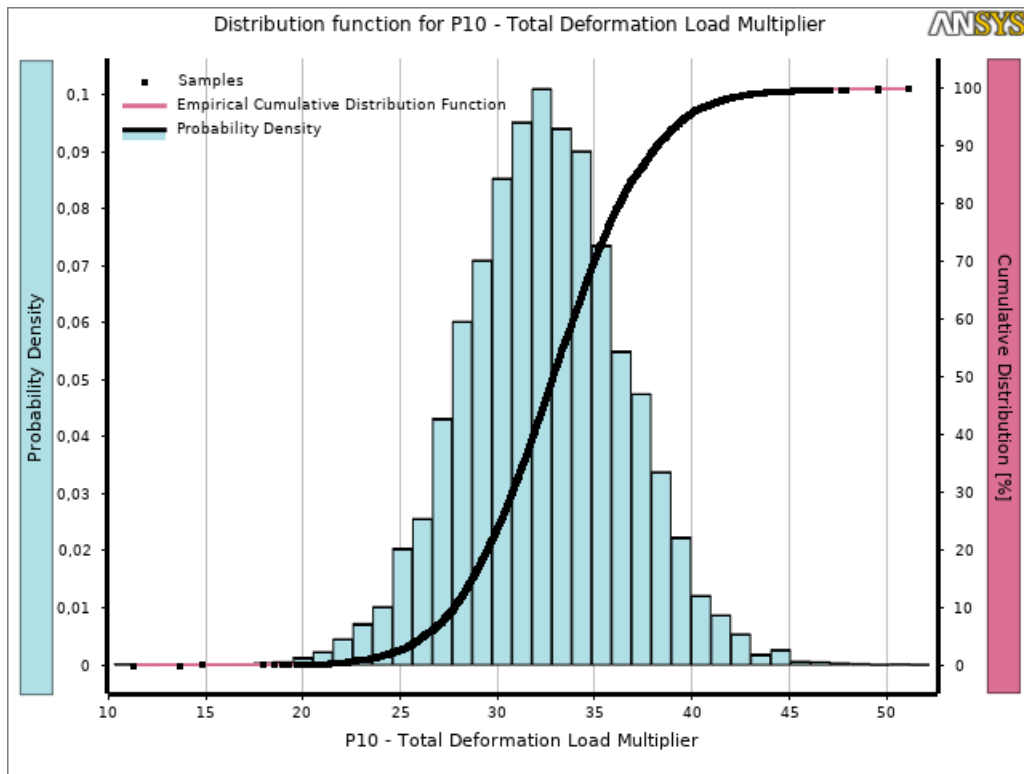| Property	Symbol	Unit	Mean	σ	COV
Spacing	S	m	1	0.05	0.05
Diameter	D	m	5	0.25	0.05
Cylinder thickness	t_s	mm	20	1	0.05
Height of stiffener	h_r	mm	210	10.5	0.05
Stiffener thickness	t_r	mm	10	0.5	0.05

Figure 6.1: Distribution function of critical buckling pressure with 5% COV for design variables.

Table 6.2 shows how the sample size varies and the corresponding maximum and minimum critical buckling pressure for each post-processor analysis, design of experiment and response surface, respectively.

Table 6.2: Sample size and range of critical buckling pressure for the analysis, design of experiment, response surface and Six-Sigma. For 5% COV for all design variables.

Analysis	Sample	Minimum	Maximum
Design of experiment	283	21.72	43.71
Response surface	∞	-33.20	63.97
Six Sigma	10000	11.31	51.22

Figure 6.1 represents the Six Sigma analysis of the uncertainty in the critical buckling pressure. The sampling range of the critical buckling pressure is 11.31 bar and 51.22 bar. The mean value and standard deviation are 32.94 bar and 4.11, respectively. The value of the cumulative distribution function in Figure 6.1 states the probability at each point that the related parameter of critical buckling pressure lays equal or below the point.

The critical buckling pressure of the pressure hull model has an uncertainty of:

$$P_{cr} = 32.94 \pm 4.11 \ [bar]$$

The Six Sigma analysis shows a probabilistic critical buckling pressure of 12.84 bar for a 1/10000 failure. Design factor from ASME VIII div. 2 represents a covariance of 5% for all variables. However, comparing the probabilistic critical pressure and the nominal critical pressure, a new design factor can be obtained, which gives a design factor of 2.77 compared to the ASME design factor of 2.5.

6.2 1% COV for Diameter

The diameter of 5000 mm and a 5% covariance corresponds to a variation of 250 mm and not really realistic. Hence, to optimise the Six Sigma analysis, a 1% covariance of the diameter and 5% covariance for the rest of the design variables is sufficient. The statistical characteristics of pressure hull dimensions are presented in Table 6.3. The result of the Six Sigma analysis for 1% COV for pressure hull diameter is presented in Figure 6.2.

Table 6.3: Statistical characteristics dimension for pressure hull with 1% COV for diameter and 5% COV the other design variables.

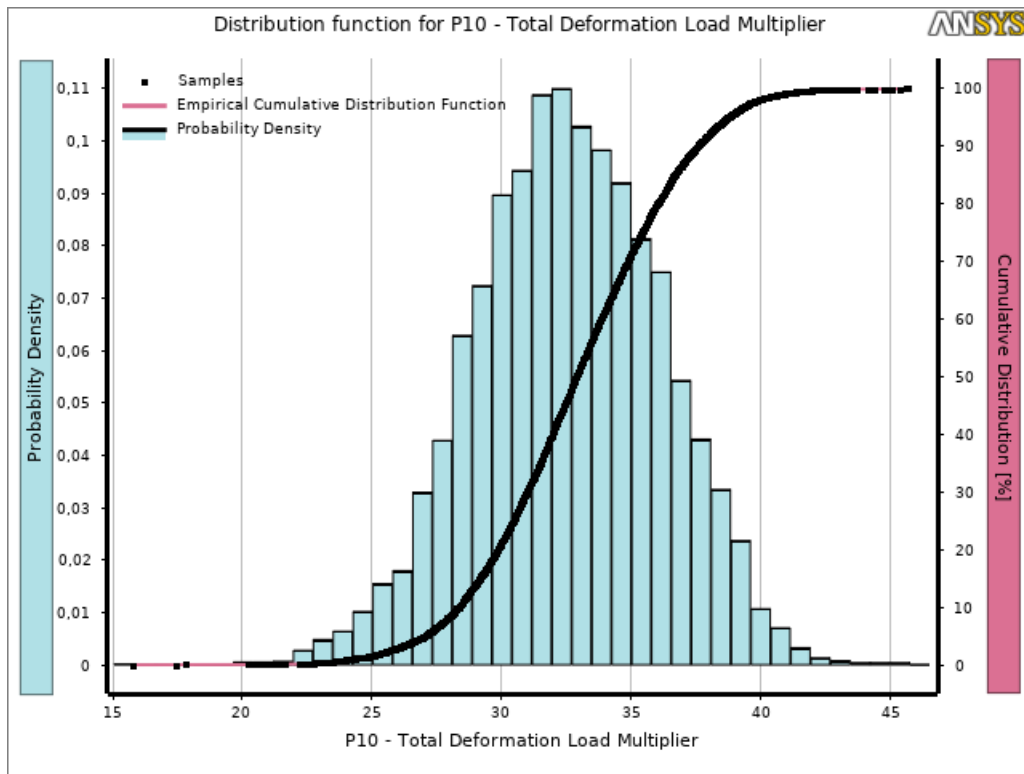| Property	Symbol	Unit	Mean	σ	COV
Spacing	S	m	1	0.05	0.05
Diameter	D	m	5	0.05	0.05
Cylinder thickness	t_s	mm	20	1	0.01
Height of stiffener	h_r	mm	210	10.5	0.05
Stiffener thickness	t_r	mm	10	0.5	0.05

Figure 6.2: Distribution function of critical buckling pressure with 1% COV for diameter variable.

The sample size varies, and the corresponding maximum and minimum critical buckling pressure for the post-processor analysis, design of experiment and response surface, and the Six Sigma analysis are shown in Table 6.4.

Table 6.4: Sample size and range of critical buckling pressure for the analysis, design of experiment, response surface and Six-Sigma. For 1% COV for diameter and 5% COV for other design variables.

Analysis	Sample	Minimum	Maximum
Design of experiment	284	23.15	40.68
Response surface	∞	-0.85	65.17
Six Sigma	10000	15.81	45.79

Figure 6.2 represents the Six Sigma analysis of the uncertainty in the critical buckling pressure. The sampling range of the critical buckling pressure is 15.81 bar and 45.79 bar. The mean value and standard deviation are 32.97 bar and 3.60, respectively.

The critical buckling pressure of the pressure hull model has an uncertainty of:

$$P_{cr} = 32.97 \pm 3.60$$

The Six Sigma analysis shows a critical buckling pressure of 16.96 bar for a 1/10000 failure. When comparing this result to the result presented in section 6.1, the critical buckling pressure of 1/10000 failure rate is significantly larger when modifying the uncertainty of the design variables. With a covariance error of 5% for all dimension, the critical buckling pressure is 12.84 bar. The mean critical pressure is more or less the same. However, the uncertainty of the critical buckling pressure is larger for a 5% covariance for all dimensions. Hence, the optimised probabilistic approach with sufficient covariance for each input parameter gives a new design factor of 2.09, which is reduced by from 2.77 given in section 6.1.

CHAPTER 7   SUMMARY AND CONCLUSION

7.1   Summary

The findings in this study suggest that design has a vital influence on the ring-stiffened cylindrical pressure hull performance.

The spacing between the ring-stiffeners has a significant influence on the critical buckling pressure. Reducing the unsupported spacing between the stiffeners increases the critical buckling pressure significantly. However, there will also be a moderate increase in pressure hull weight. The correlation between spacing, critical bucking pressure, and weight shows a low to a slight coefficient of correlation. Reduced spacing between stiffeners also gives a higher critical pressure than thicker stiffeners, even though it yields the same weight of the pressure hull. The cylinder thickness also has a significant influence on the critical buckling pressure and weight. The coefficient of correlation between the cylinder thickness and the performance variables also showed a strong to very strong correlation. By comparing models, there was evidence that a smaller unsupported length between stiffeners and a thicker ring-stiffener provided a more considerable critical buckling pressure and a significantly lighter weight of the pressure hull than the thickness of the cylinder. Hence, the cylinder thickness has a higher impact on the weight than both spacing and ring-stiffener thickness. For a failure probability of 1/10000 with enough covariance of cylinder thickness, gave a critical buckling pressure of 12.84 bar, which gives an increased in the critical buckling pressure by 7.09%, when using the ASME VIII design factor, which gave a critical buckling pressure of 13.82 bar. The design factor is reduced with 16.4% from the ASME VIII design factor of 2.5, to a design factor of 2.09.

Somewhat surprisingly, the ring-stiffener thickness indicates to have no impact on the critical buckling pressure at a certain range of cross-section stiffness of the ring-stiffeners. However, at the maximum stiffness of the various ring-stiffener thickness has some impact. As stated by Kavya *et al.* [25], the stiffeners are added to the cylindrical shell to improve the critical buckling pressure such that it is closer to the theoretically determined pressure. Bagheri et al. [18], found in his study that the unsupported spacing plays a vital role in the magnitude of the buckling pressure, which reflects the findings in this thesis. However, the weight of the welding of ring-stiffeners is not taken into account in this thesis when calculating the pressure hull weight, nor

is the manufacturing limiting spacing. Cai *et al*. [20], concluded in his study that the shell thickness plays a significant role in pressure hull performance, which also shows a significant role in the pressure hull performance in this study.

The correlation between spacing and the critical buckling pressure and weight is less than expected, whereas the eigenvalue buckling show a significant influence in critical buckling pressure and some increase in weight. The difference might be due to simplification in the correlation study. The geometrical model was kept constant as the dimension varies through the study. Hence, as the spacing was reduced, ring-stiffeners were not added to the geometry, which was done in the eigenvalue buckling analysis. A thicker cylinder shell made a significant increase in the weight of the pressure hull, which might be explained as the cylindrical shell is the main component of the pressure hull.

7.2   Conclusion

In this study, the design influence of collapse performance of a ring-stiffened cylindrical pressure hull is studied, and a collapse design optimisation is proposed. This study was done by choosing geometrical design variables for the pressure hull and analysing in a finite element model. Uncertainties in input parameters and output variables were evaluated using a probabilistic design approach. The following observations listed below are the conclusion for the present work.

- The input design parameters with a vital influence in the performance of the ring-stiffened cylindrical pressure hull are the unsupported length between the ring-stiffeners and the cylinder thickness.
- The pressure hull can reach a high strength capacity with a reduced weight of the pressure hull when combining a small unsupported spacing and a sufficient thickness of the ring-stiffeners. Compared to increased cylinder thickness, which gave a higher weight of the pressure hull.
- Probabilistic distribution of reduced failure improved the critical buckling pressure and reduced the design factor by 16.4% compared to the ASME VIII design factor of 2.5.
- When considering the uncertainties in the design variables, the critical buckling pressure may increase by 7.09%

7.3 Recommendations for Future Work

The following list contains suggested topics for further work which may provide a wider investigation on the design influence and the better optimisation of the ring-stiffened cylindrical pressure hull. To further investigate the design influence and optimise the ring-stiffened cylindrical pressure hull, future topics are suggested as followed:

- This study has used a linear elastic material, which does consider the softening or hardening in the material. The model can be developed as a non-linear ring-stiffened cylindrical shell to consider the plastic deformation in the buckling analyses, which is valid for more extensive deformation.

- Investigate how to modify the design factor in the non-linear damage assessment by comparing the elastic-plastic collapse design methods from the different codes.

- This thesis has shown that the cylinder thickness has shown a strong correlation with the critical buckling pressure, which can mean a small imperfection might make a significant impact on the collapse load. It would be beneficial to perform an imperfection sensitivity study to investigate if and how the unfavourable imperfection in the cylindrical shell influence the critical buckling pressure.

- This study has designed the pressure hull for local buckling to happen first. It would be interesting to investigate how the critical buckling pressure and weight vary when designing the pressure hull model for global buckling mode to initiate first.

REFERENCE

[1]   J. R. MacKay and F. van Keulen, "Partial Safety Factor Approach to the Design of Submarine Pressure Hulls using Nonlinear Finite Element Analysis," *Finite Elem. Anal. Des.*, vol. 65, pp. 1–16, Mar. 2013, doi: 10.1016/j.finel.2012.10.009.

[2]   C.-C. Liang, C.-Y. Hsu, and H.-R. Tsai, "Minimum Weight Design of Submersible Pressure Hull Under Hydrostatic Pressure," *Comput. Struct.*, vol. 63, no. 2, pp. 187–201, Apr. 1997, doi: 10.1016/S0045-7949(96)00342-2.

[3]   R. Burcher and L. Rydill, *Concepts in Submarine Design*. Cambridge University Press, 1994.

[4]   U. Gabler, *Submarine Construction*. Naval Ship Research and Development Center, 1972.

[5]   N. Friedman, *Submarine Design and Development*. London: Conway Maritime Press, 1984.

[6]   P. S. Granville, "Elements of the Drag of Underwater Bodies." David W. Taylor Naval Ship Research and Development Center, 1976.

[7]   M. Renilson, *Submarine Hydrodynamics*. Springer, 2015.

[8]   D. A. Jones, D. B. Clarke, I. B. Brayshaw, J. L. Barillon, and B. Anderson, *The Calculation of Hydrodynamic Coefficients for Underwater Vehicles, Technical Report DSTO-TR-1329*. Australia: Defence Science and Technology Organisation, 2002.

[9]   P. N. Joubert, *Some Aspects of Submarine Design Part 1. Hydrodynamics, Technical Report DSTO-TR-1622*. Australia: Defence Science and Technology Organisation, 2004.

[10]   P. N. Joubert, *Some Aspects of Submarine Design Part 2. Shape of a Submarine 2026, Technical Report DSTO-TR-1920*. Australia: Defence Science and Technology Organisation, 2006.

[11]   DNVGL Rules, *Part 4 Sub-Surface Ships, Chapter 1 Submarines*. 2018.

[12]   A. Alvarez, V. Bertram, and L. Gualdesi, "Hull Hydrodynamic Optimization of Autonomous Underwater Vehicles Operating at Snorkeling Depth," *Ocean Eng.*, vol. 36, no. 1, pp. 105–112, Jan. 2009.

[13]   L. Zhou, Y.-W. Mai, B. Zhang, J. Mao, and H. Jiang, "Optimal Structure Design of Elliptical Deep-Submersible Pressure Hull," in *Advanced Composites for Marine Engineering*, Switzerland: Trans Tech Publications, 2015, pp. 85–93.

[14]   E. Fathallah, H. Qi, T. Lili, and M. Helal, "Design Optimization of Composite Elliptical Deep-Submersible Pressure Hull for Minimizing the Buoyancy Factor." Hindawi Publishing Corporation, 2014.

[15]   E. Fathallah, H. Qi, L. Tong, and M. Helal, "Design optimization of lay-up and composite material system to achieve minimum buoyancy factor for composite elliptical submersible pressure hull," *Compos. Struct.*, vol. 121, pp. 16–26, Mar. 2015, doi: 10.1016/j.compstruct.2014.11.002.

[16]   E. Fathallah and M. Helal, "Optimum Structural Design of Deep Submarine Pressure hull to achieve Minimum Weight," *Int. Conf. Civ. Archit. Eng.*, vol. 11, pp. 1–22, Apr. 2016, doi: 10.21608/iccae.2016.43445.

[17]   E. Fathallah and M. Helal, "Finite element modelling and multi-objective optimization of composite submarine pressure hull subjected to hydrostatic pressure," *IOP Conf. Ser. Mater. Sci. Eng.*, vol. 683, p. 012072, Dec. 2019, doi: 10.1088/1757-899X/683/1/012072.

[18]   M. Bagheri, A. A. Jafari, and M. Sadeghifar, "Multi-objective optimization of ring stiffened cylindrical shells using a genetic algorithm," *J. Sound Vib.*, vol. 330, no. 3, pp. 374–384, Jan. 2011, doi: 10.1016/j.jsv.2010.08.019.

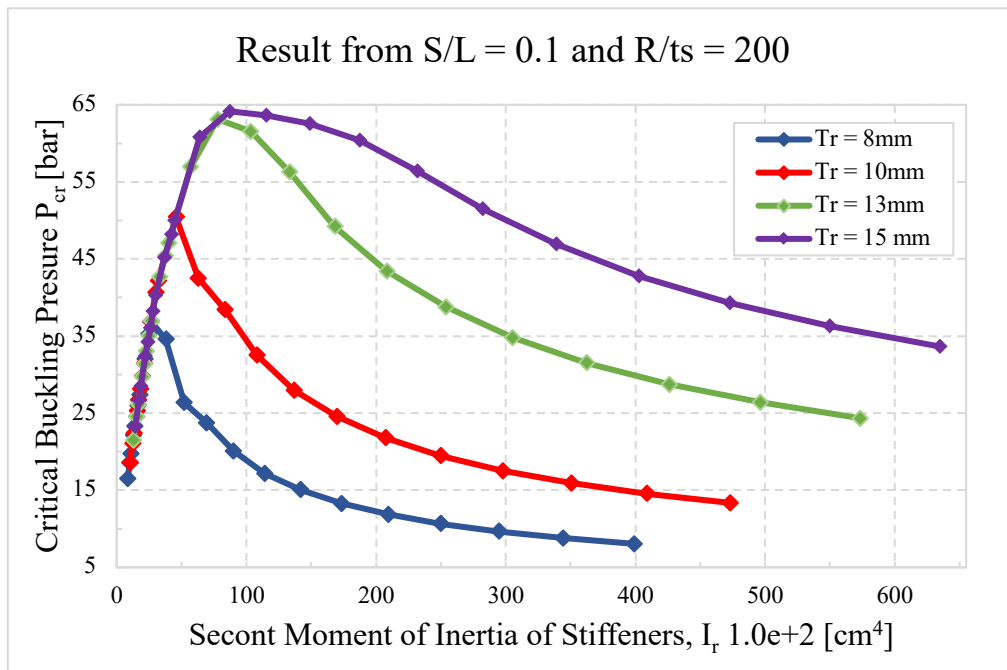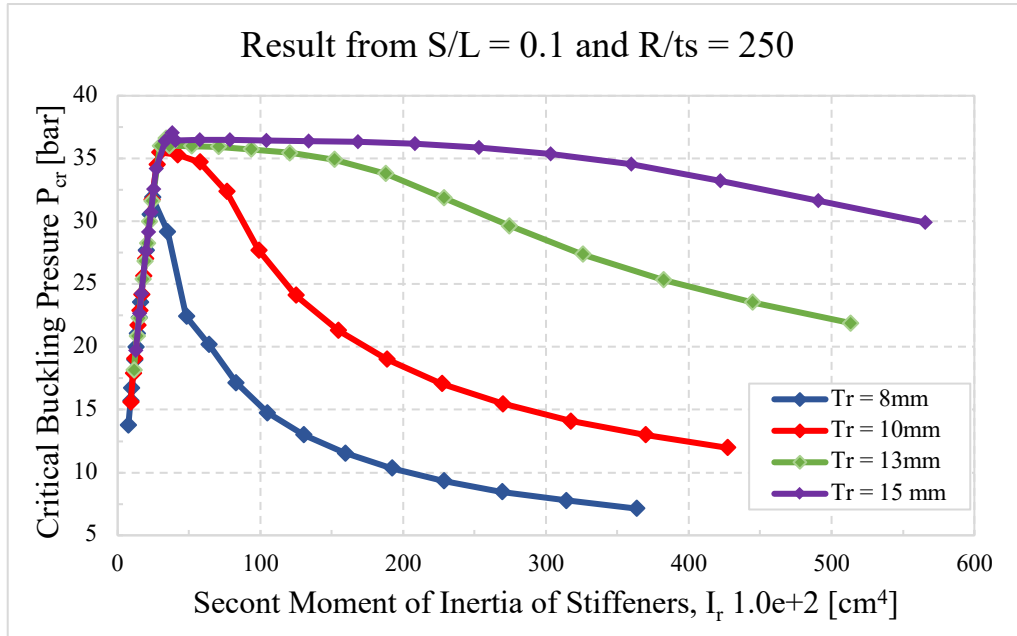[19]   C.-C. Liang, H.-W. Chen, and C.-Y. Jen, "Optimum design of filament-wound

multilayer-sandwich submersible pressure hulls," *Ocean Eng.*, vol. 30, no. 15, pp. 1941–1967, Oct. 2003, doi: 10.1016/S0029-8018(03)00044-1.

[20]　B. Cai, Y. Liu, Z. Liu, X. Tian, R. Ji, and Y. Zhang, "Probabilistic analysis of composite pressure vessel for subsea blowout preventers," *Eng. Fail. Anal.*, vol. 19, pp. 97–108, Jan. 2012, doi: 10.1016/j.engfailanal.2011.09.009.

[21]　P. F. Liu and J. Y. Zheng, "Strength reliability analysis of aluminium–carbon fiber/epoxy composite laminates," *J. Loss Prev. Process Ind.*, vol. 23, no. 3, pp. 421–427, May 2010, doi: 10.1016/j.jlp.2010.02.002.

[22]　E. Ventsel and T. Krauthammer, "Survey of Elasticity Theory," in *Thin plates and shells: theory, analysis, and applications*, New York: Marcel Dekker, 2001.

[23]　J. Prescott, "Relations Between Stress and Strain," in *Applied elasticity*, New York,: Dover Publications, 1946, pp. 13–27.

[24]　E. Ventsel and T. Krauthammer, "The General Linear Theory of Shells," in *Thin plates and shells: theory, analysis, and application*, New York: Marcel Dekker, 2001.

[25]　A. Kavya, P. Prasanna, and P. C. Jain, "Buckling Analysis of Ring Stiffened Circular Cylinders Using ANSYS." International Journal for Research in Applied Science & Engineering Technology (IJRASET), 2017.

[26]　E. Ramm and W. A. Wall, "Shell Structures—A Sensitive Interrelation Between Physics and Numerics," *Int. J. Numer. Methods Eng.*, vol. 60, no. 1, pp. 381–427, 2004.

[27]　R. D. Cook, D. S. Malkus, and M. E. Plesha, "Finite Element Method," in *Concepts and Applications of Finite Element Analysis*, 3rd ed., Wisconsin: John Wiley & Sons, INC., 1988, pp. 1–7.

[28]　E. Ventsel and T. Krauthammer, "Introduction to the General Shell Theory," in *Thin plates and shells: theory, analysis, and applications*, New York: Marcel Dekker, 2001.

[29]　Xiaolin Chen and Y. Liu, "Finite Element Modeling and Simulation with ANSYS Workbench." CRC Press Tylor & Francis Group, 2015.

[30]　A. E. H. Love, "The Small Free Vibrations and Deformation of a Thin Elastic Shell," in *Philosophical Transactions of the Royal Society of London*, Royal Society of London, 1888, pp. 491–546.

[31]　R. M. Jones, "Buckling of Circular Cylindrical Shells," in *Buckling of Bars, Plates, and Shells*, Virginia: Bull Ridge Publishing, 2006, pp. 463–689.

[32]　L. H. Donnell, "A New Theory for the Buckling of Thin Cylinders under Axial Compression and Bending, N.A.C.A. report No. 473," 1934.

[33]　U. N. Leontev and V. Z. Vlasov, "Bending of a Beam on an Elastic Foundation," in *Beams, Plates and Shells on Elastic Foundations*, 1966, pp. 47–89.

[34]　F. Millar and D. Mora, "A Finite Element Method for the Buckling Problem of Simply Supported Kirchhoff Plates." ELSEVIER, 2014.

[35]　C. R. Calladine, "Buckling of Shells: Classical Analysis," in *Theory of Shell Structure*, Cambridge University Press, 1983, pp. 473–544.

[36]　R. D. Cook, D. S. Malkus, and M. E. Plesha, "Stress Stiffening and Buckling," in *Concepts and applications of finite element analysis*, 3rd ed., Wisconsin: John Wiley & Sons, INC., 1988, pp. 429–447.

[37]　W. Schneider and A. Brede, "Consistent Equivalent Geometric Imperfections for the Numerical Buckling Strength Verification of Cylindrical Shells under Uniform External Pressure." ELSEVIER, 2004.

[38]　D. Bushnell, "Description of Types of Instability and Buckling Classical Buckling Problems," in *Computerized Buckling Analysis of Shells*, 1981, pp. 1–29.

[39]　J. L. Zeman, F. Rauscher, and S. Schindler, "General Terms and Definitions," in *Pressure Vessel Design: The Direct Route*, ELSEVIER, 2006, pp. 6–10.

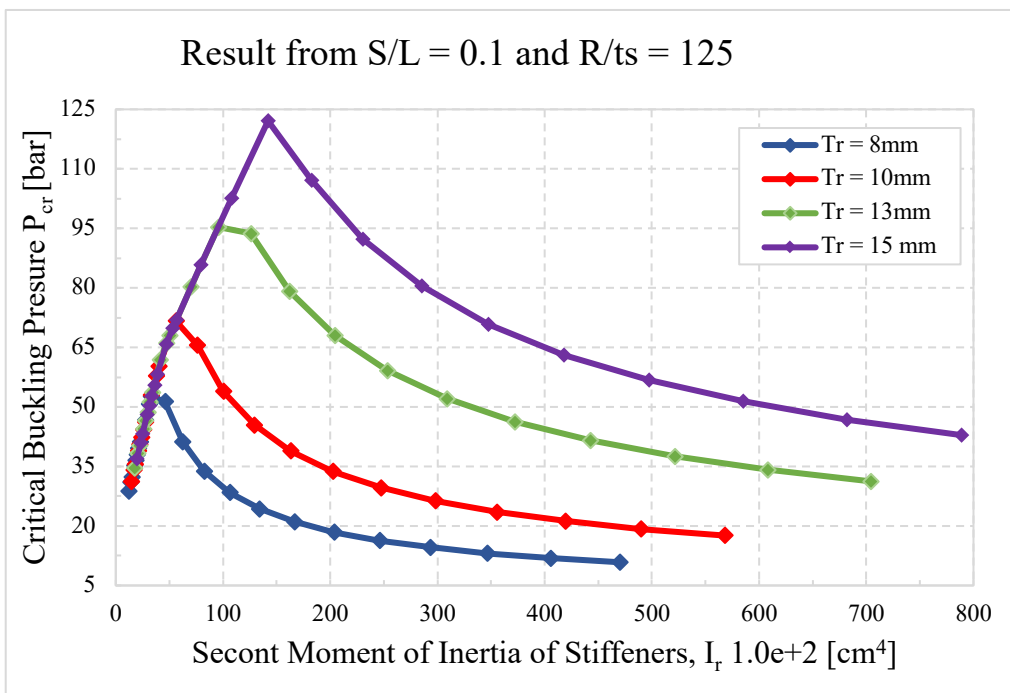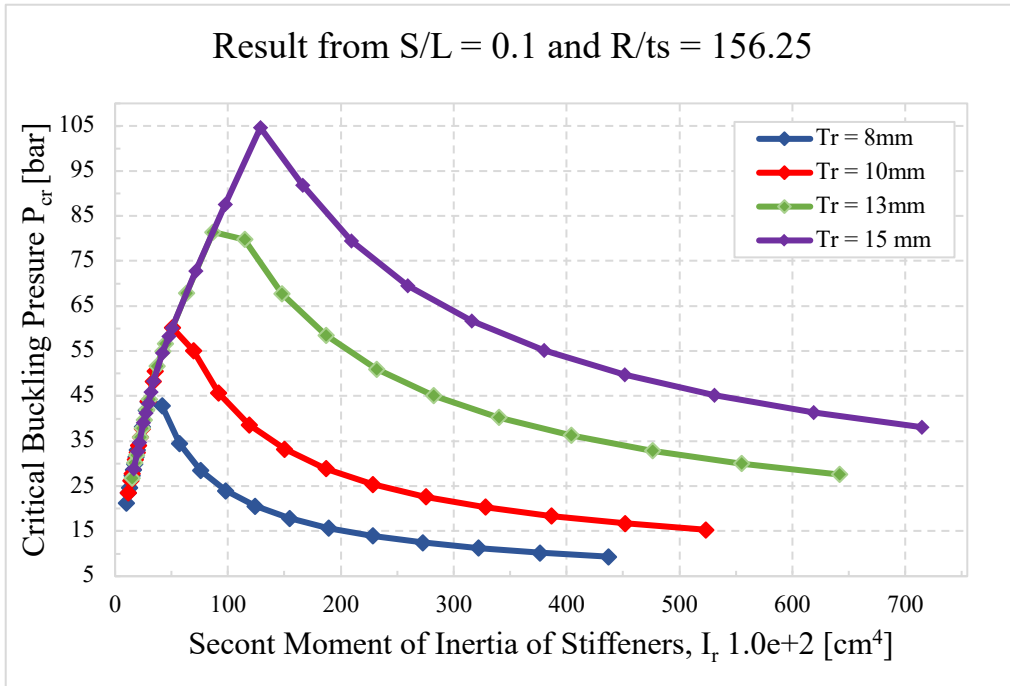[40]　B. Prabu, N. Rathinam, R. Srinivasan, and K. A. S. Naarayen, "Finite Element Analysis

of Buckling of Thin Cylindrical Shell Subjected to Uniform External Pressure." Journal of Solid Mechanics, 2009.

[41]   S. P. Timoshenko and J. M. Gere, "Buckling of Shells," in *Theory of Elastic Stability*, 2nd ed., McGraw-Hill Book Company, 1961, pp. 458–519.

[42]   D. Bushnell, "Buckling of Shells - Pitfall for Designers," in *AIAA Journal*, 9th ed., vol. 19, 1981, pp. 1183–1226.

[43]   Y. Hu, B. Chen, and J. Sun, "Tripping of Thin-walled Stiffeners in the Axially Compressed Stiffened Panel with Lateral Pressure," *Thin-Walled Struct.*, vol. 37, no. 1, pp. 1–26, May 2000, doi: 10.1016/S0263-8231(00)00010-0.

[44]   C. R. Calladine, "Understanding Imperfection-sensitivity in the Buckling of Thin-walled Shells," *Thin-Walled Struct.*, vol. 23, no. 1, pp. 215–235, Jan. 1995.

[45]   Th. von Kármán, L. G. Dunn, and H. Tsien, "The Influence of Curvature on the Buckling Characteristics of Structures," pp. 276–289, 1940.

[46]   L. A. Godoy and E. M. Sosa, "Computational Buckling Analysis of Shells: Theories and Practice." ResearchGate, 2014, Accessed: Apr. 13, 2020. [Online].

[47]   G. Cederbaum and J. Arbocz, "Reliability of Shells via Koiter Formulas," *Thin-Walled Struct.*, vol. 24, no. 2, pp. 173–187, Jan. 1996, doi: 10.1016/0263-8231(95)00027-5.

[48]   J. Arbocz and H. Abramovich, "The Initial Imperfection Data Bank at the Delft University of Technology: Part I," *Delft Univ. Technol. Dep. Aerosp. Eng. Rep. LR-290*, 1979, Accessed: Apr. 27, 2020. [Online].

[49]   M. W. Hilburger, M. P. Nemeth, and J. H. Jr. Starnes, "Shell Buckling Design Criteria Based on Manufacturing Imperfection Signatures," *NASA Cent. Aerosp. Inf.*, May 2004, Accessed: Apr. 28, 2020. [Online].

[50]   A. Chakrabarty, S. Mannan, and T. Cagin, "Finite Element Analysis in Process Safety Applications," in *Multiscale Modeling for Process Safety Applications*, Butterworth-Heinemann, 2015, pp. 275–286.

[51]   M. H. Jawad, "Basic Finite Element Equations," in *Design of Plate and Shell Structures*, The American Society of Mechanical Engineers, 2004, pp. 409–432.

[52]   "2015 ASME Section VIII division 2, Boiler and Pressure Vessel Code." ASME (American Society of Mechanical Engineers), New York, 2015.

[53]   "2017 ASME Section VIII division 3, Boiler and Pressure Vessel Code." ASME (American Society of Mechanical Engineers), New York, 2017.

[54]   "European Committee for Standardization; NS-EN 13445-3." Unifired Pressure Vessel, Brussel, 2014.

[55]   "Specification for Unfired Fusion Welded Pressure Vessels." BSi British Standard, 2009.

[56]   "EN 13445 'Unfired Pressure Vessels' Background to the Rules in Part 3 Design." Union de Normalisation de la Mècanique, 2004.

[57]   S. Reh, J.-D. Beley, S. Mukherjee, and E. H. Khor, "Probabilistic Finite Element Analysis using ANSYS," *Struct. Saf.*, vol. 28, no. 1, pp. 17–43, Jan. 2006, doi: 10.1016/j.strusafe.2005.03.010.

[58]   M. T. Heitzmann, J. P. Torres, L.-J. Vandi, and S. Schaber, "Probabilistic Design: A New Approach to Look at Composite Design." 2015.

[59]   M. W. Long and J. D. Narciso, "Probabilistic Design Methodology for Composite Aircraft Structures," U.S. Department of Transpotation - Federal Aviation Administration Technical Report, DOT/FAA/AR-99/2, 1999.

[60]   F. L. Montes and L. Molina, "Six Sigma and Management Theory: Processes, Content and Effectiveness," *Total Qual. Manag. Bus. Excell. - TOTAL QUAL MANAG BUS EXCELL*, vol. 17, pp. 485–506, May 2006, doi: 10.1080/14783360500528270.

[61]   "ANSYS, 'DesignXplorer User's Guide', 19.3 Academic ed." ANSYS.

[62]   P. Yang, Y.-W. Liu, and G.-Y. Zhong, "Prediction and parametric analysis of acoustic streaming in a thermoacoustic Stirling heat engine with a jet pump using response surface methodology," *Appl. Therm. Eng.*, vol. 103, pp. 1004–1013, Jun. 2016, doi: 10.1016/j.applthermaleng.2016.04.157.

[63]   L. An, C. Liu, and Y. Liu, "Optimization of operating parameters in polysilicon chemical vapor deposition reactor with response surface methodology," *J. Cryst. Growth*, vol. 489, pp. 11–19, May 2018, doi: 10.1016/j.jcrysgro.2018.02.030.

[64]   S. K. Rout, B. K. Choudhury, R. K. Sahoo, and S. K. Sarangi, "Multi-objective parametric optimization of Inertance type pulse tube refrigerator using response surface methodology and non-dominated sorting genetic algorithm," *Cryogenics*, vol. 62, pp. 71–83, Jul. 2014, doi: 10.1016/j.cryogenics.2014.03.019.

[65]   E. Ellobody, R. Feng, and B. Young, "Linear and Nonlinear Finite Element Analyses," in *Finite Element Analysis and Design of Metal Structures*, E. Ellobody, R. Feng, and B. Young, Eds. Boston: Butterworth-Heinemann, 2014, pp. 56–71.

[66]   J. He and Z.-F. Fu, "Mathematics for modal analysis," in *Modal Analysis*, J. He and Z.-F. Fu, Eds. Oxford: Butterworth-Heinemann, 2001, pp. 12–48.

[67]   "ANSYS, 'User's guide', 19.3 Academic ed." ANSYS.

[68]   "ANSYS Fluent User's Guide Release 15.0." ANSYS, 2013.

[69]   Y. Wang, C. Feng, Z. Zhao, and J. Yang, "Eigenvalue Buckling of Functionally Graded Cylindrical Shells Reinforced with Graphene Platelets (GPL)," *Compos. Struct.*, vol. 202, pp. 38–46, Oct. 2018, doi: 10.1016/j.compstruct.2017.10.005.

[70]   G. Meissner, "Some Correlation Basics: Properties, Motivation, Terminology," in *Correlation Risk Modeling and Management: An Applied Guide Including the Basel III Correlation Framework - with Interactive Models in Excel / VBA*, New York, SINGAPORE: John Wiley & Sons, Incorporated, 2014.

[71]   J.p. Guilford, *Fundamental Statistics In Psychology And Education*, 2nd ed. 1950.

[72]   K. Pearson, "Notes on the History of Correlation," *Biometrika*, vol. 13, no. 1, pp. 25–45, 1920, doi: 10.1093/biomet/13.1.25.

[73]   K. Pearson, "Mathematical Contributions to the Theory of Evolution. III. Regression, Heredity, and Panmixia," *Philos. Trans. R. Soc. Lond. Ser. Contain. Pap. Math. Phys. Character*, vol. 187, pp. 253–318, 1896.
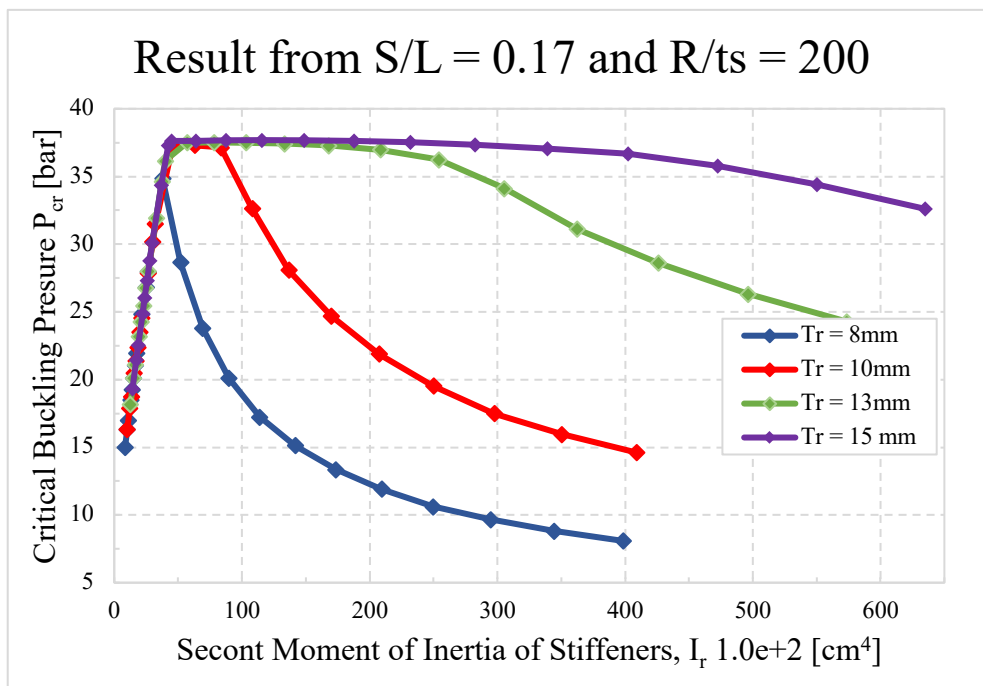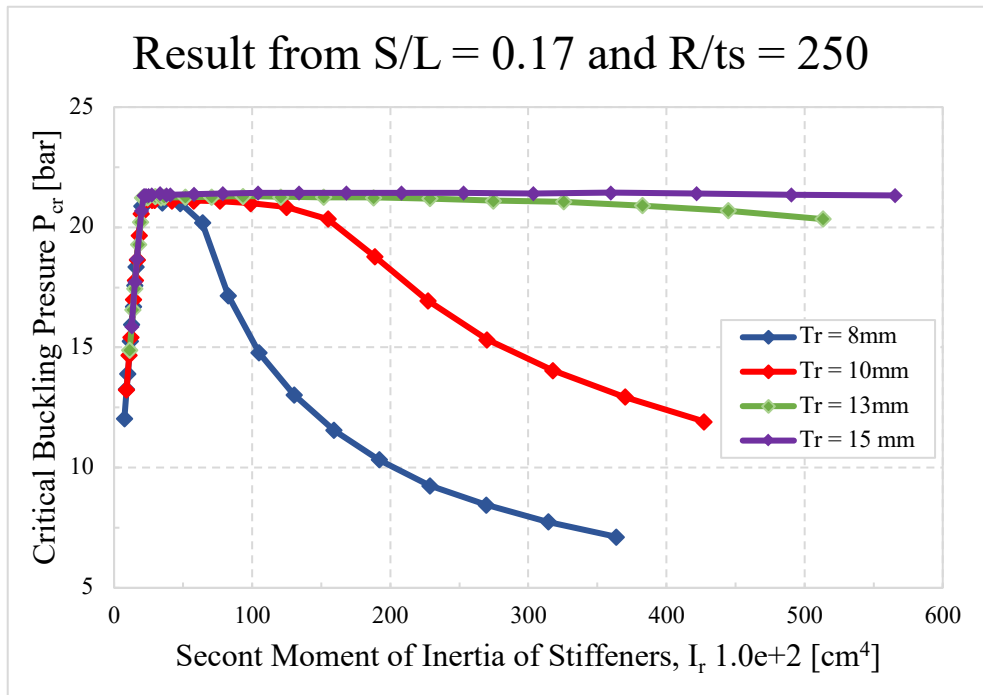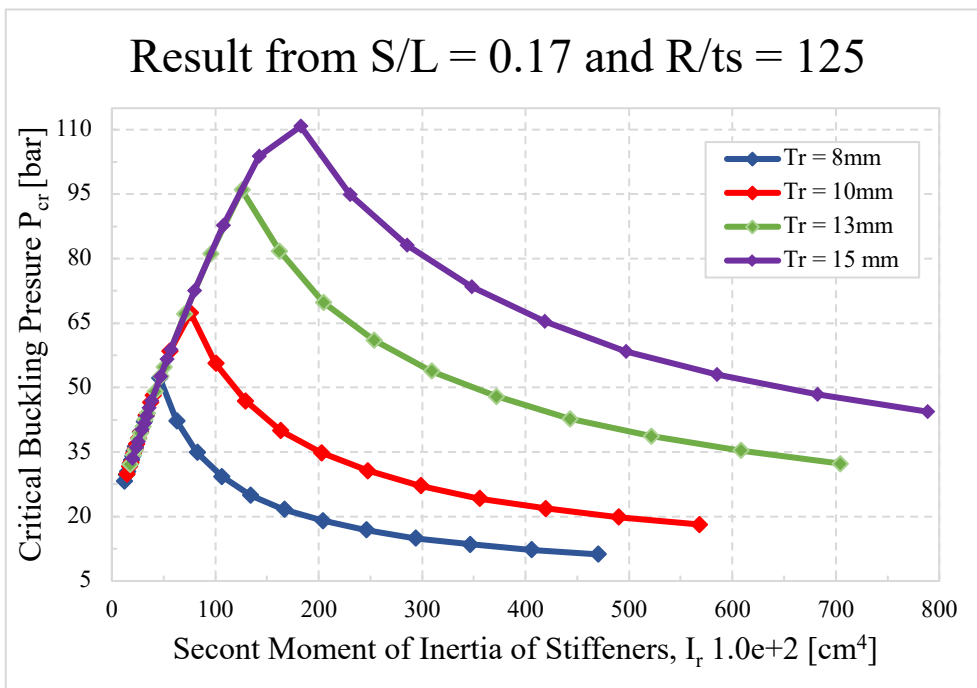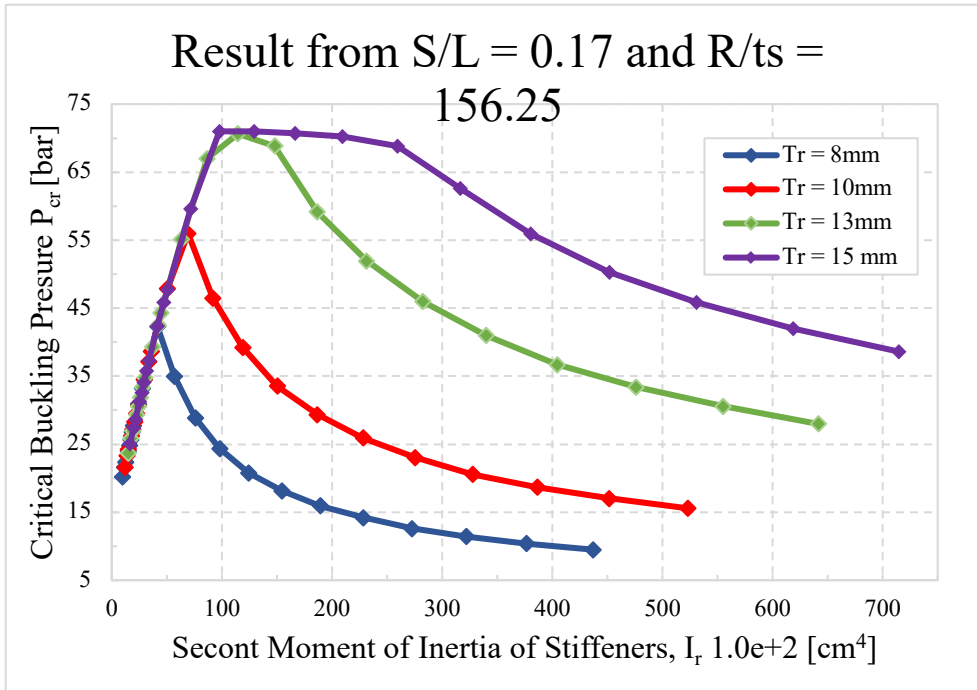
A   APPENDIX

A.1   Result from the Spacing-Length Ratio of 0.1

Result from S/L = 0.1 and R/ts = 250

Result from S/L = 0.1 and R/ts = 200

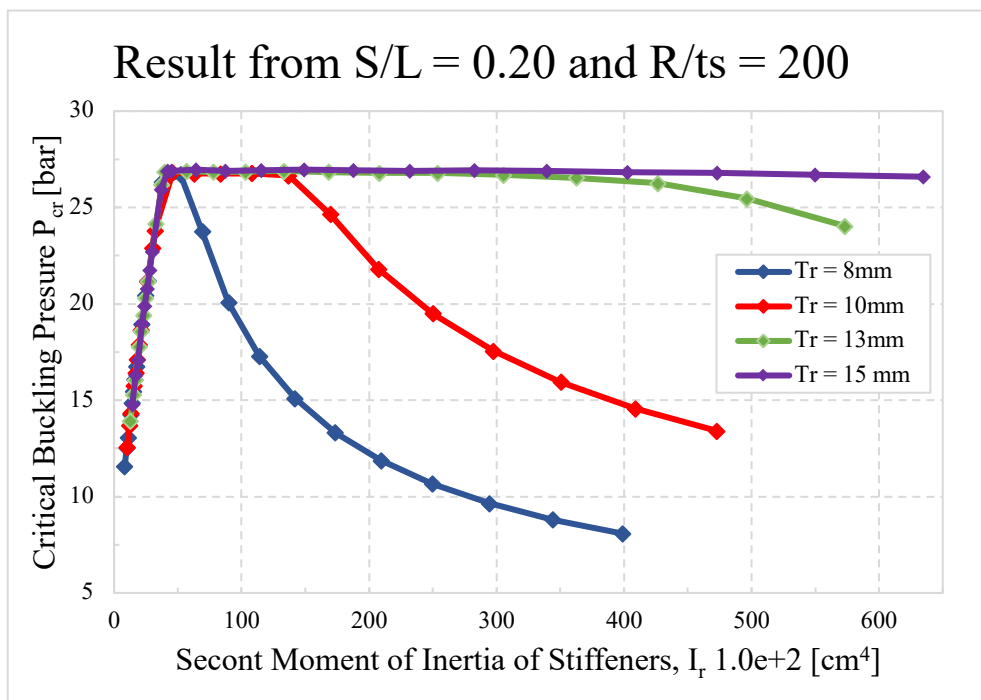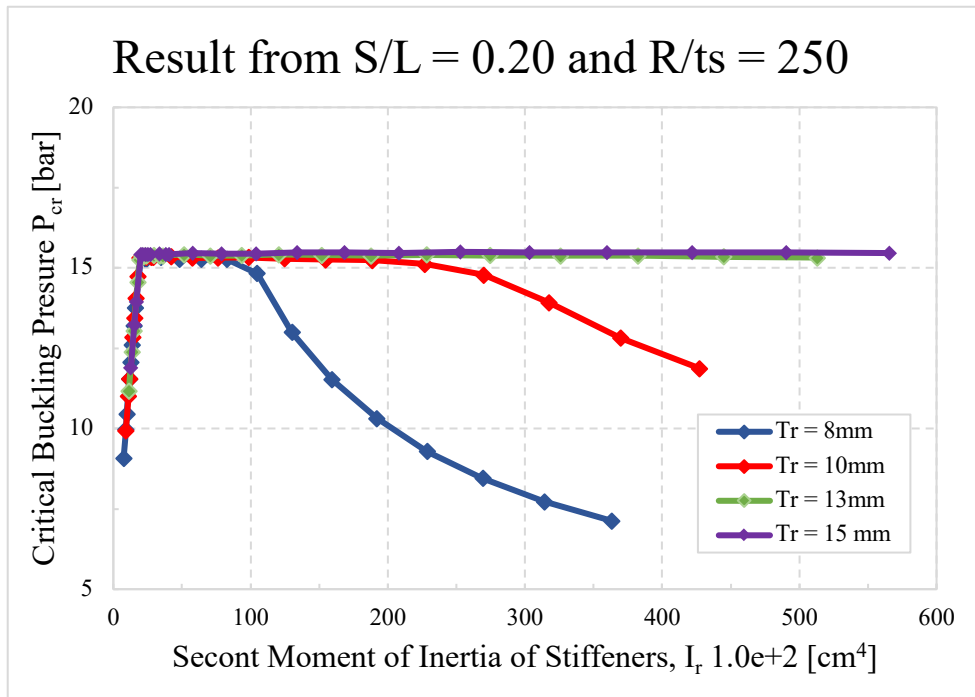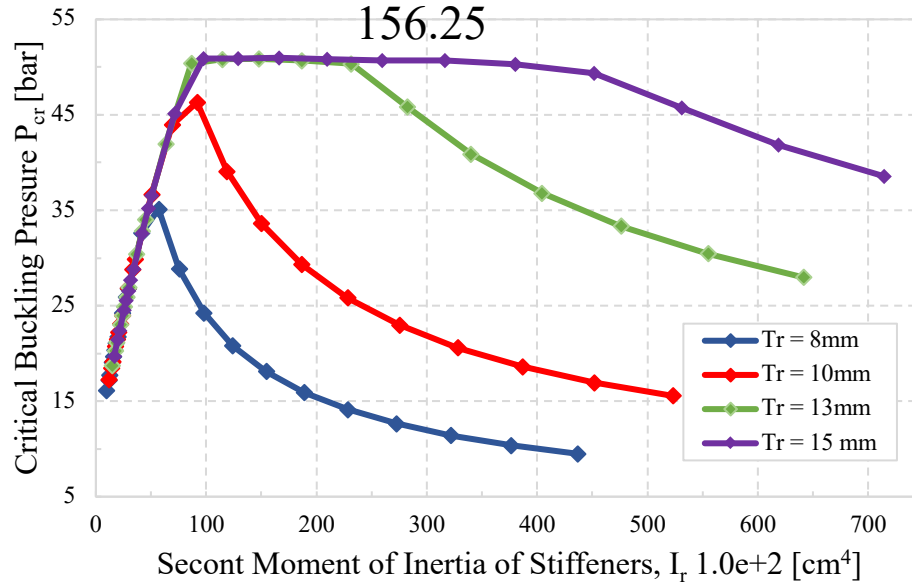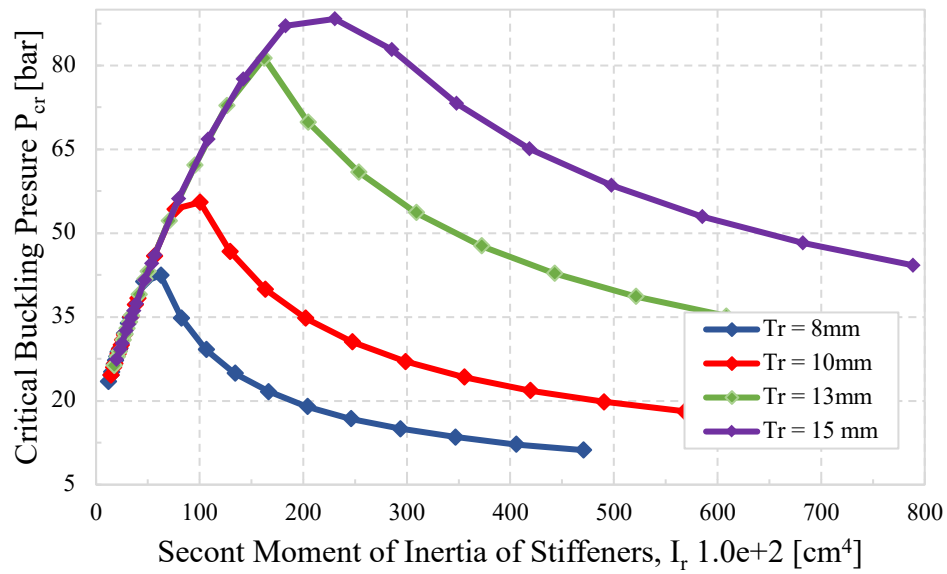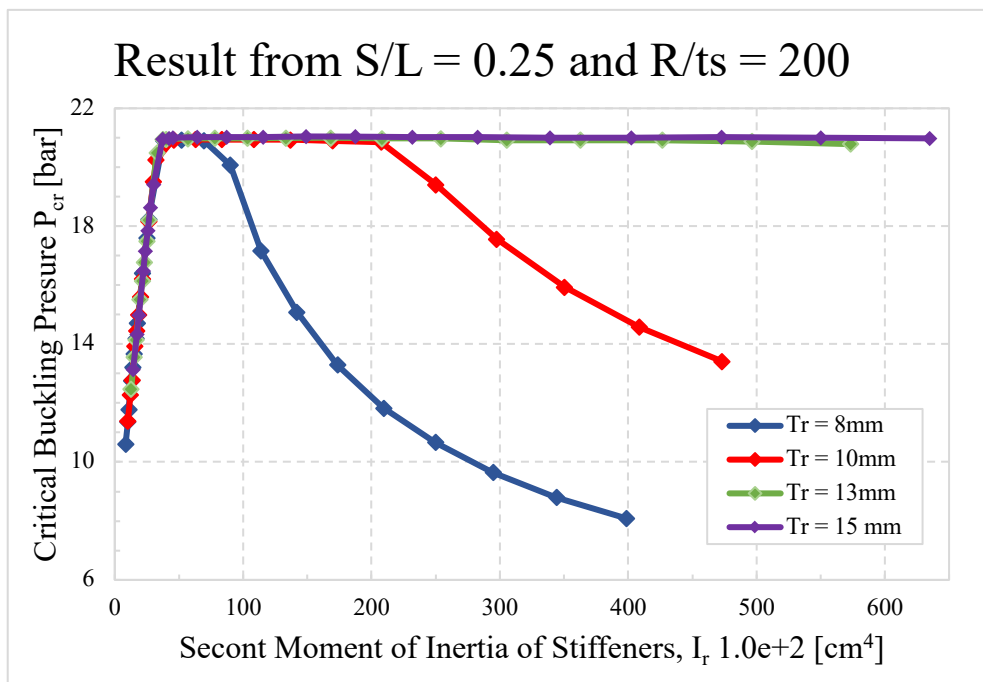Result from S/L = 0.1 and R/ts = 156.25

Result from S/L = 0.1 and R/ts = 125

A.2   Result from the Spacing-Length Ratio of 0.17

Result from S/L = 0.17 and R/ts = 250
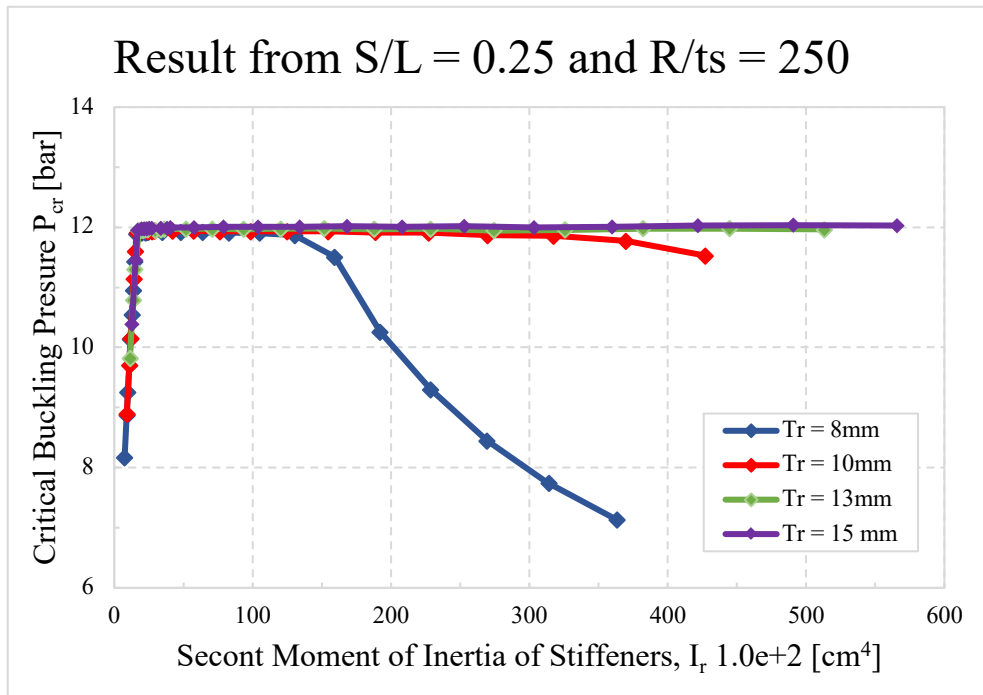

Result from S/L = 0.17 and R/ts = 200

Result from S/L = 0.17 and R/ts = 156.25

Result from S/L = 0.17 and R/ts = 125

A.3   Result from the Spacing-Length Ratio of 0.2

Result from S/L = 0.20 and R/ts = 250

Result from S/L = 0.20 and R/ts = 200
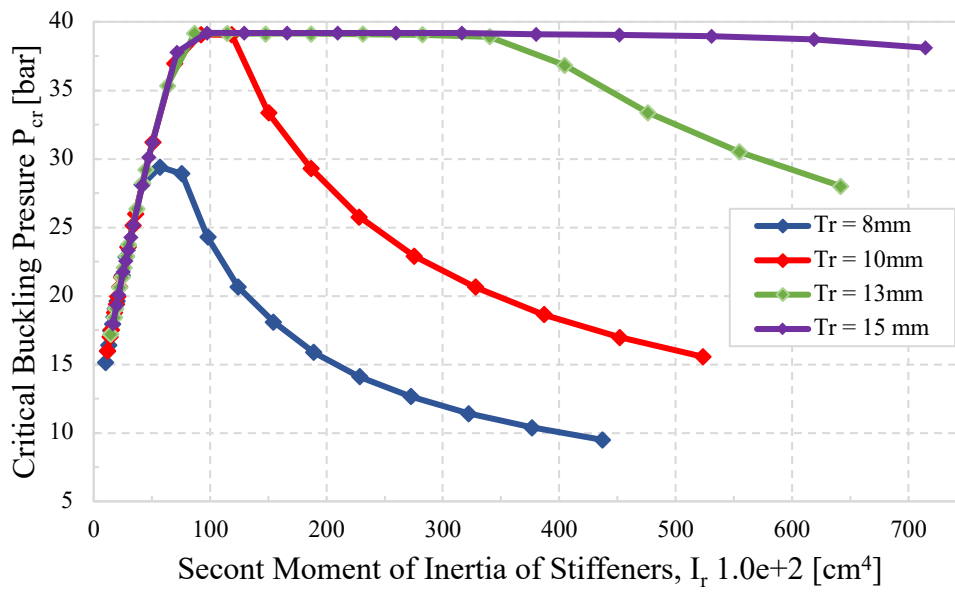
Result from S/L = 0.20 and R/ts = 156.25

Result from S/L = 0.20 and R/ts = 125

A.4   Result from the Spacing-Length Ratio of 0.25

Result from S/L = 0.25 and R/ts = 156.25

Result from S/L = 0.25 and R/ts = 125